



University of Kerbela  
College of Science  
Department of Physics

## Improvement of radiotherapy theoretically by nano – molecules as radiosensitive agent

Thesis Submitted to the Council of the College of Science, University of  
Kerbala in Partial Fulfillment of the Requirements for the Master Degree  
in Physics

By

Walaa Shalan Sarhan

B.Sc. University of Kerbala 2008

Supervised by

Assist. Prof Dr. Nagham Muhee AL-tememi

March 2024 A.D.

Ramadan 1445 A.H.


بِسْمِ اللَّهِ الرَّحْمَنِ الرَّحِيمِ

﴿تَعَالَى اللَّهُ الْمَلِكُ الْحَقُّ وَلَا تَعْجَلْ  
بِالْقُرْآنِ مِنْ قَبْلِ أَنْ يُقْضَىٰ إِلَيْكَ وَحْيُهُ  
وَقُلْ رَبِّ زِدْنِي عِلْمًا﴾

صدق الله العلي العظيم

## Supervisor Certificate

We certify that the thesis entitled " *Improvement of radiotherapy theoretically by nano – molecules as radiosensitive agent* " was prepared under our supervision by (*Walaa Shalan Sarhan*) at the Science College / Kerbala University as a partial fulfilment of the requirements for the Master degree of Science in Physics.

Signature: 

Name: **Dr. Nagham Muhee AL-tememi**

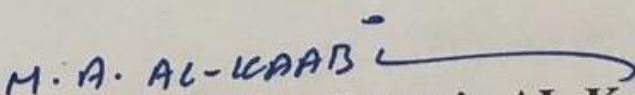
Title: Assistant Professor

Address: Department of Physics, College of Science/University of Kerbala

Date: 31/3/2024

In view of the available recommendations, I forward this thesis for debate by the examining committee.

Signature:

  
Name: **Dr. Mohammed Abdulhussain AL-Kaabi**

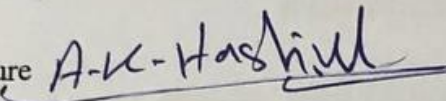
Title: Assistant Professor

Head of the Physics Department, College of Science/ University of Kerbala

Date: 31/3/2024

## Examination Committee Certification

We certify that we have read this thesis, entitled "*Improvement of radiotherapy theoretically by nano – molecules as radiosensitive agent*" and as an examining committee, examined the student "*Walaa Shalan Sarhan*" on its contents and that in our opinion it is adequate for the partial fulfillment of the requirements for the Master Degree of Science in Physics.


Signature   
Name: **Dr. Abdalsattar Kareem Hashim**

Title: Professor

Address: University of Kerbala,  
College of Science, Department of Physics.

Date: 20 / 3 / 2024

(Chairman)


Signature   
Name: **Dr. Rajaa K. Mohammad**

Title: Professor

Address: University of Kerbala,  
College of Science, Department of Physics.

Date: 20 / 3 / 2024

(Member)


Signature   
Name: **Dr. Talib Abdulridha Abdulwahid**

Title: Assist Professor

Address: University of Kufa,  
College of Science, Department of Physics.

Date: 20 / 3 / 2024

(Member)

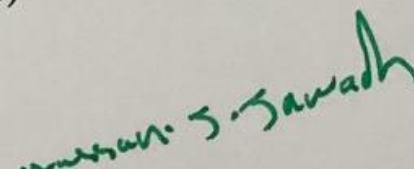
Signature   
Name: **Dr. Nagham M. Shiltagh**

Title: Assist Professor

Address: University of Kerbala  
College of Science, Department of Physics.

Date: 20 / 3 / 2024

(Member & Supervisor)

Signature:   
Name: **Dr. Hassan Jameel Jawad AL-Fatlawy**

Title: Professor

Address: **Dean of the College of Science, University of Kerbala**

Date: / /

## *Dedication*

*I dedicate the fruit of this work to God's argument in his land, to the one who will fill the earth with fairness and justice after it was filled with injustice and oppression.*

*To my master and imam, the master of the era, Zalzaman (Muhammad ibn al-Hasan ibn Ali al-Hadi), may God hasten his noble reappearance.*

*To the light of God by which those who are rightly guided are guided and by which the believers are relieved.*

*To the promised and praised light.*

*To the cause connected between earth and heaven.*

*To you, son of the Lady of Women, I offer my humble effort before you, and I ask God for acceptance and success.*

*Walaa Shalan*

## ***Acknowledgments***

*“In the name of Allah, the most beneficent and the most merciful”*

*First and foremost, I would like to thank Allah Almighty subhanahu wa-ta'ala for his endless blessing and giving me the perseverance to achieve what I have achieved today*

*I wish to express my enormous gratitude to my supervisor Assist. Prof Dr. Nahagm Muhee AL-tamemie for his continuous encouragement, guidance, advice, and a great effort from the first step till the completion of my thesis, may Allah reward him with the best reward. I also thank the Deanship of the College of Science, the Presidency of the Physics Department, and all the professors in the Physics Department.*

*I wish I had a better word than thanks to express how I feel to my father, mother, all. my family and colleagues.*

*Finally, a great "thank you" goes to anyone who helped me, or gave me advice.*

*Walaa Shalan*

## Table of contents

Number	Title	Page
	Acknowledgments	II
	Table of contains	III
	List of Figures	V
	List of Tables	VI
	List of Symbols	IX
	Abstract	XII
<b>Chapter One</b>		
1-1	Carbohydrates	2
1-2	Monosaccharide (glucose)	2
1-3	Physical and chemical properties of $\alpha$ -D glucose	4
1-4	Mechanism of absorption of glucose into the blood by human organs in the human body	5
1-5	Application nanotechnology in Medical Field	7
1-6	Silver nanoparticles in treatment	8
1-7	Radiotherapy (RT)	10
1-8	Types of radiations useful in RT	11
1-9	Medical linear accelerator LINAC in X-Ray Mode	12
1-10	Radiotherapy Action Mechanisms	13
1-11	Previous studies	14
1-12	The Aim of the Work	18
<b>Chapter Two</b>		
2-1	Introduction	20
2-2	The first part / Approximation of the Schrödinger Equation	20
2-3	Born-Oppenheimer Approximation	22
2-4	Hartree–Fock Approximation	23
2-4-1	Restricted Hartree –Fock (RHF) Method:	24
2-4-2	Unrestricted Hartree-Fock (UHF) Method:	25
2-5	The Roothaan – Hall Equations and the Linear Combination of Atomic Orbitals (LCAO)	25
2-5-1	Slater-Type Orbitals (STOs)	26
2-5-2	Gaussian-Type Orbitals (GTOs)	27
6-2	Density Functional Theory (DFT):	28
2-6-1	The Hohenberg-KohnTheorem (HK)	28

2-6-2	Kohn-Sham Method	30
2-7	Exchange-Correlation Functional	31
2-8	Density Approximations	32
2-8-1	The Local Density Approximation (LDA)	32
2-8-2	The Local Spin-Density Approximation (LSDA)	33
2-8-3	The Generalized Gradient Approximation (GGA)	34
2-9	Hybrid functional	35
2-10	Basis Sets	35
2-10-1	Minimal Basis Sets	36
2-10-2	Split Valence Basis Sets	36
2-10-3	Polarized Basis Sets	37
2-10-4	Diffuse Basis Sets	37
2-11	Programs and Computers in Use	38
2-11-1	Computers in Use	38
2-11-2	Programs	38
2-11-2-1	Gaussian 09W	38
2-11-2-2	Gauss View Program	39
2-12	Electronic properties	39
2-13	Total Energy	39
2-14	Energy Gap ( $E_g$ )	41
2-15	Atomic Charges	41
2-16	Molecular Electrostatic Potential (MEP) Surface	42
2-17	Principles of Vibrational Spectroscopy	42
2-18	Kerma concept	44
2-19	Exposure	46
2-20	Absorbed Dose	47
2-21	Biological Effectiveness Relative	48
2-22	Linear Attenuation Coefficient	49
2-23	Coefficient of Mass Energy Absorption	50
2-24	The Relationship Between Mass Attenuation Coefficient and Cross Section	51
2-25	Fractionation Dose	53
2-26	Sensitivity Enhancement Ratio (SER)	53
2-27	Deriving of Theoretical Procedure	55
Chapter Three		
3.1	Introduction	60



3-2	Nanoparticales molecular construction	60
3.3	Structural Properties .	62
3-3-1	Minimize Energy	62
3.3.2	Bond Lengths	67
3-3-3	Bond Angles	71
3-3-4	dihedral angle	72
3-3-5	Natural Population Analysis (NPA)	74
3-4	HOMO–LUMO Energy	77
3-5	Molecular Electrostatic Potential (MEP) Surface	80
3.6	Spectroscopy Properties	83
3.6.1	Vibrational Frequencies & IR spectra analysis.	83
3-6-2	Vibration of mode	85
3-7	Number of surviving lung malignant cells	93
3-8	Conclusion	106
3-9	Future work	108

## List of Tables

Number	Table	Page
1-1	physical properties of the $\alpha$ – D glucose	4
2-1	Values of the constant $\alpha/\beta$	57
3-1	Parameters of compound of pure $\alpha$ – D glucose ( $C_6H_{12}O_6$ )	62
3-2	Parameters of compound of 2 $\alpha$ – D glucose with one AgNP ( $C_{12}H_{24}O_{12}Ag$ )	62
3-3	Parameters of compound of $\alpha$ – D glucose with three AgNPs ( $C_6H_{12}O_6Ag_3$ )	62
3-4	Electronic and thermal properties different of structure of pure $\alpha$ – D glucose and $\alpha$ – D glucose with silver nanoparticles	66
3-5	Bond lengths in (Å) of pure $\alpha$ – D glucose and $\alpha$ – D glucose with AgNPs at B3LYP	67
3-6	Bond angle in (degree) of pure $\alpha$ – D glucose and $\alpha$ – D glucose with AgNPs at B3LYP	71
3-7	Dihedral angle in (degree) of pure $\alpha$ – D glucose and $\alpha$ – D glucose with AgNPs at B3LYP	73
3-8	Natural atomic charges of the ( $C_6H_{12}O_6 Ag_3$ )	74

3-9	Natural atomic charges of the ( $C_{12}H_{42}O_{12} Ag$ )	75
3-10	HOMO–LUMO gap interaction of $\alpha - D$ glucose with Ag NPs by the DFT method	77
3-11	Comparison of calculated wavenumbers ( $cm^{-1}$ ) for final adsorption geometries of studied molecules indicating to the vibrational normal modes of main functional groups	84
3-12	The number of vibrations mode of $\alpha - D$ glucose with AgNPs	86
3-13	Comparison of experimental and theoretical wavenumbers for studied molecules and previous studies	93
3-14/A	The decreasing the number of cancer call with increasing energy from(2MeV-8 MeV) with $\alpha - D$ glucose add 3 Ag NPs ( $C_6 H_{12}O_6Ag_3$ )	95
3-14/B	The decreasing the number of cancer call with increasing energy from(10MeV-15 MeV) with $\alpha - D$ glucose add 3 Ag NPs ( $C_6 H_{12}O_6Ag_3$ )	96
3-15/A	The decreasing the number of cancer call with increasing energy from(2MeV-8 MeV) with the aid of 2 $\alpha - D$ glucose add 1 Ag NPs ( $C_{12} H_{24}O_{12}Ag$ )	97
3-15/B	The decreasing the number of cancer call with increasing energy from(10MeV-15 MeV) with the aid of 2 $\alpha - D$ glucose add 1 Ag NPs ( $C_{12} H_{24}O_{12}Ag$ )	98

## List of figures

Number	Figure	Page
1-1	Different structure of $\alpha$ -D glucose (a) represent of open chain ,(b) represent of ring	3
1-2	Different cyclic structures of glucose (A) alpha –D glucose, (B) bata –D glucose	3
1-3	Structure of as (A ) sucrose ,(B) glucose and (C)fructose with the number of their corresponding oxygen atoms (in red). Carbon and hydrogen atoms are showed in white and gray color, respectively.	5

1-4	Mechanisms of AgNPs' antibacterial effect against bacteria, showing the ROS-dependent route, DNA damage, protein denaturation, and enzyme inactivation	9
1-5	AgNPs' anticancer mechanisms. AgNPs have the ability to break DNA, produce ROS and ruin the ultrastructure of cancer cells	10
1-6	(A) The linear accelerator with drift tubes, the represent (B) exterior LINAC in X-Ray Mode	13
2-1	Diagram of orbital energy levels for closed - shell systems	24
2-2	Diagram of orbital energy levels for open - shell systems	25
2-3	A comparison of the form of STO and GTO functions.	27
2-4	A molecule has two electrical energy states	40
2-5	Diagram band gap between two molecules that interact and ban of HOMO-LUMO	41
2-6	The many vibrational modes	44
3-1	(A) pure $\alpha$ -D glucose, (B) represent 2 $\alpha$ - D glucose with 1 AgNPs and (C) $\alpha$ - D glucose with 3 AgNPs drawing by camo draw program	61
3-2	full optmazation of molecules structer represent (A) pure $\alpha$ - D glucose (B) $\alpha$ - D glucose with 3AgNPs and (C) 2 $\alpha$ - D glucose with 1AgNPs	63
3-3	Total energy curve forB3LPY of structure of pure $\alpha$ - D glucose	64
3-4	Total energy curve forB3LPY of structure of 2 $\alpha$ - D glucose with one Ag	65
3-5	Total energy curve forB3LPY of structure of $\alpha$ - D glucose with three of AgNP	65
3-6	Optimized geometric structure of the bond length for represent(A) pure $\alpha$ - D glucose (B) $\alpha$ - D glucose with 3AgNPs, (C) 2 $\alpha$ - D glucose of with one Ag NP	70
3-7	The charge distbustion of $\alpha$ - D glucose with 3Ag NPs	75
3-8	The charge distbustion of 2 $\alpha$ - D glucose with one Ag NP	76

3-9	HOMO- LUMO state of $C_6H_{12}O_6$	78
3-10	HOMO- LUMO state of $C_6H_{12}O_6Ag_3$	79
3-11	HOMO- LUMO state of $C_{12}H_{24}O_{12}Ag$	79
3-12	Molecular electrostatic potential in 3D showe (A)pure $\alpha - D$ glucose (B) $\alpha - D$ glucose with 3AgNPs and (C) $\alpha - D$ glucose with 1AgNP	81
3-13	Molecular electrostatic potential contour surface show (A)pure $\alpha - D$ glucose (B) $\alpha - D$ glucose with 3AgNPs and (C) $\alpha - D$ glucose with 1AgNP	82
3-14	IR spectra of structuers of glucose with AgNPs; $\alpha$ -D-glucose- $Ag_3$ (red), and 2 $\alpha - D$ -Glucose- $Ag$ (black) including the assignment of the most influential groups	84
3-15	The most prominent kinds of effective vibration, (A) $\alpha - D$ glucose with 3AgNPs and (B) 2 $\alpha - D$ glucose with one AgNP	92
3-16	Compars SER of lung with the presence of 3 silver nanoparticles with $\alpha$ -D glucose ( $C_6H_{12}O_6Ag_3$ ) and X-ray energy ranging from 2 to 15 (MeV) with the presence of 3 silver nanoparticles with $\alpha$ -D glucose ( $C_6H_{12}O_6Ag_3$ ) and X-ray energy ranging from 2 to 15 (MeV) between thyrtical study(Blue column) and pruivous study (red column)	100
3-17	Relastionship between photon energy and mass-energy absorption coefficient of lung	101
3-18	Enhancement of lung SER with the presence of one silver nanoparticle with 2 $\alpha - D$ glucose ( $C_{12}H_{24}O_{12}Ag$ ) and X-ray energy ranging from 2 to 15 (MeV).	102
3-19	(A) Relationship between photon energy and mass-energy absorption coefficient of sliver and showe (B) relation shipe between photon energy and mass-energy absorption coefficient of $C_{12}H_{24}O_{12}Ag$	103
3-20	Relationship between energy and sessions radio tharpy existence $\alpha - D$ glucose with three sliver nanoparticales	104
3-21	Relation shipe between energy and sessions radio tharpy existence two alpha-D glucose with one sliver nanopartical	104

## List of Symbols

$\Psi$	wave function
$\hat{H}$	Hamiltonian operator.
$\hat{T}_N$	Kinetic energy operator of nuclei
$\hat{T}_e$	Kinetic energy operator of electrons
$\hat{V}_{NN}$	potential energy operators of nuclei
$\hat{V}_{ee}$	potential energy operators of electrons
$A$	Spin up of electron
$B$	Spin down of electron
$r_{ij}$	Distance between electron i and j
$\phi_{i\ spatial}$	spatial wave function
$N_n$	normalization constant,
$\zeta$	orbital exponent
GTOs	Gaussian-Type Orbitals
STOs	Slater-Type Orbitals
UHF	Unrestricted Hartree-Fock
RHF	Restricted Hartree –Fock
DFT	Density Functional Theory
HK	Hohenberg-Kohn
$E$	total energy
$\rho$	density
$V_{ext}$	external potential
KS	local potential
$V_{Coul}$	the Coulomb interaction potential
$V_{XC}$	xchange-correlation potential.
$E_{XC}$	exchange-correlation energy
LDA	Local Density Approximation
LSDA	Local Spin-Density Approximation
GGA	Generalized Gradient Approximation
B3LYP	Beckes three parameter hybrid functional with lee-yang Parr correlation functional
HOMO	Highest occupied molecular orbital
LUMO	Lowest unoccupied molecular orbital
MEP	Molecular Electrostatic Potential
$x_a$	constant of anharmonicity

IR	Infrared Spectroscopy
$g_k$	degeneracy factor
LINAC	linear accelerator
K	Kerma
CPE	charged particle equilibrium
$\epsilon_{tr}$	initial kinetic energy of secondary charged particle's
ME	Convert mass to energy or vice versa
$\psi$	Flounce
$\mu/\rho$	Mass energy transport coefficient
$\phi$	photon flux
X	Exposure
R	Roentgen
D	Dose
E	Energy
Gy	Gray
RBE	Relative Biological Effectiveness
Dx	Doses of X-rays with energy 250 kVp
Dr	Test radiation dose
I	Intensity
$\mu$	Linear attenuation coefficient
HVL	Half value layer $\mu$ m Mass attenuation coefficient
$N_A$	Avogadro's number
$\mu_e$	Electronic attenuation coefficient
$\mu_a$	Atomic attenuation coefficient
$\sigma$	microscopically cross-section
$\mu_{en}$	Linear energy absorption coefficient
$\mu_{en}/\rho$	Mass energy absorption coefficient
$\alpha$	Linear sensitivity
$\beta$	Quadratic sensitivity

$\alpha/\beta$	Real radio sensitivity to recover ability of a tissue
SER	Sensitivity enhancement ratio
DMF	Drug dose modification factor
ROS	Reactive oxygen species
$M_r$	Reduced mass
GIT	Enzymes of the gastrointestinal tract
GLUT	Enzymes Gamma glutamyl
ATP	Adenosine triphosphate,
ADP	Adenosine diphosphate,
Q	Coulomb unit
C	Coulomb
N	Mean number of ion pairs formed
$(K_{col})_{air}$	Collision kerma
$W_{air}$	Average energy expended in air
Z	Atomic number
A	Mass number
MeV	Mega electron volt
LET	Linear energy transfer
J	Joule
Kg	Kilogram

## **Abstract**

This research includes a theoretical study to enhance radiotherapy using nanoparticles as a radiation-sensitive agent. Different structures of the Alpha-D-glucose molecule ( $\alpha$ -D-glucose- $C_6H_{12}O_6$ ) were used after its adsorption on the silver nanoparticles surfaces  $C_6H_{12}O_6Ag_3$  and  $C_{12}H_{24}O_{12}Ag$ . The properties of these configurations were evaluated using density functional theory (DFT) with a hybrid B3LYP function (Becke, three-parameters, Lee-Yang-Parr) and with 6-311+G\* as a basis set for C, O, and H atoms. However, for silver (Ag) atoms the basis was LANL2DZ used.

The electronic properties and structure were studied by performing geometric optimization and obtaining the best configurations for the Alpha-D-glucose structures with silver nanoparticle's by obtaining the stability energies for  $C_6H_{12}O_6Ag_3$ ,  $C_{12}H_{24}O_{12}Ag$ , and  $C_6H_{12}O_6$ . Their values are - 687.140, - 1520.447, - 1124.712 respectively in Hartree units. The optimized structures were obtained by calculating the lengths of the bonds, bond angles and dihedral angles were also calculated, the electronic properties were studied, including the electronic energies, the distribution of electronic charges, and the energy gap for each compound, Vibrational modes were calculated for each compound.

On the other hand, FTIR spectra were analyzed and studied, where it was found that there is agreement between the theoretical and practical studies after studying the properties with stability of these molecules. They were used with high-energy photons resulting from linear accelerators or from radioactive sources.

The purpose of using these molecules is to increase the absorbed dose of radiation within infected cells in human organs (lungs). The goal of this reaction is to increase the cross-sectional area of interaction within the tumor by alpha-D glucose with silver nanoparticles in order to increase the absorbed dose within the tumor without damaging the healthy cells surrounding the tumor.



These molecules interacted with high energies of X-ray Radiation with a range of 2-15 MeV, the sensitivity to radiation (SER) is theoretically  $C_6H_{12}O_6Ag_3$  compound E=2Mev, E=4Mev, E=6MeV equal 13.86 while E=8 MeV, E=10 MeV equal 14.75, E=12 Mev equal 13.95, E=14 Mev equal 14.84. At the maximum energy value of 15 MeV, equal 15.64 while  $C_{12}H_{24}O_{12}Ag$ . E=2MeV equal 13.7, E=4MeV, E=6MeV, E=8MeV and E=10MeV equal 12.9, E=12MeV equal 12.5, E=14MeV equal 12.8. At the maximum energy value of 15 MeV, equal 12.9

These values of radiation sensitivity resulted in a reduction of the number of radiotherapy sessions by approximately half the duration of treatment time.

# **Chapter One**

## **Introduction**

## 1-1 Carbohydrates

Carbohydrates are food groups whose chemical composition is determined by a set of nutritional and physiological characteristics. The classification of carbohydrates depends on main factors, including the nature of the individual monomer, the degree of polymerization, and the type of bond (alpha or beta). according to what was agreed upon by the World Health Organization in 1997) [1].

Carbohydrates are divided into four main groups:

- 1- Monosaccharide (glucose).
- 2- Disaccharides.
- 3- Oligosaccharides.
- 4- Polysaccharides.

## 1-2 Monosaccharide (glucose)

D-glucose is the most prevalent carbohydrate and the most abundant organic component (when all of its mixed forms are taken into account ) [2]. Andreas Marggraf extracted glucose from raisins for the first time in 1747[2]. Jean Dumas invented the term glucose in 1838 [3], derived from the Greek word gleucos, which means 'sweet' or 'sugar[2]. D-glucose is polyalcohol as well as an aldehyde, and it is classified as an aldose, which is a sugar with an aldehyde group. The suffix -ose denotes a sugar group, whereas -ald denotes an aldehyde group [2]. Overall, the chemical formula of glucose is  $C_6H_{12}O_6$  and is the most prevalent monosaccharide [4]. It is classified as a hexose, a subtype of monosaccharides, because it contains six carbon atoms. One of the sixteen aldohexose stereoisomers is D-glucose, that is often known as dextrose and a common d-isomer found in nature[2]. In equilibrium, the glucose molecule can

exist in both open-chain (acyclic) and ring (cyclic) forms [5], as show in figure (1-1).

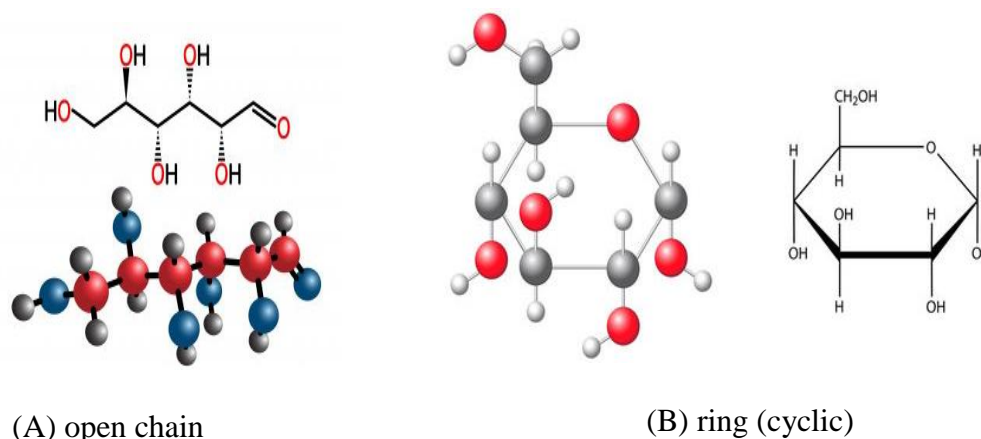


Figure 1-1: Different structures of glucose (A) open chain, (B) represent of ring [5].

As seen in the figure (1-2), there are two forms of glucose that have different cyclic structures depending on where the hydroxyl group is connected to the carbon atom: alpha- and beta-glucose [6].

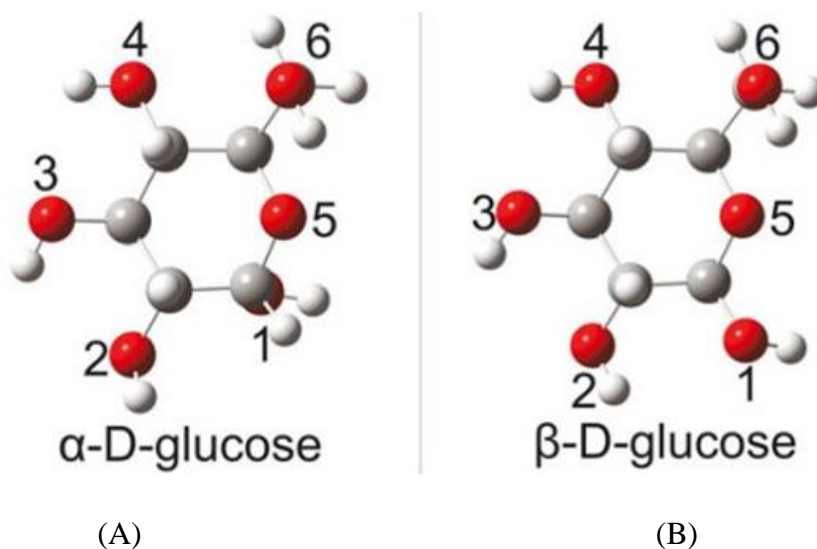


Figure1- 2: Different cyclic structures of glucose (A) alpha –D glucose, (B) bata –D glucose[ 6] .

At equilibrium, cyclic structure of glucose is the consequence of an intramolecular interaction between the aldehyde C atom and the C-5 hydroxyl group that results in the formation of an intramolecular hemiacetal. The cyclic form of glucose is sometimes known as glucopyranose because the ring comprises five carbon atoms and one oxygen atom, similar to the structure of

pyrin. Except for the fifth atom, which is connected to a sixth carbon atom outside the ring, each carbon in this ring is linked to a hydroxyl side group [2].

In biology, glucose is a common fuel. It provides energy to being from bacteria to humans via aerobic respiration, anaerobic respiration (in bacteria), or fermentation. Glucose is the primary source of energy in the human body, supplying around 3.75 kilocalories (16 kilojoules) of dietary energy per gram [7]. Glucose and oxygen provide nearly all of the energy for the brain [8]. As a result, its availability has an impact on psychological processes. When glucose levels are low, psychological functions that require mental effort (e.g., self-control, effortful decision-making) suffer [9-11]. The level of glucose in the brain, which is primarily dependent on glucose and oxygen for energy, is typically 4 to 6 mM (5 mM = 90 mg/dL). However, when fasting, it drops to 2 to 3 mM.[12]. Below-1 1 mM, confusion ensues, and at lower levels, coma occurs [12].

### 1 – 3 Physical and chemical properties of $\alpha$ -D glucose

Alpha-glucose's molecular structure, which features an alcohol ring with a linear aldehyde group, is crucial in highlighting the substance's physical and chemical characteristics. These forms, as indicated in table 1-1, are thought to be the efficient aggregates to exhibit the physical characteristics of  $\alpha$  -D glucose[2].

Table 1-1: Physical properties of the glucose [2].

<b>physical properties</b>	<b>Characteristics</b>
<b>Appearance</b>	White, crystalline
<b>Molecular weight</b>	180.16 g mol <sup>-1</sup>
<b>Melting point</b>	150 °C
<b>Density</b>	1.5620 g cm <sup>-3</sup>
<b>Solubility in;</b>	
<b>Water</b>	Very soluble
<b>Ethanol</b>	Slightly soluble
<b>Ethyl ether</b>	Insoluble
<b>Pyrimidine</b>	Soluble

However, because of its low molecular weight, the hydroxyl group that gives carbohydrates their overall chemical characteristics also governs the chemical processes. Hence, it is thought to have the biggest role in the occurrence of chemical reactions and characteristics [13, 14].

#### 1-4 Mechanism of absorption of glucose into the blood by human organs in the human body

The types of sugar compounds are glucose ( $C_6H_{12}O_6$ ), sucrose ( $C_{12}H_{22}O_{11}$ ) and fructose, levulose ( $C_6H_{12}O_6$ ). Glucose and fructose the same of formula but different molecular structure as shows in figure( 1-3)[15] . A kenotic simple sugar present in many plants, where it is frequently linked to glucose to produce the disaccharide sucrose. It is one of three dietary monosaccharides, along with glucose and galactose, which are absorbed directly into the blood of the portal vein by the gut after digestion. The liver subsequently transforms both fructose and galactose into glucose, making dissolved glucose, also known as blood sugar, the sole monosaccharide present in circulating blood [16] .

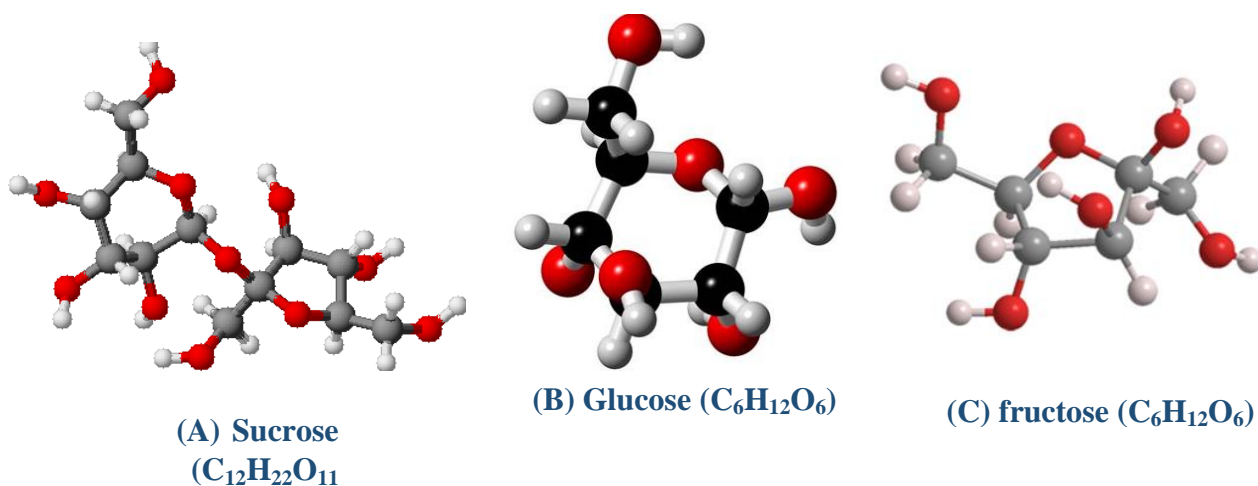


Figure1-3: Structures of as (A) sucrose, (B) glucose and (C) fructose with the number of their corresponding oxygen atoms (in red). Carbon and hydrogen atoms are showed in white and gray color, respectively[15].

Glucose is a significant macronutrient and a critical homeostatic element in the regulation of energy metabolism that is maintained in a limited range of 4.4 to 6.1 m mol/L, or roughly 1.0 g/L, in the fasting blood of healthy adults.

However, glucose is not the main component of mixed foods, and its main source in the diet is poly- and oligosaccharides, which are hydrolyzed to monomers by enzymes in the small intestine during luminal and membrane digestion [17]. Postprandial glucose concentrations in the GIT lumen can vary greatly depending on the food composition, location of the gastrointestinal tract (GIT), and time of day and can be many times higher than those in the blood. In humans, the quantity of gut luminal glucose was reported to be around 48 mmol/L in upper intestine samples obtained 2 hours after eating a meal [18]. This demonstrates that the stomach acts as both a barrier to glucose transit and a regulatory mechanism to keep blood glucose levels stable. Thus, glucose absorption, intake, and metabolism are all interrelated processes that determine blood glucose levels, as well as its accessibility to organs and tissues [19]. Glucose absorption is an important aspect of the homeostatic system that keeps blood glucose levels stable, and it may provide negative feedback to the brain's control of food intake [20]. The "glucostatic" hypothesis of appetite suggested by Jean Mayer in the 1950s was based on the relative changes or fluctuations of blood glucose levels as determined by simultaneous processes of glucose supply and consumption [19]. In both healthy and disease conditions pathological states, the physiological mechanisms required for nutrition intake and glucose metabolism [21]. Under normal physiological settings, glucose is the primary oxidizable substrate of the lungs [22]. The first step in glucose consumption by tissues is cellular absorption, which happens in most cells via carrier-mediated facilitated diffusion via GLUT family glucose transporters [23].

Cancer is characterized by increased glucose absorption. Therapeutic techniques for inhibiting tumor growth by interfering with glucose uptake and metabolism in cancer cells are being researched [24-26]. Otto Warburg's first observations that tumors used glucose anaerobically even in the presence of oxygen were consistent with increasing glucose need [27]. The conversion of glucose to

lactate produces just 2 moles of ATP per mole of glucose, whereas mitochondrial oxidative phosphorylation produces 30 moles of ATP per mole of glucose [28]. Warburg reasoned that mitochondrial malfunction was at the root of cellular transformation and that the transformed cell needed to enhance its glucose intake and fermentation to compensate for the inefficient respiration in order to meet the metabolic needs of the cell [27]. However, demonstrate that mitochondrial function is not decreased in cancer cells [29], and is essential for neoplastic transformation [30]. The reduced mitochondrial activity observed by Warburg in cancer cells could have been caused by the Crabtree effect, which states that high rates of glucose uptake and glycolysis in cancer cells which can inhibit mitochondrial respiration, most likely due to competition for ADP and inorganic phosphate between glycolysis and oxidative phosphorylation [31].

The topic of why cancer cells need to boost their glucose absorption and glycolytic metabolism even in the presence of oxygen remains unanswered. Although no definite explanation has been offered, multiple lines of evidence have shown that glycolysis is preferred to mitochondrial respiration in rapidly proliferating tissues, during neoplastic transformation, and in normal physiological activities [32, 33]. Increased glucose uptake and decreased mitochondrial utilization of glucose in rapidly proliferating tissues provides a quick source of energy via ATP.

## **1 – 5 Application Nanotechnology in Medical Field**

Particulate dispersions or solid particles with a size range of 1–100 nm in size are referred to as nanoparticles [34] . The use of smaller materials in nanotechnology enables the manipulation of molecules and substances at the nanoscale level, which might improve material's mechanical qualities or provide access to bodily parts that are not easily accessible by physical means [35, 36] Nanomaterials, particularly silver nanoparticles, are employed in a variety of applications, including anti-cancer [37]. Nanoparticles have played an important



role in the advancement of radiation therapy by acting as both a therapeutic agent and a carrier for other medicines [38].

## **1 – 6 Silver nanoparticles in treatment**

The chemical element silver (Ag) has an atomic number of 47 and its atomic weight is 107.87 g/mole. Its density is 10.49 g/cm<sup>3</sup> (25°C), while its melting and boiling points are 961.78 and 2162 °C, respectively [39]. Because of their stability in the majority of interactions, silver nano atoms have found application in the medical and therapeutic domains, including radiotherapy.

These atoms are distinguished by having radiation sensitivity similar to that of Nano atoms of gold [40]. Owing to their high atomic number, silver nano atoms exhibit significant physical and chemical characteristics[39]. It has been used as an antibacterial in many diseases due to the stability of the reaction [37]. AgNPs have been extensively researched for their antimicrobial and anticancer effects. Research has demonstrated that AgNPs possess broad-spectrum antibacterial capabilities against a variety of pathogens, such as viruses, fungi, and bacteria. AgNPs have strong antibacterial action, the precise processes are still unclear. AgNPs' antibacterial mechanisms have been explained by a variety of theories, such as [41].

- i) Breaking down the bacterial membrane and leaking cell contents.
- ii) Producing reactive oxygen species (ROS) and inhibiting respiratory chain.
- iii) Breaking down the DNA structure and preventing DNA replication; and IV deactivating enzymes and denaturing proteins as show in the Figure 1-4.

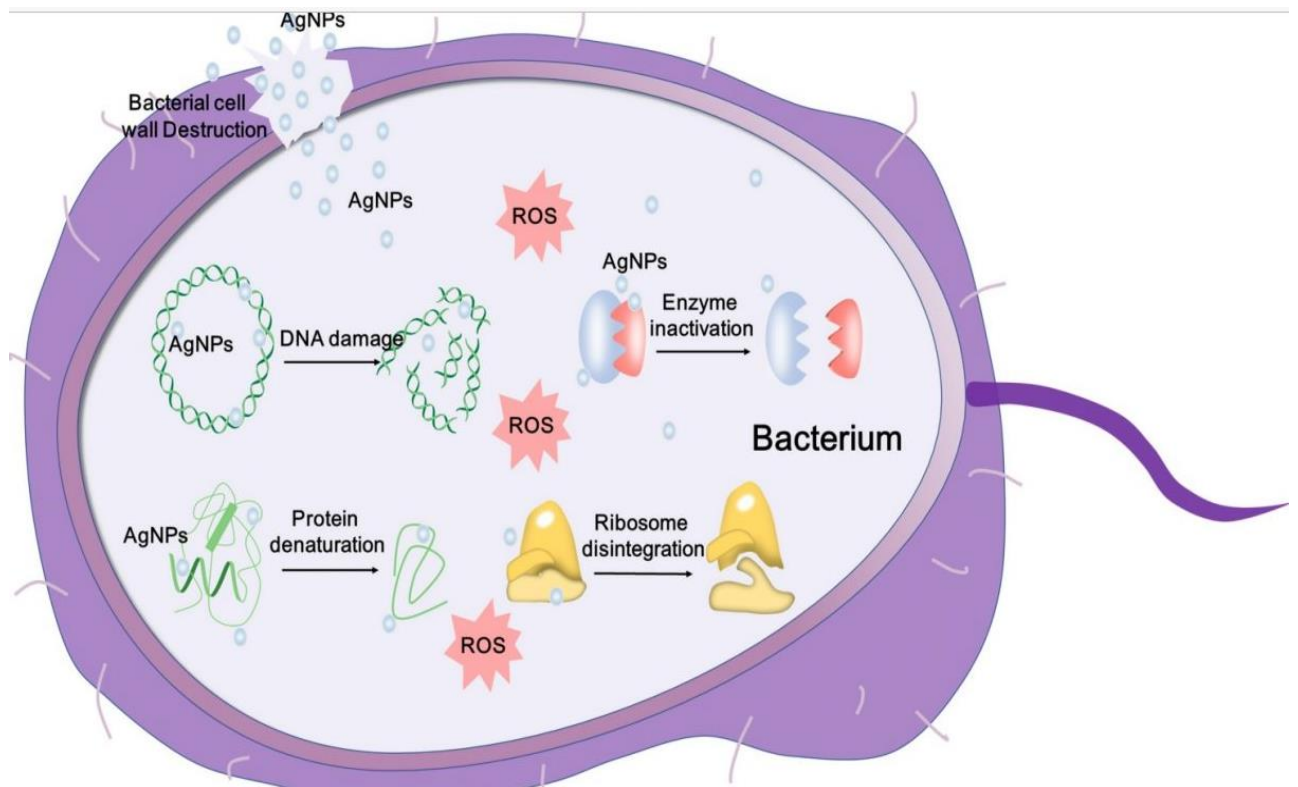


Figure1-4: Mechanisms of AgNPs' antibacterial effect against bacteria, showing the ROS-dependent route, DNA damage, protein denaturation, and enzyme inactivation [41].

AgNPs have the ability to directly interact with DNA to cause DNA mutations or to produce ROS, which can upset DNA structure [42, 43]. Elevated reactive oxygen species (ROS) have the ability to cause damage to the double helix of DNA in a concentration-dependent manner. This damage can include breaking single or double-stranded DNA and altering base modifications and DNA cross-links [42, 44] as show in the figure1-5.

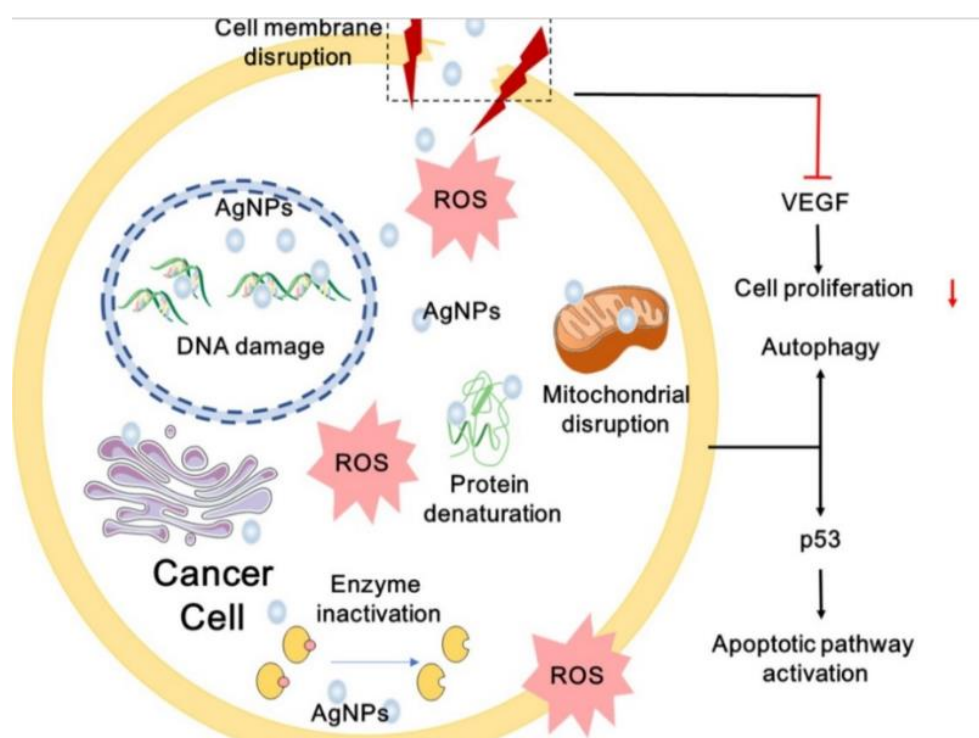


Figure1-5: AgNPs' anticancer mechanisms. AgNPs have the ability to break DNA, produce ROS and ruin the ultrastructure of cancer cells [42].

## 1-7 Radiotherapy (RT)

Radiotherapy (RT), often known as radiation therapy, is a therapeutic approach that uses high-energy rays or radioactive element to destroy tumor cells and stop their growth and proliferation. For more than a century, RT has been a successful method for treating cancer, either alone or in combination with other therapies [45]. It is still a key therapeutic method for the treatment of several types of cancer today. It is predicted that around two-thirds of all cancer patients will undergo RT as a stand-alone treatment or as part of a more sophisticated therapeutic program [46]. Prior to the development of ionizing particle beams, medicine had limited choices for treating both malignant disorders. The picture quickly altered once Wilhelm Conrad Rontgen discovered X-rays in 1895 [47]. Emil Herman Grubbe employed X-rays to treat a patient with breast cancer one year after their discovery [48]. There have been discoveries of new radioactive isotopes, ray types, and radiation techniques.

Scientists began to get a better understanding of the nature of radiations, their modes of action, and the link between radiation duration and dose on cell survival. Nonetheless, it wasn't until the 1920 that doctors realized that administering a complete radiation dosage in fractionated doses was superior than a single therapy session in terms of cancer management and fewer adverse effects [49].

The experiments done over the next three decades (Megavoltage period) were also focused on the creation of more creative radio-therapeutic devices capable of treating tumours in the deep tissues. During this time, Cobalt 60 therapy was introduced, which produced high-energy  $\gamma$ -rays [50] and of more potent electron linear accelerators (also known as electron linacs [51], capable of delivering megavoltage X-rays. The new devices could give a larger dose of energy than the old ones, allowing for the treatment of deeper tumors with higher skin saving. Because of the challenges in regulating these sources and the potential of causing excessive radiation in the tissue around cancer, unique multi-field irradiation strategies were developed [52].

## 1-8 Types of radiations useful in RT

Radiotherapy is based on the use of two kinds of radiation:

- A. **Non-ionizing radiation** (radiation that cannot ionize materials)
- B. **Ionizing radiation** (has the ability to ionize materials).

There are two types of ionizing radiation;

1. Radiation that directly ionizes (charged particles). Heavy ions, electrons, protons, alpha particles.
2. Radiation that ionizes indirectly (neutral particles). Neutrons, photons (x-rays, gamma rays).

Radiation can be administered both **externally** and **internally**. **In the first** modality, the beam of radiation is supplied by an external radiation source; **in the second**, a radioactive source is internally inside the lesions that must be

treated. In general, the therapy that must be employed is determined by its location, size, and complexity.

### **1-9 Medical Linear Accelerator LINAC in X-Ray mode**

Linear accelerator is based on the idea that the electric field accelerates electric charges. A linear accelerator is made up of a long row of hollow metal cylinders, one end of which is connected to a source of charged particles to be accelerated and the other end is connected to the target. The lengths of the metal cylinders vary. Connecting odd number cylinders (first, third, fifth, etc.) to one polar generating vibrations device (oscillator) and connecting even number cylinders (second, fourth, and sixth, etc.) to the other end of the oscillator. The timing of polar transition must match with the acceleration of particles exiting each cylinder. As a result, it must increase the length of each cylinder in proportion to the increase in speed.

Proceed particles must to be accelerated in all cylinders at the same rate. As the number of utilized cylinders increases, so does the speed of the accelerated particles [53]. A high intensity of X-ray beam is thought to be effective for deep tumor therapy. Compton scattering is the primary interaction between high energy X-rays and tumors. Linear accelerators may generate high-energy X-rays. A linear accelerator is a medical device that converts electrons to photons with kinetic energy ranging from 4 MeV to 25 MeV. The kinetic energy of the accelerated electron varies with the length of the cylinders, ranging from 30 cm at 4 MeV to 150 cm at 25 MeV [54]. Electrons are accelerated by straight-line cylinders. A series of linked cylinders that are all empty of air., as seen in figure1-6 [55].

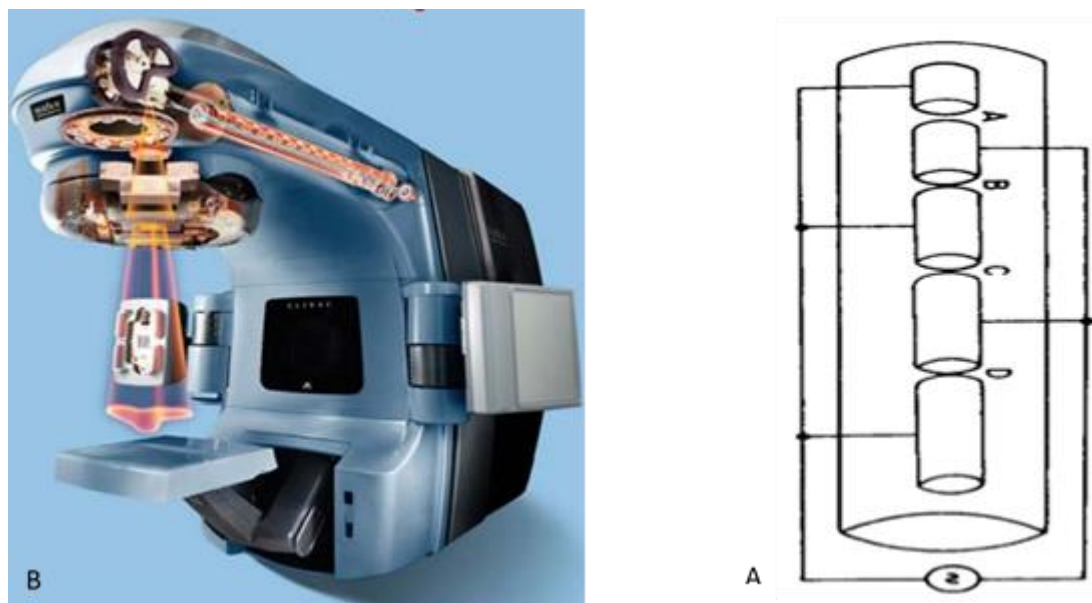


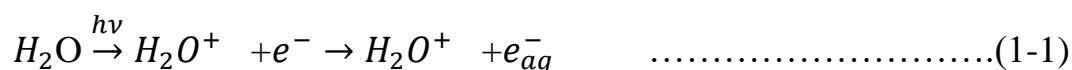
Figure1-6: (A) The linear accelerator with drift tubes, (B) exterior LINAC in X-Ray Mode [55].

### 1-10 Radiotherapy Action Mechanisms

In indirect action, the radiation reacts with other molecules and atoms (mostly water, as around 80% of a cell is made up of water) within the cell to form free radicals, which can then damage the important target within the cell via diffusion. Chemical sensitizers can modify indirect action. The following are the steps involved in creating biological harm by the indirect impact of x rays [56]:

- 1- Primary photon interaction (photoelectric effect, Compton Effect, pair formation) results in a high energy electron or positron.
- 2- When a high-energy light-charged particle moves through tissue, it generates free radicals in the surrounding water.
- 3- Free radicals can cause chemical alterations in DNA by breaking chemical links.
- 4- Biological impacts are caused by changes in chemical bonding.

The following radiochemical processes help explain the stages involved in destroying cancer [56].





The highly reactive species created in water by radiochemical reactions include  $e_{aq}^-$ ,  $OH^\cdot$  and  $H^\cdot$ . By interacting with and destroying the molecules in cells, these reactive species cause indirect radiation harm to biological systems. Because they have an unpaired valence electron, free radicals like  $H_2O^+$  (water ion) and  $OH^\cdot$  (hydroxyl radical) that break chemical bonds and create chemical changes that cause cellular harm are extremely reactive molecules[56].

### 1-11 Previous studies

(LU X iong et al , 2015) Glucose molecules were used as a reducing agent during the synthesis of copper nanoparticles. They came to the conclusion based on density functional theory that the antibacterial activity of nanoparticles may be due to the variation in their free surface energy [57].

(Yao Hao et al , 2015) used cryolatin, silatin, and gold nanoparticles with high atomic numbers, using spectra with high energy potentials. They studied analytical methods for calculating the dose of radiation enhancement in the lung. They concluded that gold nanoparticles are more radiation enhancing than cryolatin and silatin nanoparticles [58].

(Salim M. Khalil et at , 2016) investigated the role of carbohydrates as aluminum inhibitors utilizing density functional theory and full geometric form optimization in the presence of the B3LYP / 6-31G(d , p) function. They discovered that sucrose corrodes metal the least effectively and glucose corrodes aluminum the most effectively [59].

(Zio Ouyang et at ,2016) examined the use of titanium dioxide nanoparticles in the presence of Shiro-Penkov radiation. They calculated the total radiation

inside a 2 cm diameter lung tumor exposed to radiation 6 MeV for 14 days using radiation transfer modeling, and they discovered a discernible increase in the death of cancer cells [60].

(Alejandro J . Ganzalez Fa et at , 2017) used to confirm the production of silver particles using honey with a pH of 5–10. By using absorption spectroscopy to measure the plasmon resonance at 411 nm, the kinetic variables of the compositions were examined at room temperature. They discovered that glucose works well as an agent to reduce silver [61].

(S.N. Sunil Gowda et at , 2018) investigated the production of silver nanoparticles utilizing the antioxidant folic acid. It functions to lessen and stabilize silver nanoparticles. An X-ray was applied to the A549 cells within the lung tumor at 8 MeV. Through analysis of the cells' proteins and genetic makeup following irradiation, they discovered that the nanoparticles stopped cancer cells from the risk of developing a new malignant tumor [62].

(R. E. Ambrusi et at , 2019) used time-dependent density functional theory to assess the adsorption energies on the silver surface with alpha-glucose and gluconate-ion molecules. By examining the features of the UV absorption spectra and analyzing the observed charge on the surface of carbon dots, they were able to identify the active groups COOH- and COO- that excite them on silver [63].

(Masoumeh Zangeneh et at , 2019) investigated the augmentation of the radiation dosage of zinc oxide nanoparticles doped with high-atomic-number gadolinium under 6 MeV high-energy X-ray irradiation. Through the use of combined plasma mass spectrometry and TEM, the cellular uptake of cells was assessed. It was established how lethal MTT nanoparticles were. A survival assay was used to calculate the radiation enhancement dosage, and it was



discovered that the value of the dose increased as the quantity of nanoparticles increased [64].

(Jeison Manuel Arroyave et al., 2020) investigated the hybrid nanoparticles' theoretical and experimental outcomes to verify the interaction between C-dot and AgNPs. The theory behind the practical results involved the calculation of the negative charge energies on the AgNPs surface and the analysis of the active aggregates in the COO- and OH-infrared spectra using density functional theory [65].

(Jinghua Han et al., 2022) investigated the use of ALA-5-coated polyaspartamide-DOX nanoparticles as a radiosensitizing agent to target lung cancer when exposed to high-energy X-ray radiation. Because radiation sensitivity has harmful side effects, researchers discovered that acid-coated nanoparticles effectively destroy cancer cells. They came to the conclusion that this combination suppressed tumors without endangering healthy tissues [66].

(G. Venkatesh et al., 2022) studied the geometric characteristics and physical-chemical absorption of the molecule 2-Deoxy-Dglucose with groups of transition elements (gold, silver, and copper) using density functional theory. The basis sets for B3LYP-LAN2DZ were used to test them. In addition to the findings of molecular dynamics simulations, they discovered that the combination may have anti-cancer capabilities and that the chemical qualities rely on the mass size [67].

(Ivana Vukoje et al., 2022) synthesized hydrocolloids of silver nanoparticles, ranging in size from 15 to 30 nanometers, by stabilizing and reducing glucose, sucrose, and dextran. They used DFT to investigate this preparation's characteristics to ascertain the adsorption energies and molecular charges. The improved adsorption energies by silver were discovered to be much greater [68].

(Roshni Iyer et al., 2022) used the creation of dual catalyst nanoparticles, or E-DSNPs, containing the radiation-sensitizing compound NU7441. The membrane known as ephrin A2/EphA2 on the surface of lung cancer cells is the target tissue. They discovered that there was a significant radiosensitivity absorption by the cancer cells in the membrane, along with a 0.019 and 0.19 reduction in cell survival, respectively [69].

(Yao Chen et al., 2023) investigated the effects of radiosensitization on tumor-bearing animals with lung cancer using albumin and gold nanoparticles (Alp-GNPs). Outstanding radiosensitization was discovered, with a SER of 1.432 much greater than that of X-ray radiation alone. Significant radiosensitization and anti-tumor activities were demonstrated by this combination [70].

(Hamed Nosrati et al., 2023) used X-ray radiation and high atomic number nanoparticles to target breast cancer in mice. Gd<sub>2</sub>O<sub>3</sub>@BSA-Aunps. A battery of laboratory tests was used to assess the radiosensitizing ability. When administered in vivo, they discovered that it improves tumor suppression and is thought to be a better cancer treatment when combined with high-energy X-rays and nanomaterials [71].

(Weishu Ni et al., 2023) A functional density was used to demonstrate the uneven glucose-nanoparticle bonding. According to their findings, heterogeneous cross-linking dramatically lowers the energy barrier, which helps to explain why chemotherapy works better and speeds up the enzymatic reaction of glucose. This method is thought to be efficient anti-tumor and anti-cancer procedure [72].

## **1-12 The Aim of the Work**

Studying the effect of nano-molecules (AgNPs) as radiosensitive agent on the radiotherapy Promotion theoretically and this is by the following steps;

- 1- Building the molecule glucose; DFT method will be involved as the theory investigation to in order to find their most stable configurations, study the structural and electronic properties of glucose structure with AgNPs.
- 2- Calculate the radiation dose for tumor lung that will be used with aid of nanomolecules and without nano-molecules.
- 3- Increase sensitivity enhancement ratio (SER), SER is a ratio of the number of surviving cells by the presence of nanoparticles added to glucose to the number of cells without nanoparticles at the same dose.
- 4- Incorporating new radiation tables to treat lung cancer using high energies and nanocomposites that differ from the prevailing traditional tables.

# **Chapter Two**

## **Theoretical Part**

## 2-1 Introduction

This chapter includes the theoretical investigation of our work and is divided into two parts, the first provides a comprehensive overview of molecular modeling approaches (computational techniques) for describing big, medium, and tiny systems with a focus on the DFT method. The programs and basis set types are described. The theoretical underpinning for the electronic properties obtained in this research is then discussed, and an overview of the vibrational properties of the molecular structures employed in this investigation. The second part involves theoretically enhancing radiotherapy for lung cancer patients by using molecule nanoparticles and employing them in special mathematical equations and foundations that will be explained in detail in this chapter.

### The first part

## 2-2 Approximation of the Schrödinger Equation

Bohr proposed quantum assumptions to describe the hydrogen atom in 1913, while De Broglie introduced the wave-particle concept for moving particles like electrons in 1924. Schrödinger integrated these concepts to create a novel description of electrons.

Schrödinger equation in general can be written as [73] :

$$\hat{H}\Psi = E\Psi \quad \dots\dots\dots (2-1)$$

$\Psi$ : eigenfunction, which is the name given to the wave function,  $E$ : is the Hamiltonian's eigenvalue, and  $\hat{H}$ : is the Hamiltonian operator.

The non-relativistic Hamiltonian for a system composed of  $n$  electrons and  $N$  nuclei is given by (all equations are represented in atomic units, where  $m = e = \hbar = 1$  [74]).

$$\hat{H} = -\frac{1}{2} \sum_A^N \nabla_A^2 - \frac{1}{2} \sum_i^n \nabla_i^2 - \sum_i^n \sum_A^N \frac{Z_A}{r_{Ai}} + \sum_{A>B}^N \frac{Z_A Z_B}{R_{AB}} + \sum_{i<j}^n \frac{1}{r_{ij}} \dots\dots\dots(2-2)$$

In its simplest form, the Schrödinger equation is:

$$\hat{H}(\vec{r}, \vec{R}) = \hat{T}_N(\vec{R}) + \hat{T}_e(\vec{r}) + \hat{V}_{eN}(\vec{r}, \vec{R}) + \hat{V}_{NN}(\vec{R}) + \hat{V}_{ee}(\vec{r}) \dots\dots\dots(2-3)$$

where  $\hat{T}_N(\vec{R})$  and  $\hat{T}_e(\vec{r})$  are the kinetic energy operator of nuclei and electrons, respectively,  $\hat{V}_{eN}(\vec{r}, \vec{R})$ ,  $\hat{V}_{NN}$ ,  $\hat{V}_{ee}(\vec{r})$  are both the actual and potential energy operators of nuclei and electrons.  $(\vec{R})$  is a set of nuclear coordinates,  $(\vec{r})$  is the set of electron coordinates. The coordinates of electron  $i$  are represented by,  $r_{Ai}$  and the coordinates of nuclei  $A$  are represented. The kinetic energy of the nuclei is represented [74]

$$\hat{T}_N(\vec{R}) = -\sum_A^N \frac{1}{2M_A} \nabla_A^2 \dots\dots\dots(2-4)$$

The kinetic energy of the  $n$  electron is given below:

$$\hat{T}_e(\vec{r}) = -\sum_i^n \frac{1}{2M_e} \nabla_i^2 \dots\dots\dots(2-5)$$

Where  $M_A$  : represents the nucleus' mass,  $M_e$  : represents the electron's mass., Potential energy consists of the following elements:

$$\hat{V}_{eN}(\vec{r}, \vec{R}) = -\sum_A^N \sum_i^n \frac{Z_A}{r_{Ai}} \dots\dots\dots(2-6)$$

$$\hat{V}_{ee}(\vec{r}) = \sum_{i<j}^n \frac{1}{r_{ij}} \dots\dots\dots(2-7)$$

$$\hat{V}_{NN} = \sum_{A<B}^N \frac{Z_A Z_B}{R_{AB}} \dots\dots\dots(2-8)$$

where  $Z_A$  and  $Z_B$  are the charges of nuclei  $A$  and  $B$ , respectively.  $r_{Ai}$  : is the separation between nuclei  $A$  and electron  $i$ ,  $r_{ij}$  : is the separation amid electron  $i$  and electron  $j$ .  $R_{AB}$  : is the separation between nuclei  $A$  and nuclei  $B$ .

$\nabla_i^2$  : is the electron  $i$  Laplacian operator and  $\nabla_A^2$  : is the nuclei  $A$  Laplacian operator[74, 75].

### 2-3 Born-Oppenheimer Approximation

Known as the Born-Oppenheimer approximation, this first major step in quantum mechanics toward simplifying the general molecular issue. This approximation is based on the fact that nuclear masses are substantially bigger than electron masses, hence nuclei move much more slowly, and nuclei are essentially immobile in comparison to electron motion [76]. Because the nuclear to electron mass ratio is at least 1/1836, electrons move far faster than nuclei. Because  $T_N$  is less than  $T_e$ , the kinetic energy of nuclei  $T_N$  can be ignored.  $T_N$  is ignored because  $V_{NN}$  is assumed to be constant[77]. As a result, equations (2-3) can be reduced to:

$$\widehat{H}(\vec{r}, \vec{R}) = \widehat{T}_e(\vec{r}) + V_{eN}(\vec{r}, \vec{R}) + V_{ee}(\vec{r}) \dots\dots\dots(2-9)$$

Because electrons may respond essentially and instantaneously to changes in the relative locations of the nuclei, the molecular wave function can be divided into two components, one for nuclear variables and the other for electron variables[78]. Using the Born-Oppenheimer approximation and ignoring relativity, the Hamiltonian is obtained as the following:

$$\widehat{H} = -\frac{1}{2} \sum_i^n \nabla_i^2 - \sum_i^n \sum_A^N \frac{Z_A}{r_{ij}} + \sum_{i<j}^n \frac{1}{r_{ij}} \dots\dots\dots(2-10)$$

Following that, the Hamiltonian equation will be employed to solve the Schrödinger equation.

The representation of a whole molecular wave function can be expressed as a product of an electronic and a nuclear portion using the Born-Oppenheimer approximation[79].

$$\Psi(r, R) = \Psi_e(r, R) \Psi_N(R) \dots\dots\dots(2-11)$$

Where  $\Psi_e$  and  $\Psi_N$  able to calculated by passing through two separately Schrödinger equations.

## 2-4 Hartree–Fock Approximation

The Hartree-Fock hypothesis [80, 81] ranks among the most fundamental wave function notions. The fundamental approximation is the central field estimate, indicating that the potential for electron repulsion potential is calculated making use of the total electron integral. Therefore, there is net electron and electron repulsion. but the impact of their electrons together are ignored. In the same year as the Hartree technique, Fermi and Thomas devised a computerized representation for estimating the energy of atoms by roughly estimating how electrons are distributed within an atom during 1927 [82]. Hartree presented his solution to the Schrödinger equation and his hypothesized which the total wave function of an electron system could be described as a composite of single electron functions  $\Psi_1, \Psi_2, \dots, \Psi_n$ .

$$\Psi(1,2,3, \dots, n) = \Psi_1(1) \Psi_2(2) \Psi_3(3) \dots \Psi_n(n) \dots \dots \dots (2-12)$$

The orbital the sum of every single electrons functional  $\Psi(1,2,3, \dots, n)$ . Prior to date, via Pauli Exclusion Rule did refuse to take electron spin entering consideration[83].

It is impossible for both electrons to have an identical quantum number. On the other hand, an orbital may house a up to a double electron maximal, Moreover, that electron rotations are connected. As the position exchange involving two electrons need to be asymmetrical. We obtain, the whole wave function of many-electron systems can be expressed using a Slater determinant.

Fock used a Slater determinant to substitute Hartree's full function of waves  $\Psi(1,2,3, \dots, n)$ . As the result, within the approximate Hartree-Fock, the wave function additionally have written is what is referred to as the Slater determinants. In this determinant, electron spin obeys Pauli's exclusion principle. Electrons can have different values  $(+\frac{1}{2})$  and  $(-\frac{1}{2})$  for spinning up (A) and spinning down (B). The wave function of an N-electronic system can be expressed using the Slater determinant as [84].



$$\Psi(r_1, r_2, \dots, r_N) = \frac{1}{\sqrt{N!}} \begin{vmatrix} \Psi_1 r_1 & \Psi_2 r_1 & \dots & \Psi_N r_1 \\ \Psi_1 r_2 & \Psi_2 r_2 & \dots & \Psi_N r_2 \\ \dots & \dots & \dots & \dots \\ \Psi_1 r_N & \Psi_2 r_N & \dots & \Psi_N r_N \end{vmatrix} \dots\dots\dots(2-13)$$

$\Psi$  : is the electronic spin-orbit wave function.  $\frac{1}{\sqrt{N!}}$  : is the normalization factor .

This method can be used to solve the Schrödinger formula for a quantum system including n nuclei and n electrons. Hartree Fock methods are classified into two types [85].

**2-4-1 Restricted Hartree –Fock (RHF) Method**

In order to account for the Pauli principle, electron spin must be included in wave functions. The orbitals generated by the Hartree-Fock technique are actually spin orbitals that are the product of a spatial wave function and a spin function[85].

$$\phi_i = \phi_{i \text{ spatial}}(x,y,z) A \quad \text{or} \quad \phi_i = \phi_{i \text{ spatial}}(x,y,z) B \quad \dots\dots\dots(2-14)$$

In the spin orbital  $\phi_{i \text{ spatial}}(x,y,z)$  : is the spatial wave function that describes the likelihood of detecting an electron in space, and A or B are spin wave functions. During the solution of the self-consistent field (SCF) equations for a closed shell system with all electrons coupled. The solution can be restricted so that the spatial wave functions for paired electrons are the same. This is known as a restricted Hartree-Fock calculation (RHF), and it is typically employed for systems in which all electrons are coupled figure(2- 1) shows this[86].

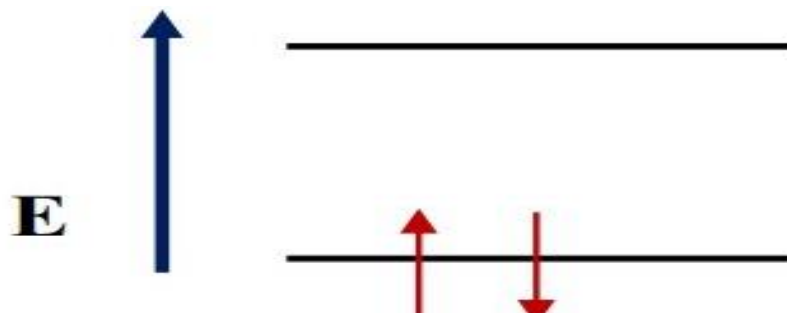


Figure 2-1: Diagram of orbital energy levels for closed - shell systems [86].

### 2-4-2 Unrestricted Hartree-Fock (UHF) Method

The assumption made in the restricted Hartree-Fock approach does not work for open shell systems with unpaired electrons. Additionally, there are various methods to this type of problem [85]. The unrestricted Hartree-Fock method (UHF) is one approach that require pairs of electrons to occupy the same spatial orbital. This approach employs twin spatial orbital groups: one has spin upward (*A*) electrons the another has downward spins (*B*) electrons. As seen in figure (2-2), this results in two sets of orbitals.

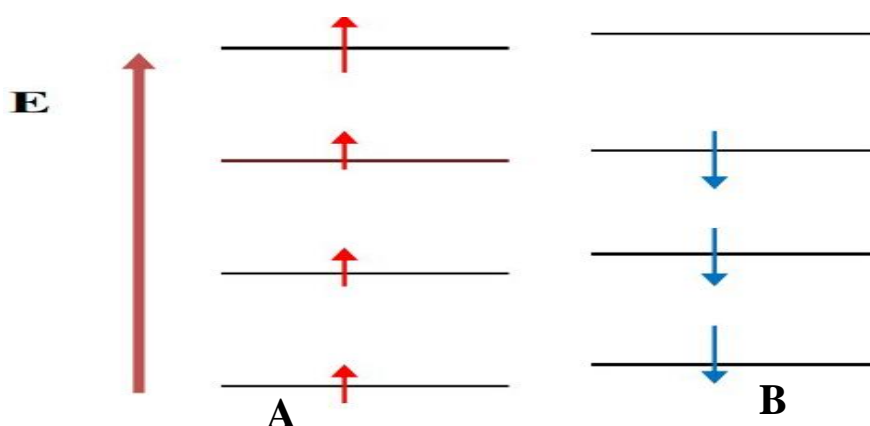


Figure: 2-2 Diagram of orbital energy levels for open - shell systems [85].

### 2-5 The Roothaan – Hall Equations and the Linear Combination of Atomic Orbitals (LCAO)

The formulae for Roothaan-Hall include constructed from HF equation using a linear combination of orbitals of atoms (LCAOs) and the notion of variation. In theory, Hartree Fock problem can be solved using any traditional technique for solving integro-differential equations. HF formulas solution with reaching HF limitation means typical for atoms with can as achieved numerically combination For large molecules, But solutions that are getting close to the HF limitation cannot be practical. In reality, the HF technique yields a intricate group of nearly unsolvable integrodifferential problems that are solvable using ease for just one variable. In a non-orthogonal basis set, the Hartree-Fock

formula is expressed by the Roothaan formulas that can maybe Slater-type or Gaussian [87].

### 2-5-1 Slater-Type Orbitals (STOs)

The molecular wave function is known to be given by the LCAO approximation.

These wave functions are given in spherical polar coordinates.[88].

$$\phi_{nlm}^{STO}(r, \theta, \phi) = R_{nl}(r) Y_{lm}(\theta, \phi) \dots\dots\dots(2-15)$$

at which m, l, and n refer to the fundamental, orbital angular momentum, with magnetic quantum numbers, correspondingly.  $Y_{lm}(\theta, \phi)$  : is a globular harmonics.  $R_{nl}(r)$ : The atomic functions of the radial element,  $R_{nl}(r)$  in the knowledge that (STOs) can written in following way:

$$R_{nl}(r) = N_n r^{n-1} \exp(-\zeta r) \dots\dots\dots(2-16)$$

$$Y_{lm}(\theta, \phi) = \theta_l(\theta) \phi_m(\phi) \dots\dots\dots(2-17)$$

$N_n$  : represents the normalization constant,  $\zeta$ : is the orbital exponent, and these functions are generated by a potential.

$$\zeta = \frac{z-s}{n^*} \dots\dots\dots(2-18)$$

The atomic number is z, while the shielding parameter is s and  $n^*$  indicates the effective main quantum number. Based on n and l, the shielding parameter s, is given an empirical value [89]. Slater-type orbitals (STOs) are functions of Eq. (2-15). The value of  $\zeta$  is determined for each STO for a particular element by minimizing the atomic energy with regard to  $\zeta$ . These values apply to every atom of that element, regardless of molecular context. The STO foundation is simple because it mimics the exact solution for a single electron atom. Carbon's precise orbitals, for example, are not hydrogenic orbitals, but are similar to them. Unfortunately, many of the integrals that must be evaluated to generate

the Fock matrix can only be solved using an infinite series with STOs. The truncation of an infinite series produces errors that can be big mistakes.

### 2-5-2 Gaussian-Type Orbitals (GTOs)

The orbitals of Gaussian include widely employed within molecules and atoms simulations today. The readily built functions that are polycentric are the most useful variety among these roles. Because they lack a cusp at the origin, they are less suitable as representations of atomic orbitals than STO. Though the values of their exponents are different, (GTOs) and (STOs) share the same overall form [90].

$$\Phi_{nlm}^{GTO}(r, \theta, \phi) = R_{nl}(r) Y_{lm}(\theta, \phi) \dots\dots\dots (2-19)$$

$$R_{nl}(r) = N_n r^{n-1} \exp(-\zeta r^2) \dots\dots\dots (2-20)$$

In GTO, the radial type is relies by  $\exp(-\zeta r^2)$  rather than  $\exp(-\zeta r)$ . Understanding integrals of electron-electron repulsion can be calculated analytically presently, while STOs is confined to numerical techniques. As fundamental problem from GTOs as exponent falls to zero very quickly as  $r$  increases, and there is no correct "cusp" in the center, shown in the illustration (2-3)[91].

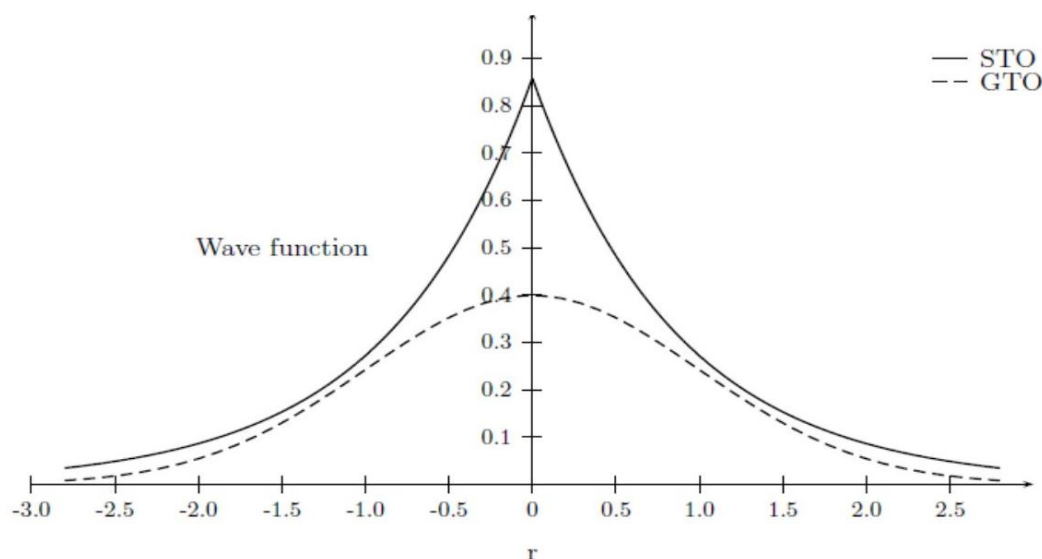


Figure 2-3: An analysis of STO and GTO function forms compared [91].

## 2-6 Density Functional Theory (DFT)

The density functional theory (DFT) is one of the most powerful theories, providing greater precision to Hartree-Fock theory, Ab-initio, and semi-empirical techniques. DFT can be applied to atoms, molecules with heavy atoms, and solids, as well as nuclei, quantum and classical fluids [92, 93]. It describes a system's ground state characteristics, and the electronic density is critical. Density functional theory predicts a wide range of molecular properties, including molecular structure, atomization energies, vibrational frequencies, electrical and magnetic properties, and ionization energies, among others. The advantage of employing the electron density over the wave function is the significantly lower dimensionality. DFT may now be applied to considerably bigger systems, with hundreds or even thousands of atoms. Furthermore, DFT is computationally straightforward. DFT has been a popular approach in first-principles calculations aiming at explaining or even forecasting the behavior of molecular and condensed matter systems [94, 95].

A functional is a function that is defined by another function; for example, a density functional is used to calculate the energy for the electron density. Thus, a wave function and an electron density are functions, whereas energy based on a wave function or an electron density is a functional [96]. The first publications on density functional theory were written with Pierre Hohenberg (Hohenberg and Kohn, 1964) [97] and Lu J. Sham (Kohn and Sham, 1965) [98].

### 2-6-1 The Hohenberg-Kohn Theorem (HK)

Theorems stated by Hohenberg and Kohn in 1964 form the formal foundations of DFT [97]. The two Hohenberg-Kohn theorems (HK) established DFT's theoretical foundation. The initial HK theorems only applied to non-degenerate ground states in the absence of a magnetic field, but they have now been

expanded to include these [99] . The theory is made up of two theorems that Hohenberg and Kohn stated and proved:

- **1st HK Theorem:** The first HK theorem shows that A density of electrons that depends about only three positions in space uniquely determines characteristics of a many-electron structure in the state of ground. It lays the framework to lower the many-body problem from  $3N$  coordinates in space of  $N$  electrons to 3 spatial coordinates using the functional the density of electrons [100] . In addition to an additive constant, an understanding of the ground-state density of electrons  $\rho_0(\mathbf{r})$  essentially defines the potential from the outside  $V_{\text{ext}}(\mathbf{r})$  for each system that includes interacting particles in an external potential  $V_{\text{ex}}(\mathbf{r})$ .
- **2nd HK Theorem:** The concept of the density could indicate utilized of describe the widely applicable  $F[\rho]$  regarding energy in general  $E[\rho]$ . The global lowest level associated with this functional energy is the precise ground case energies. . On the other side, the system's ground case energy is provided by the functional  $F[\rho]$ . The lowest amount of energy would be produced by the functional  $F[\rho]$  if both the entry and ground-state density were equal.. As a result, of function might be lowered by adjusting the density to obtain the energy in the ground indicates given the external potential [101].

A final hypothesis can to demonstrate toward considering the calculation for the structure's total energy (E) using densities ( $\rho$ ):

$$E(\rho) = F(\rho) + \int V_{\text{ext}}(\vec{r}) \rho(\vec{r}) d(\vec{r}) \dots\dots\dots(2-21)$$

Where  $V_{\text{ext}}(\vec{r})$  is both the external potential and  $F(\rho)$  the generalized functional density given by:

$$E(\rho) = T(\rho) + E_{\text{int}}(\rho) + \int d\vec{r} V_{\text{ext}}(\vec{r}) \rho(\vec{r}) \dots\dots\dots(2-22)$$

Because the kinetic idiom  $T(\rho)$  additionally to the electron-to-electron connection or internal electron interaction  $E_{int}(\rho)$  both mostly impacted through density of charge, they are comprehensive  $F(\rho)$ .

### 2-6-2 Kohn-Sham Method

The Kohn-Sham approach has been used in solid-state physics for nearly fifty years. The growth of exact functional of density is raised adoption using this technique between chemicals as well as physical, primarily because that enables appropriate handling for molecular frameworks created earlier unattainable utilizing further traditional methods for the study of quantum mechanics [102]. Kohn and Sham devised an imaginary system of virtual particles with no interaction electrons in 1965 to solve the kinetic energy problem of conventional DFT. This last one is traveling with a localized externally active potential, and its lower- levels characteristics and energy are similar relative to a typical many-body interaction style [98].

KS : A means to indicate local potential is as the following:

$$V_{KS}(\vec{r}) = V_{ext}(\vec{r}) + V_{Coul}[\rho(\vec{r})] + V_{XC}[\rho(\vec{r})] \dots \dots \dots (2-23)$$

where  $V_{ext}(\vec{r})$  represents the external potential, nuclei interaction potential,  $V_{Coul}[\rho(\vec{r})]$  represents the Coulomb interaction potential, and  $V_{XC}[\rho(\vec{r})]$  represents a correlation-exchange potential.

The functional of exchange-correlation  $V_{XC}[\rho(\vec{r})]$  can be calculated as the following:

$$V_{XC}[\rho(\vec{r})] = \frac{\delta E_{KSC}}{\delta \rho(\vec{r})} \dots \dots \dots (2-24)$$

The total energy E can be calculated as the following:

$$E(\rho) = \int V_{ext}(\vec{r}) \rho(\vec{r}) dr + T_S[\rho] + J[\rho] + E_{XC}[\rho] \dots \dots \dots (2-25)$$

Where  $T_S[\rho]$  represents the KS pseudo particle technique's kinetic energy,  $J[\rho]$ : represents a defined densities functional, and  $E_{xc}[\rho]$ : represents an energy of exchange-correlation. The fundamental benefit from KS technique this  $T[\rho] - T_S[\rho]$  is now minimal, which indicates that  $T_S[\rho]$  accounts for the majority kinetic energy contributions  $E_{xc}[\rho]$  contains the leftover fractional of the precise kinetic energy of the many-body unit. Since there is no mutual interaction between the electrons in the KS system, a significance is  $T_S[\rho]$  the precise with may be calculated as the following:

$$T_S[\rho] = \frac{1}{2} \sum_i^N \nabla^2 \varphi(\vec{r}_i) \dots\dots\dots(2-26)$$

$\varphi(\vec{r}_i)$  with representing the KS eigen system calculations' KS orbitals (eigenfunctions) provided [103]:

$$\left(-\frac{1}{2} \nabla^2 + V_{KS}(\vec{r})\right) \varphi_i(\vec{r}) = \varepsilon_i \varphi_i(\vec{r}) \dots\dots\dots(2-27)$$

The KS system's kinetic energy  $T_S[\rho]$  wasn't stated clearly stated nonetheless, it is implicitly density functional in terms of the density. because of(precise) the density  $\rho$  is supplied regarding the KS the orbitals [104].

$$\rho(\vec{r}) = |\varphi_i(\vec{r})|^2 \dots\dots\dots(2-28)$$

The last unidentified parameter in Equation (2-25) is there a functional exchange-correlation  $E_{xc}[\rho]$ , which comprises all contributions of no classical electron-electron interaction except for just a tiny amount of the actual electronic system's kinetic energy [104].

## 2-7 Exchange-Correlation Functional

Correlation describes interactions between electrons inside the same molecule [105]. It is useful in the theoretical description of many electron atoms to consider The general potential of every electron should be equal **correlation energy** of the difference between both the energy predicted by the



implied theory of field and the precise non-relativistic energy[106]. Physically, it relates to the velocity of the linked electrons. Hohenberg's density functional theory, Kohn Sham's theory depends on the notion the total of a uniform electron gas's exchange and correlation energy can be calculated precisely given only its density [107]. The exchange-correlation functional is clearly critical to the density functional approach's success (or failure). One of the reasons DFT is so tempting is that even extremely simple approximations to the exchange-correlation functional can produce good results [108].

## **2-8 Density Approximations**

The following are the kinds of approximations density functional theory's exchange-correlation energy functional, which depends purely Nearly the electronic densities quantity at every point in space:

### **2-8-1 The Local Density Approximation (LDA)**

The so-called local density approximation (LDA) is a common approximation that locally substitutes the exchange-correlation energy density of an inhomogeneous system by that of an electron gas assessed at the local density. While the LDA accurately describes many ground state features (lattice constants, bulk moduli, etc.) [106]. The main idea behind the local density approximation (LDA) is to apply the known conclusion for a homogeneous system to a non-homogeneous system locally[109]. The local density approximation involves describing the functional dependency of the exchange-correlation energy on density as a simple dependence on the density's local value. Because the LDA is precise in homogeneous systems, it has been assumed to be appropriate for describing physical systems where the charge density varies slowly, such as metals[110].

The main issue with DFT is that, with the free electron gas, the exact functional for exchange and correlation is unknown. As a result, the exchange-correlation

energy functional  $E_{xc}$  of a non-uniform system is calculated locally to that of a uniform free electron gas with the same density  $\rho(r)$  as an integral of some function of total electron density.

$$E_{xc}^{LDA}[\rho(r)] = \int \rho(r) E_{xc}[\rho(r)] dr \dots\dots\dots(2-29)$$

Where  $\int \rho(r) E_{xc}$  is the exchange-correlation energy per particle of a uniform electron gas of density  $\rho(r)$  weighted with the probability  $\rho(r)$  that an electron exists at this point in space [111, 112].

**2-8-2 The Local Spin-Density Approximation (LSDA)**

There are various enhancements to the exchange-correlation functional, one of which is the introduction of spin dependent densities.

$\rho \uparrow(r)$  and  $\rho \downarrow(r)$  where  $\rho \uparrow(r) + \rho \downarrow(r) = \rho(r)$  to distinguish between spin-up and spin-down electrons and to construct a local spin-density approach (LSDA). The exchange-correlation functional is then calculation as the following [113].

$$E_{xc}^{LSDA}[\rho \uparrow(r), \rho \downarrow(r)] = \int \rho(r) \mathcal{E}_{xc}[\rho \uparrow(r), \rho \downarrow(r)] dr \dots\dots\dots(2-30)$$

where  $\int \rho(r) \mathcal{E}_{xc}[\rho \uparrow(r), \rho \downarrow(r)]$  is the exchange-correlation energy per particle of an electron gas with  $\rho \uparrow(r), \rho \downarrow(r)$  uniform spin densities[114]. As a result, the exchange-correlation functional (Eq. 2-30) can be divided into two terms as the following:

$$E_x^{LSDA}[\rho \uparrow(r), \rho \downarrow(r)] = \int \rho(r) [\mathcal{E}_x[\rho(r), \xi]] dr \dots\dots\dots(2-31)$$

$$E_c^{LSDA}[\rho \uparrow(r), \rho \downarrow(r)] = \int \rho(r) [\mathcal{E}_c[\rho(r), \xi]] dr \dots\dots\dots(2-32)$$

Finally write the exchange-correlation functional as the following:

$$E_{xc}^{LSDA}[\rho \uparrow(r), \rho \downarrow(r)] = E_x^{LSDA}[\rho \uparrow(r), \rho \downarrow(r)] + E_c^{LSDA}[\rho \uparrow(r), \rho \downarrow(r)] \dots\dots\dots(2-33)$$

This was used in numerous practical applications of density functional theory. The LSDA can handle systems having one or more unpaired electrons, as well

as situations where electrons are becoming unpaired, such as molecules far from their equilibrium geometries; it can even handle conventional molecules. For closed shell systems  $[\rho \uparrow(r) = \rho \downarrow(r)]$ , LSDA is equivalent to LDA, and because this is the most common situation, LDA is frequently used interchangeably with LSDA, however this is not true in general [115, 116].

The reason that LSDA generally outperforms LDA is that the spin-dependent approximation local exchange-correlation functionals are better than the spin-independent ones. It is also so accurate for solids that it is still commonly employed in condensed matter physics [113].

### 2-8-3 The Generalized Gradient Approximation (GGA)

(GGA) stands for generalized gradient approximate. It is still local, but it also takes of gradient the density when same dot into account:

$$E_{xc}^{GGA}[\rho \uparrow(r), \rho \downarrow(r)] = \int \rho(r) \epsilon_{xc}^{GGA}[\rho \uparrow(r), \rho \downarrow(r), \nabla \rho \uparrow, \nabla \rho \downarrow] dr \quad (2-34.)$$

Where the density gradients  $\nabla \rho \uparrow$ , and  $\nabla \rho \downarrow$  are introduced as extra local ingredients or arguments of  $\epsilon_{xc}^{GGA}$  [113, 117]. The most often used of this type is the exchange-correlation energy of **Perdew, Burke, and Ernzerhof** (PBE) in 1996 [118].

When compared to the LDA, the approximation usually provides a superior description of the structural properties of genuine materials, yielding ground-state bond lengths accurate to within 0.0015 nm and binding energies correct to within around 0.207 eV [119, 120].

As a result, the success of KS-DFT is due primarily to the fact that simple approximations (local-density approximation LDA and generalized gradient corrections GGA) for  $\epsilon_{xc}[\rho(r)]$  and its functional derivative give practical estimates of thermodynamical, structural, and spectroscopic characteristics of atoms, molecules, and solids [121].

## 2-9 Hybrid functional

Hybrid functionals are a type of approximate in density functional theory(DFT) to the exchange-correlation energy functional that mixes a part of the precise exchange from Hartree-Fock theory with the remaining exchange-correlation energy from different sources (semi-empirical or Ab-initio). Because of exact Rather than the density, the exchange energy functional is represented by means of the Kohn-Sham orbits., it is referred to as an implicit density functional. **B3LYP**, which stands for "**Becke, 3-parameter, Lee-Yang-Parr**," is one of the most widely used variations.

Axel Becke pioneered the hybrid approach to constructing density functional approximations in 1993 [122]. Hybridization with Hartree-Fock (HF) exchange (also known as exact exchange) is a simple scheme for improving the calculation of many molecular properties, such as atomization energies, bond lengths, and vibration frequencies, which are typically poorly described by simple "Ab-initio".

The well-known B3LYP (Becke, 3-parameter, Lee-Yang-Parr) exchange-correlation functional, as the following:

$$E_{xc}^{B3LYP} = (1 - a) E_x^{LSDA} + a E_x^{HF} + b \Delta E_X^B + (1 - c) E_c^{LSDA} + c E_c^{LYP} \dots\dots(2-35)$$

Where a=0.20, b=0.72, and c=0.81  $E_X^B$  is a generalized gradient approximation: the Becke 88 exchange functional,  $E_c^{LSDA}$  is the local spin density approximation to the correlation functional, and  $E_c^{LYP}$  is the Lee, Yang, and Parr correlation functional for B3LYP [123, 124].

## 2-10 Basis Sets

A group of mathematical functions called a basis set is utilized to build a system's quantum mechanical wave function [125]. These roles include frequently atomic nuclei as its focal point, with several basic responsibility indicating the arrangement of electrons around every atom; the electron

distribution across the molecule is obtained by integrating atomic basis functions. A Slater-kind orbital (STO), a sort of basis function, provides an excellent estimate of the wavefunctions of atomic orbitals. However, because it is challenging to assess; to approximate the STOs, most basis sets use different combinations of Gaussian-type orbitals (GTOs). In a basic basis set, just of bare The minimal quantity of basis functions equals required to explain each atom's whole set of electrons [126]. The following are some kinds of basis sets:

### **2-10-1 Minimal Basis Sets**

The smallest possible basis set represents the having of fewest quantity of function bases [127]. The sign STO-3G indicates that the basis set approximates the shape of the STO orbital using a single contraction of three Gaussian functions [128]. Minimal basis sets (Al-Adely) are used for exceedingly large molecular as well as qualitative results in which accuracy could be compromised. Although minimum sets of base are less computationally expensive than their larger counterparts, they often produce significantly less accurate results [126].

### **2-10-2 Split Valence Basis Sets**

In basic groups with divided valence, inner or core orbitals of atoms are defined using a single basic functional, whereas valency atomic orbitals are represented by two [106]. People devised basic groups with divided valence, these allow the single zeta in the core and the double zeta in the valence region to alter in orbital size during bonding, because most chemistry focuses on the interaction of valence electrons [106].

Most basis sets, including split-valence sets, have basis functions that are comprised of a collection of Gaussian functions rather than a single Gaussian function. The standard 6-31G split-valence foundation defines of contraction scheme [106].

The impulse represents of border from the valence (right) to the core (left). In this case, each core basis function is composed of six Gaussian functions.

The valence space is separated into two basic functions, which are commonly referred to as the "inner" and "outer" functions. Polarization functions are a collection of roles that can useful applied to foundational groups to enable the comprehensive [129]. Pople basis sets are available in the following sizes: 3-21G, 4-31G, , 6-21G, 6-311G, and [130].

### 2-10-3 Polarized Basis Sets

Functions of polarization, which include supposedly roles the larger angular quantum quantity, are a very fundamental and still useful idea [131]. As soon as the wave function contains functions of polarization, and basis-set must be increased to approach the precise electrical energy more closely. The basis determined will include at least a set of d-functions, while added functionalities include sometimes called functions of polarization. The fundamental group's flexibility is increased with the addition of polarization functions, particularly in defining electron density in bonding zones.

Calculations of relativity Hartree-Fock for group 15 elements along with certain diatomic compounds. In particular, polarization example, maybe included as \* type or (d): Non-hydrogen atoms are inserted with d-type functions. It may be presented as p-type functions appended to hydrogens (d, p) or \*\* type [132], example: 6-31G (d) or 6-31G\*.

### 2-10-4 Diffuse Basis Sets

It is the diffuse functions that inverse of functions of valence-size. That's more advanced variant of the s- with p- Different kinds of functions. Their allow orbitals to encircle a greater region of space. Basic group diffused parameters were useful with relation to applications with electrons positioned comparatively far removed from the nucleus, like anions, effective mechanisms

with a negative charge, lone pair systems of excited states, molecules, structures that have tiny ionized potential, as well as soon in addition to the 6-31G+ + (d) basis set, the 6-31+G(d) basic groups includes + heavy atom diffuse functions [129].

## **2-11 Programs and Computers in Use**

### **2-11-1 Computers in Use**

- i. Laptop core (TM)i7
- ii. System: Windows 10
- iii. Hard disk: 512 GB.
- iv. CPU: 2.6 GHZ (6 cores)
- v. RAM: 32 GB.

### **2-11-2 Programs**

#### **2-11-2-1 Gaussian 09W**

A computer application called Gaussian that was initially distributed in 1970 on Carnegie-Mellon University research group led by John Pople[133, 134]. It's already continually restart since then. The name taken of the phrase orbital or Gaussian function, that was selected for improve the preceding software's ability to process that used the Slater type function or orbital. In statistics, Gaussian functions are frequently employed to define normal distributions [135]. All computational calculations were performed using the Gaussian 09 software (M. J. Frisch) and the GaussView graphical user interface [136]. Gaussian analyzes the molecule's energy shapes, and molecule structures' vibrational frequencies, in addition to numerous molecule attributes created by this core computational kinds, starting with the fundamental principles of quantum mechanics. It's applicable to study chemicals and stable species under a range of circumstances, including as short-lived intermediates and transition states, that are difficult or impossible to identify experimentally [137].

The Roothaan-Hull equation and the ability to determine the greatest number of elements in the structure of the periodic table are the foundations of the Gaussian program. The program's computations' correctness is dependent using a basis group or wave function value utilized, with larger numbers resulting in more significant results [138].

All numbers used in internal Gaussian calculations are in atom quantities to simplify Formulas for mathematics by creating numerous One is equal to all basic factors. An energy unit called a Hartree that is easily convertible to other units in computational chemistry [138].

### **2-11-2-2 Gauss View Program**

This is feasible to construct A schematic illustration of chemical compositions by studying using the Gauss view software interface. This is a graphic editor designed for the Gaussian software allows you to easily build an input file and starting configuration for the Gaussian software as well as view Results of the midway and final computations. Gauss view 06 -16 is a compilation of common elements that function by tandem in the primary. Such enables the creation of a graphical depiction of molecular structures [139].

### **2-12 Electronic Properties**

#### **2-13 Total Energy**

A molecular system's total energy is the sum of total electronic energy and the energy of inter-nuclear repulsion. A molecule's total energy,  $E_{\text{molecule}}$ , can be calculated as the sum of its electronic energy, vibrational energy, and rotational energy:

$$E_{\text{molecule}} = E_{\text{electronic}} + E_{\text{vibration}} + E_{\text{rotation}} \dots\dots\dots(2-36)$$

Both vibrational and rotational energy are connected to the motion of the nuclei of the molecule's constituent atoms. A molecule's vibrational and rotational



energies, like its electronic energy, are quantized, which means they can only take particular discrete values. As a result, each molecule has an own collection of vibrational and rotational energy levels. The following are typical values for the disparities between nearby electronic, vibrational, and rotational energy levels:

$$\Delta E_{\text{elec.}} = 1-10 \text{ eV} \quad (\text{in the visible and near-ultraviolet range})$$

$$\Delta E_{\text{vib.}} \sim 10^{-1} \text{ eV} \quad (\text{infrared range})$$

$$\Delta E_{\text{rot.}} \sim 10^{-4} \text{ eV} \quad (\text{microwave range})$$

Hence, Elec.  $\gg$  Evib.  $\gg$  Erot. As a result, each electronic level can support an array of vibrational sub-levels, and each vibrational level can similarly accommodate an array of rotational sub-levels. Fig (2-4) Like atoms, molecules can absorb and release radiation by transitioning between the energy levels associated with their electrons, i.e, by changing their electronic energy [140, 141].

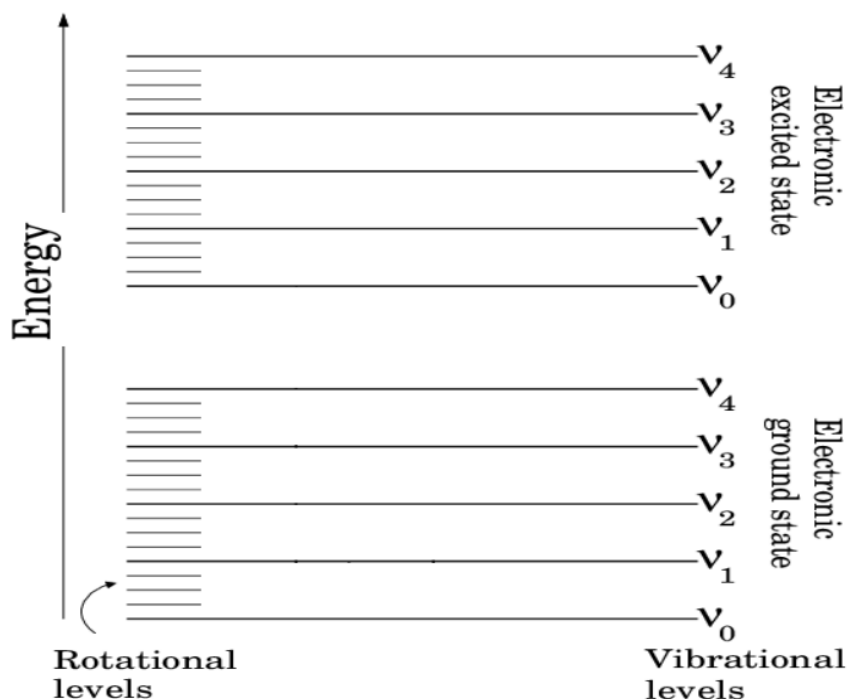


Figure 2-4: A molecule has two electrical energy state.[141].

### 2-14 Energy Gap ( $E_g$ )

The energy gap, according to Koopmans theorem, which separates the lowest unoccupied molecular orbital (LUMO) from the highest occupied molecular orbital (HOMO) [142].

$$E_g = E_{\text{LUMO}} - E_{\text{HOMO}} \dots\dots\dots(2-37)$$

Energy difference formed by LUMO and HOMO helps to determine of molecule's reactivity to chemicals kinetic stability, and how it interactions in conjunction with different species. It molecular combination possessing a small energy gap exhibits strong polarization, has strong reaction of chemicals, with has limited kinetic stabilization. This referred to in the softest molecular state [143, 144]. Figure (2-5) depicts the illustration is (HOMO) with (LUMO) energy state and gap between bands for different molecule-to-molecule interactions [145].

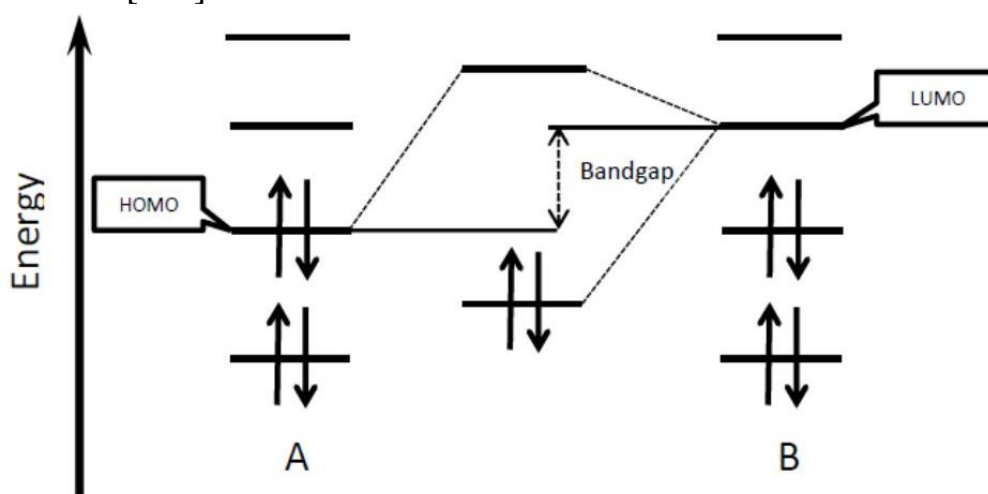


Figure 2-5: Diagram bandgap between two molecules that interact HOMO-LUMO [145].

### 2-15 Atomic Charges

Effective atomic computations were critical in applying chemical computations into the structure of molecules. this simulations examine how atomic charges affect electronic arrangement, polarizability of molecules, dipole moment, and other characteristics of molecules properties [146-148] [147-149] . It is

frequently used to define electrostatic potential [149]. Of course, Mulliken is both the most cost-effective and fastest technique of computing costs. However, the approach the method yields purely in terms of results is better. The cause of that is obvious. This distributes the equivalent standard orbitals for each of the involved atoms, thus there will be absence of polarizing. An further problem is that they are dependent on the basic groups, as well expanding of basis set worsens the description [144].

### **2-16 Molecular Electrostatic Potential (MEP) Surface**

Anytime, the MEP position of amount of energy needed for create one, which was positive charge up to that distance from infinity [150]. It is a localized three-dimensional attribute that may of assessed with dot in a system's area. That may represent the allocations of charges within the molecule three-dimensionally with color grading to show and demonstrate molecule size, shape, and electrostatic potential value [151]. The MEP surface has been demonstrated to be a highly helpful approach for examining the link Chemical and physical characteristics and structure of molecular properties of molecules such as Molecules of biology and medicines. That may of utilized in discriminate among electron-rich (electrophilic assaults) with electron-poor (nucleophilic attacks) regions of surface [152]. An extremely high energy of electrostatic potential indicates relative lack with electrons, whereas a minimal energy of electrostatic potential indicates the abundance of electrons [153].

### **2-17 Principles of Vibrational Spectroscopy**

Molecular spectra are more complicated and include more information than atomic spectra. Their greater complexity arises from the more complicated structures of molecules, whereas the spectra of atoms are due only to their electronic transitions, the spectra of molecules arise from electronic, vibrational, and rotational transitions [154]. Hooke's Law can estimate the stretching

frequency of a bond. In this approximation, two atoms and the connecting link are represented as a simple harmonic oscillator made up of two masses (atoms) coupled by a spring. A molecule can vibrate in a variety of ways, each of which is referred to as a vibrational mode. The absorbance wave number  $\nu$  may be determined using Eq. (2-41), which is derived from the harmonic oscillator model [155].

$$\nu = \frac{1}{2\pi} \sqrt{\frac{k}{\mu}} \dots\dots\dots(2-38)$$

In which  $k$  is the atomic scale force constant and the macroscopic model spring constant, and  $M_r$  is the reduced mass and  $m_1, m_2$  mas of atomas, defined by [155].

$$M_r = \frac{m_1 m_2}{m_1 + m_2} \dots\dots\dots(2-39)$$

The wavenumber unit  $\bar{\nu}$ , which is represented in  $\text{cm}^{-1}$ , is commonly used in vibrational spectroscopy. The reciprocal wavelength is the number of waves in one centimeter and is provided by the following:

$$\bar{\nu} = \frac{1}{\lambda} = \frac{\nu}{c} \dots\dots\dots(2-40)$$

Where  $\lambda$  is the wavelength and  $c$  is the vacuum velocity of light ( $2.997925 \times 10^8$  m s<sup>-1</sup>). When the force constant is greater, the vibrational frequency increases, indicating that the bonding between the two atoms is stronger.

These anharmonic oscillator's energy levels are roughly described by [155].

$$E_{\text{vib}} = h\nu_o \left[ \left( \nu + \frac{1}{2} \right) - x_a \left( \nu + \frac{1}{2} \right) \right]^2 \dots\dots\dots(2-41)$$

Where  $x_a$  is the constant of anharmonicity.

A polyatomic molecule's vibrations can be thought of as a system of connected anharmonic oscillators. If the molecule has  $N$  atoms, the nuclear masses in the molecule will have a total of  $3N$  degrees of freedom of motion. Subtraction of

the entire molecule's pure translations and rotations yields  $(3N-6)$  vibrational degrees of freedom for a non-linear molecule and  $(3N-5)$  vibrational degrees of freedom for a linear molecule [156]. Stretching vibrations (changes in bond lengths) and deformation vibrations (changes in bond angles) can be distinguished by the direction of the vibrational movement. Deformation vibrations are classified as bending modes, twisting or torsion modes, wagging modes, and rocking modes. Further subdivision relates to the symmetry of the vibration (e.g., symmetric or antisymmetric, in-plane or out-of-plane) [157]. Figure 2-6 shows these modes [158].

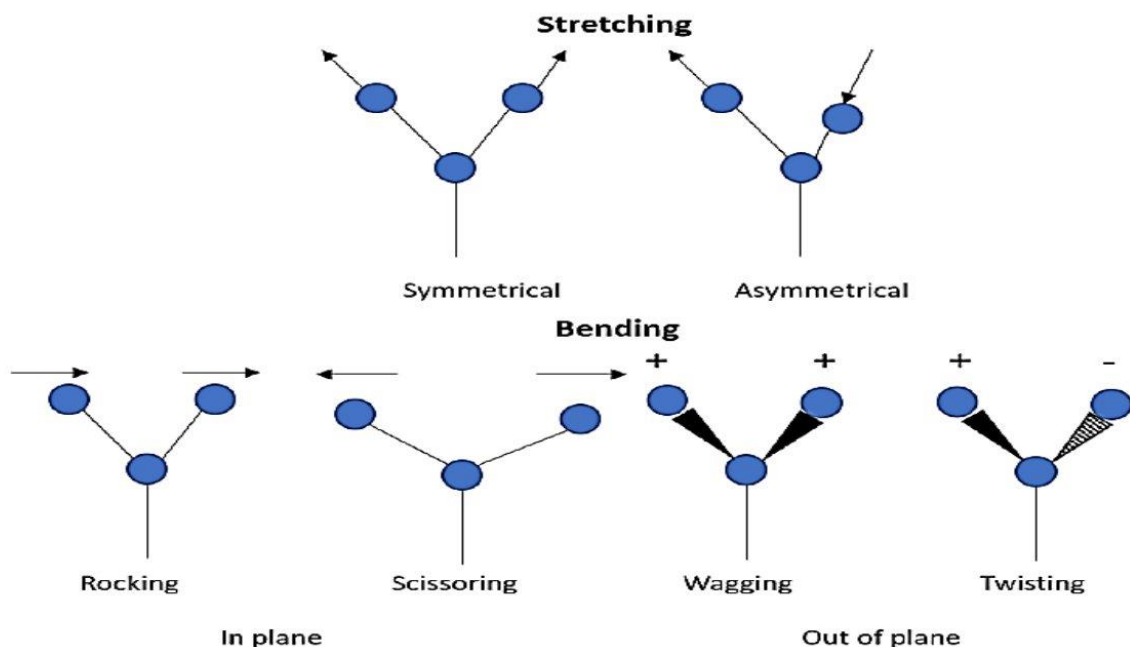


Figure 2-6: The many vibrational modes [158].

## The Second Part (radiotherapy)

### 2-18 Kerma Concept

Kerma understands it as a function of kinetic energy released per unit mass. It is used to indirectly ionize radiations such as photons. The advantage of kerma is that it can identify the average energy transferred from indirectly ionizing

radiations to directly ionizing radiations. Photon interactions, photoelectric effect, Compton scattering, and pair production photon transfer energy to electron of medium, then electron transfer energy to medium based on ionization or excitation. As shown in the equation below, Kerma determines average energy transmitted from photon to electron of medium per unit mass [53, 159].

$$K = \frac{dE_{av.}}{dm} \dots\dots\dots (2-42)$$

The Kerma unit is joule per kilogram, often known as gray (Gy). 1 Gy= 1J/1Kg. Some of the secondary charged particles produced by photon interaction inside a given area of material transferred energy outside the area in which it was produced. To estimate the radiation dosage, charged particle equilibrium (CPE) must be attained. CPE occurs when a particle departs the reaction zone carrying a particular amount of energy to be replaced by another particle with the same energy created outside the interaction zone. In the case of CPE, the initial kinetic energy of secondary charged particles generated by photons is denoted by

$$\epsilon_{tr} = \sum ME \dots\dots\dots(2-43)$$

where ME indicates converting mass to energy or vice versa; in this case, kerma equals [160, 161] .

$$K = \frac{d \epsilon_{tr}}{dm} \dots\dots\dots(2-44)$$

In absence of CPE, kerma is given an energy flow  $\Psi$  (J/m<sup>2</sup>) and a mass energy transfer coefficient  $\frac{\mu_{tr}}{\rho}$  in units of (m<sup>2</sup> /kg).

$$K \text{ (Gy)} = \Psi \frac{\mu_{tr}}{\rho} = \phi h\nu \left( \frac{\mu_{tr}}{\rho} \right)_{air} \dots\dots\dots(2-45)$$

$(\frac{\mu_{tr}}{\rho})_{air}$  represents the mass energy transfer coefficient for air at photon energy  $h\nu$  and  $\phi$  photon flux.

Two approaches were used to get energy from photons created by charged particles (electrons).

1. collision contact (soft and hard collisions)
2. Radiation interacts (bremsstrahlung and electron-positron annihilation).

These approaches distinguish two types of kerma: collision kerma  $K_{col}$  and radiation kerma.  $K_{rad}$ , Kerma of collision  $K_{col}$  denotes kerma formed as a result of electron energy loss during ionization. Kerma caused by radiation  $K_{rad}$  is kerma produced by secondary photons produced by bremsstrahlung. As a result, the total kerma  $K$  can be found by the sum of two kermas [161].

**2-19 Exposure**

The total charge  $dQ$  (coulomb unit) of the ions of one sign created in air when all the electrons and positrons generated by photons in mass  $dm$  (kilogram), is defined as **exposure X (R)**. It may alternatively be described as the number of ions per unit volume mass of air generated by radiation. The exposure unit is called roentgen (R).

1 roentgen( R) =  $2.58 * 10^{-4}$  C / Kg [162].

$$X = \frac{dQ}{dm} \dots\dots\dots(2-46)$$

"The transfer of energy (kerma) from the photon beam to charged particles at a specific location does not result in the absorption of energy by the medium (absorbed dose) at the same location, due to the limited range of secondary electrons released through photon interactions." [53]

The initial kinetic energy (KE) of a charged particle the mean number of ion pairs created (N) yields the average energy lost in air per ion pair formed.  $W_{air}$ , In standard conditions,  $W_{air}$  equals initial kinetic energy (KE) divided by the mean number of ion pairs created (N) equals  $33.97 \times 1.602 \times 10^{-19}$  J/ion.

Exposure in air equal multiplying quantity of charges formed per joule of energy deposited ( $e / W_{air}$ ) by collision kerma [162-164]

$$X = (K_{col})_{air} (e / W_{air}) \dots\dots\dots(2-47)$$

The existence of radiation can be recorded by observing the ionization of atoms in the medium through which the radiation permeates [53].

$$X = \frac{dQ}{dm} \dots\dots\dots(2-48)$$

**dQ** is the quantity of electric charges in coulombs, **dm** is the mass of air in kilograms, and **X** is the exposure in roentgen (R).

The following factors are used to calculate X-ray exposure: parameters  $E_{air}$ , the energy flounce, the mass energy absorption coefficient ( $\frac{\mu_{en}}{\rho}$ )<sub>air</sub>, the charged particle energy released per unit mass of air is  $\Psi (\frac{\mu_{en}}{\rho})_{air}$  [165].

$$\text{Exposure (R)} = \Psi (\frac{\mu_{en}}{\rho})_{air} (\frac{e}{E_{air}}) \dots\dots\dots (2-49)$$

Where e denotes the charge of an electron.

**2-20 Absorbed Dose**

The International Commission on Radiation Units and Measurements (ICRU) defines absorbed dose as "the energy absorbed by the medium that is exposed to radiation per unit mass at the measurement point [166].

The absorption dose can be stated mathematically as the following [166].

$$D = \frac{dE}{dm} \dots\dots\dots(2-50)$$



E: Radiation energy delivered to a particular volume mass of the material exposed to radiation. The energy supplied to the exposed medium is equal to

$$E = (E_{in})_n + (E_{out})_n + (E_{in})_c + (E_{out})_c + \sum E \dots\dots\dots(2-51)$$

Where  $(E_{in})_n$  : denotes the energy emitted by non-charged particles entering the measuring region,  $(E_{out})_n$ : Energy emitted by non-charged particles as they exit the measuring region.

$(E_{in})_c$ : Radiated energy emitted by charged particles entering the measuring region+ $(E_{out})_c$  : Radiated energy emitted by charged particles that result in the measuring region,  $\sum E$  : It denotes the amount of energy converted to mass (a negative value) or mass converted into energy (a positive value), i.e., the mass of an irradiated medium. The dose absorbed is measured in joules per kilogram (J/kg). The gray (Gy) is the term for the unit of absorbed dose [166].

**2-21 Biological Effectiveness Relative**

The absorbed dose (D) is the amount or quantity of radiation energy that transfers to the medium. However, it should be emphasized that identical doses of different forms of radiation do not result in comparable biologic effects, with one gray of neutrons producing a higher biologic effect than the same dose of X-rays. This is due to the differential in energy deposition pattern at the tiny target [53]. This gives birth to the idea of relative biologic efficacy. The relative biologic effectiveness (RBE) of test radiation (r) compared to 250 kVp X-rays is defined as the ratio of X-ray doses to test radiation doses necessary to have the same biological impact in the target [163].

$$RBE = \frac{D_x}{D_r} \dots\dots\dots(2-52)$$

where  $D_x$  and  $D_r$  are the dose quantities of 250 kVp X-rays and the actual radiation dose, respectively [167].

**2-22 Linear Attenuation Coefficient**

When a photon beam of intensity  $I_0$  collides with an attenuator of thickness  $(x)$ , the intensity  $I(x)$  of the photon beam is attenuated by the attenuator. [168].

$$I_0 = I_x e^{-\mu x} \dots\dots\dots(2-53)$$

$I_0$  : The first incident photon beam.,  $I_x$ : attenuating photon beam,  $\mu$  ( $\text{cm}^{-1}$ ) : The linear attenuation coefficient is social with photon energy and attenuator kind (atomic number). known as attenuation per length unit of the attenuator. The half value layer (HVL or  $x_{1/2}$ ) is the thickness necessary to lower the original photon beam to half its initial value [169].

$$X_{1/2} = \text{HVL} = \frac{0.693}{\mu} \dots\dots\dots(2-54)$$

The linear attenuation coefficient  $\mu$  ( $\text{cm}^{-1}$ ) is related to the mass attenuation coefficient  $\mu_m$  ( $\text{cm}^2/\text{g}$ ), the atomic attenuation coefficient ( $\text{cm}^2/\text{atom}$ ), and the electronic attenuation coefficient  $\mu_e$  ( $\text{cm}^2/\text{electron}$ ) as the following [162]:

$$\mu = \mu_m \rho = \frac{\rho N_A}{A} \mu_a = \frac{\rho N_A Z}{A} \mu_e \dots\dots\dots(2-55)$$

where,  $Z$  and  $A$  are the density, atomic number, and mass number of the attenuator, respectively, and Avogadro's number ( $N_A$ )  $N_A = 6.022 \times 10^{23}$  atoms/mol. If the mass attenuation coefficient  $m$  is independent of the attenuator density, then the mass attenuation coefficient is important for usage in the application. For mixes and compounds, the mass attenuation coefficient is calculated by adding the mass attenuation coefficients of their constituents [170].

$$\frac{\mu}{\rho} = \left( \sum_i \frac{\mu}{\rho} \right)_i \dots\dots\dots(2-56)$$

Both the mass energy attenuation coefficients and the density of the attenuating material influence photon beam attenuation. When the target is biological tissue, attenuation is done via the Compton effect and is dependent on the electron density, however at higher photon energies more than 6 MeV, pair creation occurs and is dependent on the atomic number of the target [171].

**2-23 Coefficient of Mass Energy Absorption**

When photons interact with a target, they produce either charged or uncharged particles that carry a portion of the photon energy outside of the initial location. The energy is transferred to the distant point from the initial location by secondary photons (Compton scattering, annihilation, bremsstrahlung) and deposited in that secondary location. As a result, linear energy absorption coefficient concept appears, which is connected to linear attenuation coefficient as the following:

$$\mu_{en} = \mu E_{\text{fraction}} \dots\dots\dots(2-57)$$

$E_{\text{fraction}}$  is the fraction of photon energy that is transmitted to the medium outside of the primary target.

When a photon interacts with matter, some of its energy is transmitted as secondary electron kinetic energy. The energy will be deposited by an alternative secondary electron away from the target. Because energy is lost outside the target during contact, two essential coefficients in the medical profession emerge: the  $\mu_{tr}$  energy transfer coefficient and  $\mu_{en}$  the energy absorption coefficient [162].

$$\mu_{tr} = \mu \frac{E_{tr}}{h\nu} \dots\dots\dots(2 - 58)$$

The average energy transmitted to charged particles (electrons and positrons) in the attenuator is denoted by  $E_{tr}$ .

$$\mu_{en} = \mu \frac{E_{en}}{h\nu} \dots\dots\dots(2-59)$$

$E_{en}$  is the average energy deposited in the attenuator by charged particles. The mass energy absorption coefficient ( $\frac{\mu_{en}}{\rho}$ ) is defined as the fraction of incoming photon energy that converts to kinetic energy for charge particles in a unit area. The relevance of the mass energy absorption coefficient in radiotherapy is to correctly calculate absorbed energy inside tissue . Mean proportion of incident photon energy converted to charged particle kinetic energy per mass-per-unit-area distance, excluding energy lost as radiation. At low photon energies, there is a relationship between the mass energy absorption coefficient and the mass attenuation coefficient for soft elements. When photon energy rises and reaches greater energies. bremsstrahlung and annihilation occur, there is a difference between the mass energy absorption coefficient and the mass attenuation coefficient prevails [171, 172].

## 2-24 The Relationship Between Mass Attenuation Coefficient and Cross Section

The likelihood of interaction happening between the particle interactions and the target is defined as the **cross section**. The barn is the unit of cross-section used (1 barn =  $10^{-24}$  cm<sup>2</sup>) [170]. Photon energy and the atomic number of the medium are two parameters that influence cross section. Pair production interaction will be dominant in the case of high photon energy and high atomic number[170]. There are two sections. The microscopic cross section ( $\sigma$ ), which is the chance of a certain reaction occurring between a photon and a target, is represented in units of area cm<sup>2</sup> [170].

The other cross-section is referred to as the macroscopic cross-section ( $\mu$ ). The macroscopic cross section is the likelihood of a certain reaction occurring per unit of photon transit. It is connected to the microscopic cross section ( $\sigma$ ) by the relationship illustrated below [170].

$$(\mu) = N (\sigma) \dots\dots\dots(2-60)$$

( $\mu$ ) : is the represent Macroscopic cross section (linear attenuation coefficient) ( $\text{cm}^{-1}$ ), N : is the represent Number of material atoms ( $\text{atoms}/\text{cm}^3$ ) and ( $\sigma$ ) : is the represent microscopical cross-section ( $\text{cm}^2$ ). The total cross section for cross sectional areas is calculated by adding all cross sectional areas together as shown in Eq (2-56) [171] .

$$\sigma_{total} = \sum_i \sigma_i \dots\dots\dots(2-61)$$

Whereas  $\sigma_{total}$  total cross section,  $\sigma_i$  individual cross section The cross section ( $\sigma$ ) and mass energy absorption coefficient ( $\mu$ ) are connected in the following equation [171]:

$$\frac{\mu_{en}}{\rho} = \frac{\sigma N_A}{A} \dots\dots\dots(2-62)$$

$N_A$  : is represent Avogadro's number , A : is represent Mass number .

The total mass energy absorption coefficient may be calculated using equations (2-61) and (2-62):

$$\left(\frac{\mu_{en}}{\rho}\right)_{total} = \sum \left(\frac{\mu_{en}}{\rho}\right)_i \dots\dots\dots(2-63)$$

The calculation of total mass attenuation coefficients is more significant than cross sections in radiology. The energy of the photon is one of the numerous parameters that impact the effect of a photon beam on tissue. The photon energy

and atomic number of the target are important parameters on which the mass energy absorption coefficient is dependent [173, 174].

### **2-25 Fractionation Dose**

The total dose will be divided into a number of smaller doses called fractions, which are given on different days ". Higher total doses of radiation are often utilized for curative therapy. For 3–8 weeks, a fraction of the amount will be taken once a day, Monday through Friday. The overall dose is divided into various therapy sessions with weekend rest periods, giving the healthy cells time to recuperate [175] The foundation of fractionation is based on five fundamental biological elements known as the five Rs of radiotherapy [176].

- Radiosensitivity.
- Repair
- Repopulation
- Redistribution
- Reoxygenation

The division of the dose into several parts protects normal tissues by repairing sublethal damage between dose fractions and repopulating cells. The repair of sublethal damage is stronger in late responding tissues, whereas cell repopulation is larger in early responding tissues. Through reoxygenation and relocation of tumor cells, fractionation promotes tumor damage [176]. In general 2 Gy is necessary to eliminate proliferative cell capability [176].

### **2-26 Sensitivity Enhancement Ratio (SER)**

Radiotherapy is the use of incident ionizing radiation on a cancer tumor in order to eradicate cancer cells. During radiotherapy, there are both remaining cancer cells and dead cancer cells. SER is a relationship between survival cancer cells

and destroyed cancer cells with and without nanoparticles, where SER " is the ratio of survival cells to the beginning cells for irradiation without and with nanoparticles " The incorporation of nanoparticles into malignant tumors is thought to be an ideal strategy for increasing (SER). Increased SER indicates an increase in killed cancer cells and a decrease in surviving cancer cells with and without nano particles [177, 178].

It is mathematically described by the following equation [179].

$$SER = \frac{\text{number of survival maligninat cells with out NPs} - \text{number of survival maligninat cells with NPs}}{\text{umber of survival maligninat cells with out NPs}} \dots\dots\dots(2-64)$$

A drug's dose modification factor ( DMF) is defined as the amount of radiation necessary to create an effect without and with a medicine [179].

If DMF = 1 there will be no medication

DMF < 1 effect.

DMF > 1 Improvement

The notion of DMF is analogous to the displacement of the response curve by radiation sensitizers. Radiosensitizers, such as nanoparticles, increase radiation damage in vivo and in vitro cancers. The sensitizer enhancement ratio is commonly used to represent the magnitude of the sensitizing effect [180-182].

### 2-27 Deriving of Theoretical Procedure

The total mass energy absorption coefficient of an organ may be calculated using a nano-agent as the following:

$$\left(\frac{\mu_{en}}{\rho}\right)_{total} = \left(\frac{\mu_{en}}{\rho}\right)_{organ} + \left(\frac{\mu_{en}}{\rho}\right)_{nanoparticles} \dots\dots\dots(2-65)$$

This equation may be used to calculate the dose(d) for different media [169].

$$d(\text{Gy}) = 8.9 \times 10^{-3} \frac{\mu_{en}/\rho_{media}}{\mu_{en}/\rho_{air}} \times X \dots\dots\dots(2-66)$$

The exposure in roentgen (R) units may be determined theoretically using the following equation [183].

$$X = 1.8 \times 10^{-8} E \mu_{en}/\rho_{air} \phi \dots\dots\dots(2-67)$$

Where E is photon energy (MeV), and  $\phi$  is photon flow (photon/cm<sup>2</sup>).

The dose fractionation equation using nanomaterial will thus be as the following:

$$d(\text{Gy}) 8.9 \times 10^{-3} \frac{\mu_{en}/\rho_{organ} + \mu_{en}/\rho_{nanoparticules}}{\mu_{en}/\rho_{air}} \times X \dots\dots\dots(2-68)$$

$\left(\frac{\mu_{en}}{\rho}\right)_{organ}$  : is the organ's mass attenuation coefficient,  $\left(\frac{\mu_{en}}{\rho}\right)_{nanoparticules}$  : is the nanoparticle mass attenuation coefficient. Equation (2-66) is an irradiation dosage fractionation equation [171, 184, 185]

In radiotherapy, the biological effect (BE) on malignant cells exposed to one radiation dose is  $ad$ , which means the cells cannot repair themselves during a single radiation shoot. In LET, the demonstrate death in this case is mitotic and



apoptotic. When two radiation shoots hit malignant cells, the biological effect is  $\beta d^2$  where the quadratic coefficient constant is,  $\beta$  the demonstrate death in this case is mitotic, and the total biological effect on malignant cells exposed to radiotherapy is given by [186].

$$BE = \alpha d + \beta d^2 \dots\dots\dots(2-69)$$

The biological impact on malignant cells exposed to n fractions dosage is determined by two factors: fraction numbers and applied dose, which are described by the linear quadratic irradiation equation shown below [187].

$$BE = n ( \alpha d + \beta d^2 ) \dots\dots\dots(2-70)$$

Where n is the number of fractions and d is the dose per fraction.

$\alpha$  ( $Gy^{-1}$ ) constant for linear sensitivity (real tissue radiosensitivity). The logarithm of the number of cells damaged irreparably per gray of ionizing radiation dosae is the rate of cell death by single-ionizing events.

$\beta$  ( $G y^{-2}$ ) constant for quadratic sensitivity (tissue healing ability) Repair capacity: the logarithm of the number of cells sterilized in a repairable way per gray squared, the maximum rate of cell killing by two ionizing events observed when there is no repair of sublethal lesions during radiation exposure, but total dose (D) given by multiplying the number of fractions with a single dose [187, 188].

$$D = n d \dots\dots\dots (2-71)$$

There is another way to construct the dose equation (2-69) for the biological effect (BE).

$$BE = \alpha D + \beta D d \dots\dots\dots(2-72)$$

Where D is the biological effect of the same event, and D is the biological effect of a different event. The biological effect is rewritten in the following manner [189, 190]:

$$BE = n d ( 1 + \beta d ) \dots\dots\dots(2-73)$$

Divide both sides of the equation to get:

$$\frac{BE}{\alpha} = n d (1 + \frac{\beta d}{\alpha} ) \dots\dots\dots(2-74)$$

$$\frac{BE}{\alpha} = n d (1 + \frac{d}{\alpha/\beta} ) \dots\dots\dots(2-75)$$

Where  $\alpha/\beta$  : is the ratio of true radio sensitivity to tissue recovery ability after radiation exposure, it is an essential factor and has a table for many examples indicated in table (2-1) [176] .

Table 2-1: Values of the constant  $\alpha/\beta$  [176].

Tumor classification	$\alpha/\beta$
"for early responding tissues "	10
" for late responding tissues "	3

Alpha is a parameter for linear cell kill that is proportional to the dosage supplied, and Beta is a parameter for quadratic cell kill that is proportional to dose<sup>2</sup>. Equation (2– 75) is referred to as **the linear-quadratic equation** .

The ratio of surviving cancer cells to original malignancy cells is the survival curve for X-ray [191].

$$S = \frac{N_s}{N_i} \dots\dots\dots(2-76)$$

The surviving cells following radiation dose(d) [192].

$$S = \text{EXP}^{- (\alpha d + \beta d^2)} \dots\dots\dots(2-77)$$

We get by substituting an expression (2-76) for an equation (2- 77).

$$N_S = N_i \text{EXP}^{- (\alpha d + \beta d^2)} \dots\dots\dots(2-78)$$

Surviving fraction is represented by equation (2-78), By substituting the fraction dosage value into the previous equation [193, 194].

$$N_S = N_i \text{EXP}^{- \left( 1 + \frac{d}{\alpha/\beta} \right)} \dots\dots\dots(2-79)$$

Where  $N_S$ : surviving cell number after irradiation.  $N_i$  starting cell number before irradiation.  $\alpha/\beta$  : is a radio-sensitivity factor.

We derive the irradiation equation modification by replacing equation (2-66) in equation (2-79)

$$N_S = N_i \text{EXP}^{- \left( 1 + \frac{8.9 \times 10^{-3} (\mu_{en}/\rho_{organ}) + (\mu_{en}/\rho_{nano}) \times X}{\mu_{en}/\rho_{air}} \right) \alpha/\beta} \dots\dots\dots(2-80)$$

The radiotherapy equation (2- 80) is also completed by applying the exposure equation (2- 66).

$$N_S = N_i \text{EXP}^{- \left( 1 + \frac{8.9 \times 10^{-3} (\mu_{en}/\rho_{organ}) + (\mu_{en}/\rho_{nano}) \times 1.8 \times 10^{-8} (EMev) \frac{\mu_{en}}{\rho_{air}}}{\alpha/\beta} \right)} \dots\dots (2-81)$$

# **Chapter Three**

## **Results and Discussion**

### 3.1 Introduction

The findings of the structural and electronic features that were calculated using the DFT method are reported in this chapter. These parameters include the surface potential energy. The lowest energy required to achieve the optimum structure, bond lengths, and bond angles. Electronic characteristics such as total energy, dipole moment, and atomic charges. Infrared spectroscopy is one of the spectroscopic characteristics. The hybrid B3LYP and density functional theory at one function generalization approximation are applied to get the result of the glucose particles and their adsorption with silver nanoparticles. Gaussian 09 was used to complete all computations. Gauss view 06 was used as a supplement to locate the optimization geometries.

On the other hand, after obtaining the most stable molecular configurations of  $\alpha$  – D glucose with nanoscale silver and studying its properties, the radiation dose used in the treatment of lung cancer was calculated, as was the radiation sensitivity of cancer cells, using special mathematical methods.

### 3-2 Nanoparticales molecular construction

Two different structures were built of two molecules of  $\alpha$  – D glucose that have been adsorbed by one silver atom ( $C_{12}H_{24}O_{12}Ag$ ). There are 12 carbon atoms, 12 oxygen atoms, 24 hydrogen atoms, and one silver atom in this structure. The second structure ( $C_6H_{12}O_6Ag_3$ ) is made up of one  $\alpha$  – D glucose molecule and its adsorption by three silver atoms, to get its structural and electrical characteristics. It was created with the Gauss View 6 software program and optimized with the Gaussian 09 program. the final one is made up of six carbon atoms, twelve hydrogen atoms, six oxygen atoms, and three nano silver atoms as shown fig (3-1). These characteristics were calculated using the density functional theory DFT and the hybrid function B3LYP using the mix basis set

that selected for C, O, and H atoms was 6-311 + G\*, whereas the LANL2DZ basis set was used for Ag atoms.

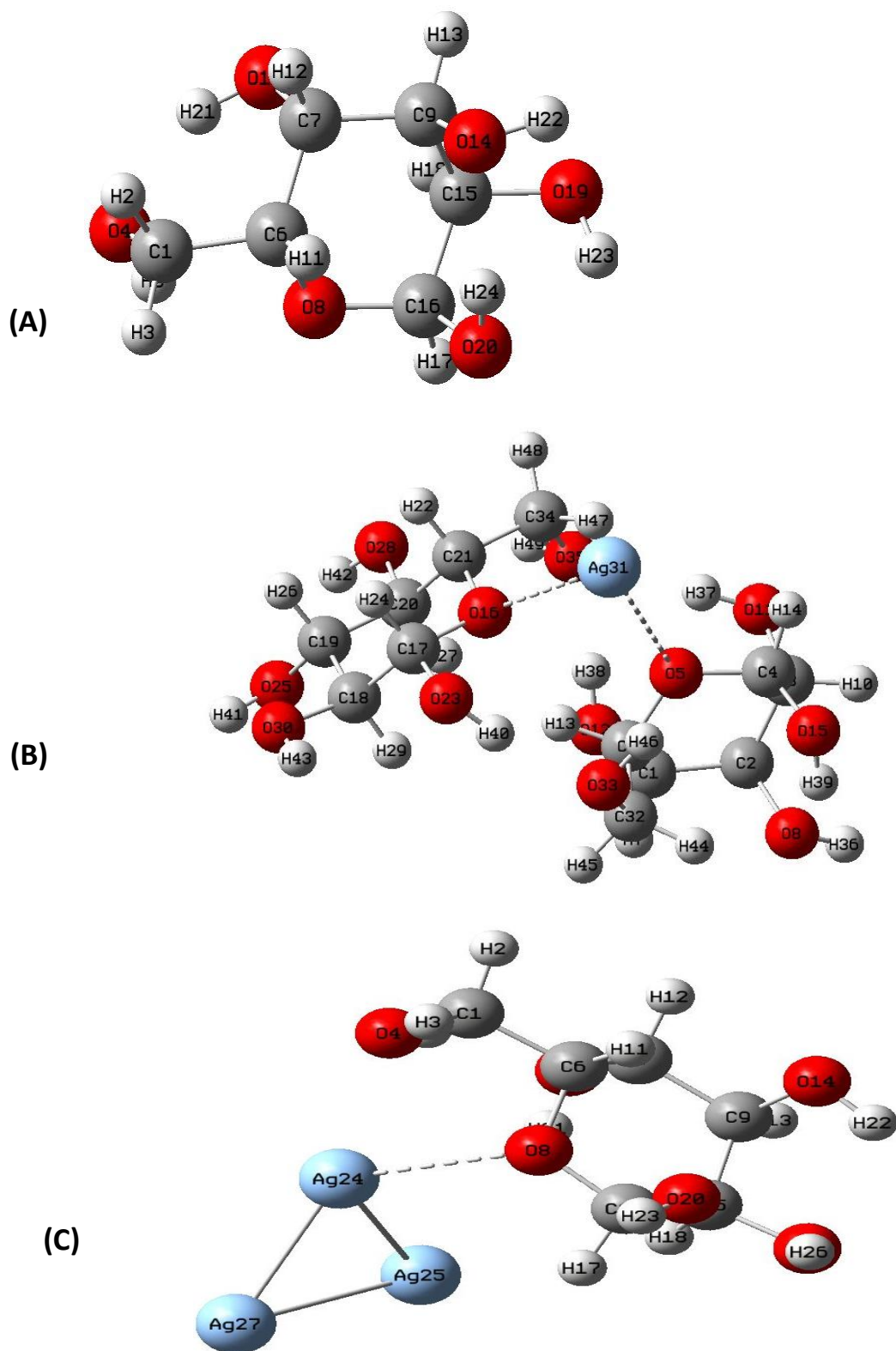


Figure 3-1: (A) pure alpha D glucose (B) 2-alpha D glucose with AgNP, and (C) alpha D-glucose with 3 AgNPs drawing by camo draw program.

### 3.3 Structural Properties

#### 3-3-1 Minimize Energy

Figure (3-2) illustrates a fully optimized geometric structure, including numbering and naming atoms. The internal coordinates represent the location of the atoms in terms of bonds, angles, and dihedral angles. To optimize the geometries, use theoretical B3LYP with mix basis set that selected for C, O, and H atoms was 6-311 + G\*, whereas the LANL2DZ\_basis set was used for Ag atoms and no symmetry constraints. The computations are converged to optimal geometries that correspond to real energy minima by allowing all parameters to become more relaxed. The absence of imaginary frequencies and the convergence of the four parameters (maximum force, RMS force, maximum displacement, and RMS displacement) improve energy minimization. As show in tables (3-1), (3-2)and (3-3)

Table 3-1: Parameters of compound of pure alpha -D glucose ( $C_6H_{12}O_6$ ).

Parameters	Numerical values	approach
Maximum force	0.000001	Converged
RMS force	0.000000	Converged
Maximum displacement	0.000015	Converged
RMS displacement	0.000004	Converged

Table 3-2: Parameters of compound of 2alpha -D glucose with one AgNP ( $C_{12}H_{24}O_{12}Ag$ ).

Parameters	Numerical values	approach
Maximum force	0.000002	Converged
RMS force	0.000000	Converged
Maximum displacement	0.000040	Converged
RMS displacement	0.000012	Converged

Table 3-3: Parameters of compound of alpha-D glucose with three AgNPs ( $C_6H_{12}O_6Ag_3$ ).

Parameters	Numerical values	approach
Maximum force	0.000000	Converged
RMS force	0.000000	Converged
Maximum displacement	0.000003	Converged
RMS displacement	0.000001	Converged

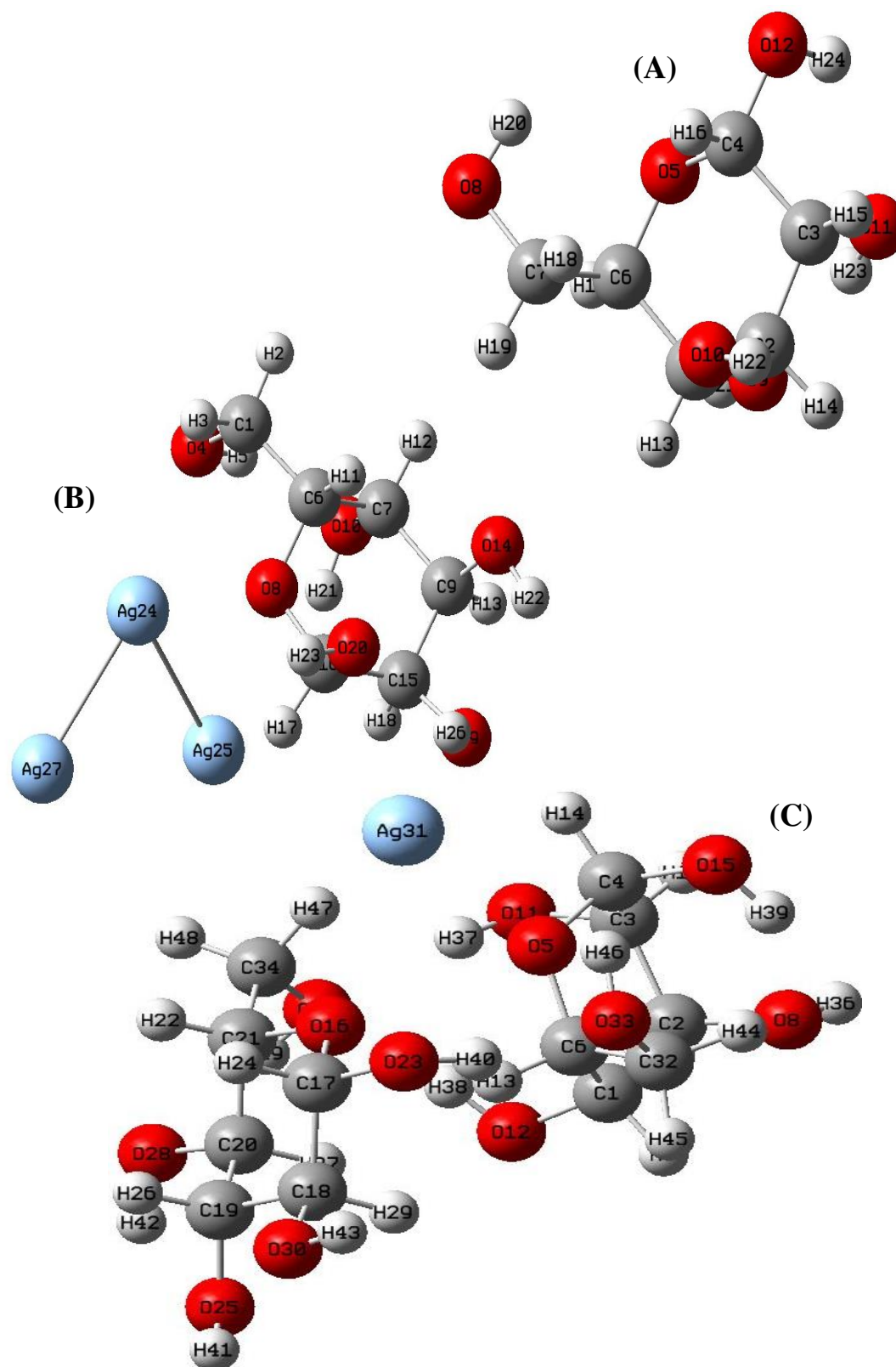


Figure3-2 : Fully optimization structure are represent (A) pure alpha D- glucose, (B) alpha D- glucose with 3AgNPs and (C)2alpha D- glucose with AgNP.



The molecule that resulted was discovered to have converged to optimum geometries with minimal energy equal to -687.140 Hartree, -1520.447 Hartree and -1124.712 Hartree respectively, the value of pure  $\alpha$ -D glucose, 2  $\alpha$ -D glucose with AgNP and  $\alpha$ -D glucose with 3AgNPs. These molecular structures are the most stable configurations. Figures (3-3), (3-4) and (3-5) depict the relationship between the number of improvement steps and total energy for the B3LPY. The best results for the thermal and electrical characteristics of both molecule configurations ( $C_{12}H_{24}O_{12}Ag$ ), ( $C_6H_{12}O_6Ag_3$ ) were obtained by engineering optimization, as indicated in the table (3-4)

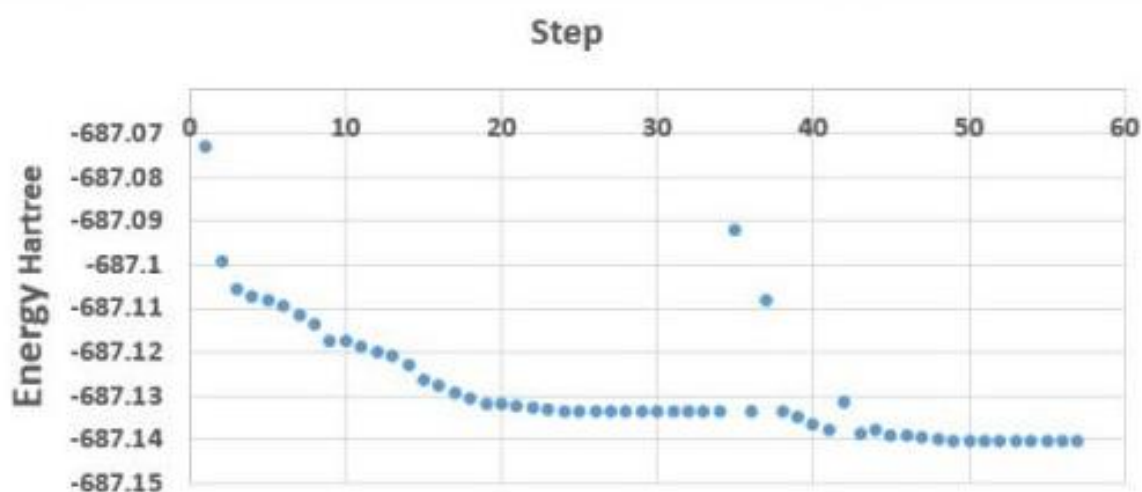


Figure 3-3 : Total energy curve for B3LPY of structure pure  $\alpha$ -D glucose.

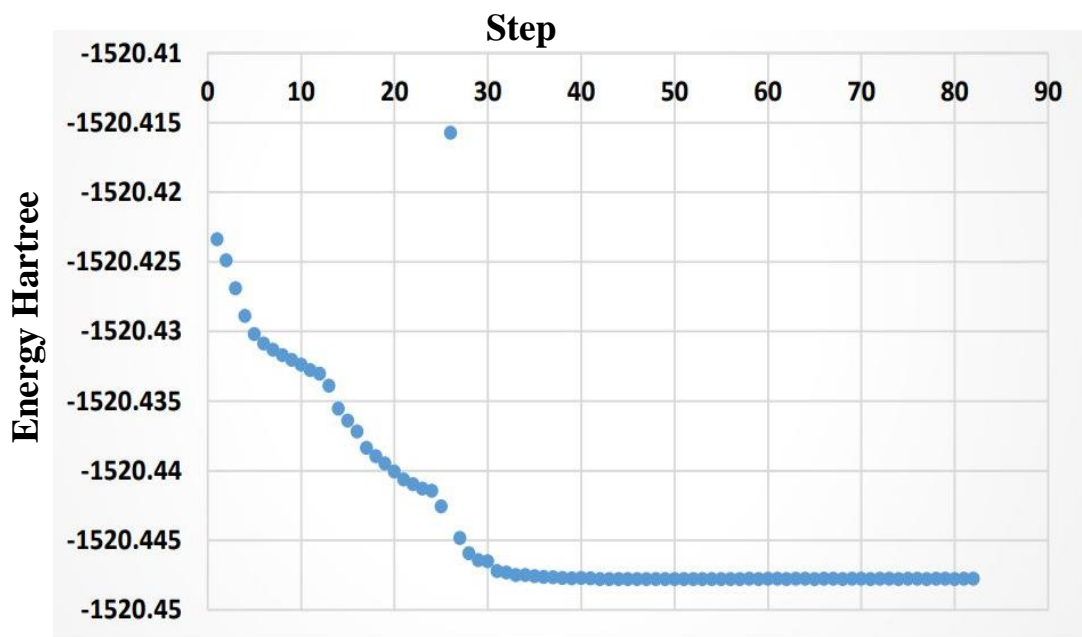


Figure 3-4: Total energy curve for B3LPY of structure of 2- $\alpha$  D glucose with one AgNP.

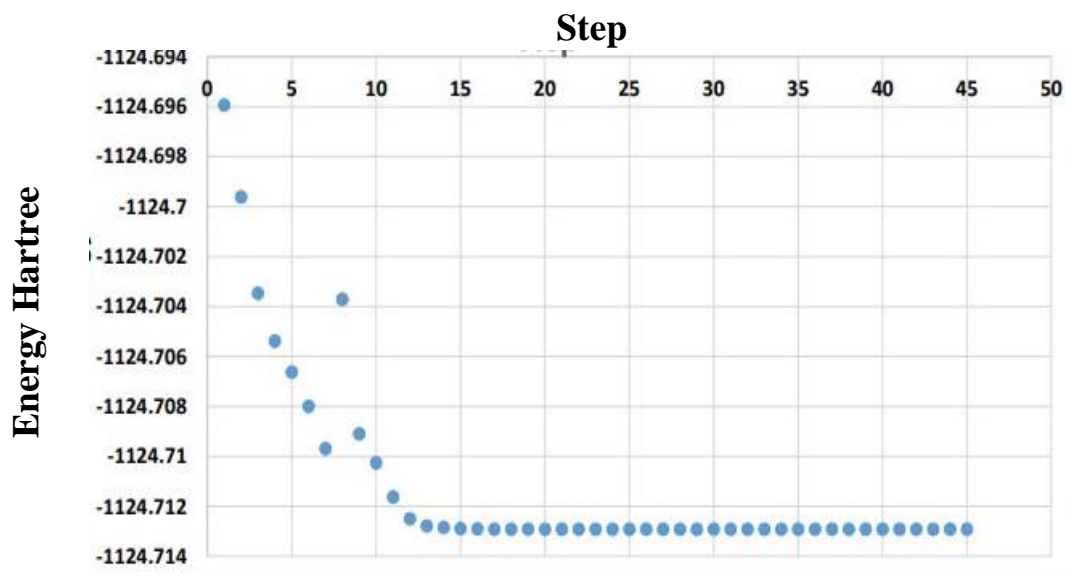


Figure 3-5: Total energy curve for B3LPY of structure of  $\alpha$  - D glucose with three of AgNPs.

Table 3-4: Electronic and thermal properties different of structure of pure  $\alpha$ -D glucose and  $\alpha$ -D glucose with silver nanoparticles.

<b>molecular structures</b>	<b>Properties</b>	<b>Numerical values</b>
<b>Pure <math>\alpha</math>-D-glucose</b>	Total Energy	-687.140287 Hartree
	Dipole Moment	4.439068 Debye
	Polarizability	83.005667 a.u.
	Temperature	298.150 Kelvin
	Pressure	1.00000 atm
	Zero Point Energy Correction	0.196287 Hartree
	Thermal Correction to Energy	0.208289 Hartree
	Thermal Correction to Entropy	0.209233 Hartree
	Thermal Correction to Free Energy	0.159299 Hartree
	E Thermal	130.704 kcal/mol
	Heat Capacity	46.82 cal/mol-kelvin
	Entropy	105.096cal/mol-kelvin
	<b>2 <math>\alpha</math>-D-glucose-Ag</b>	Total Energy
Dipole Moment		3.3422 Debye
Polarizability		223.1100
Temperature		298.150 Kelivin
Pressure		1 atom
Zero Point Energy Correction		0.399687Hartree
Thermal Correction to Energy		0.427419 Hartree
Thermal Correction to Entropy		0.428363 Hartree
Thermal Correction to Free Energy		0.338296 Hartree
E Thermal		260.210 Kcal/mol
Heat Capacity		103.053cal/mol. Kelivin
Entropy		189.563 cal/mol. Kelivin
<b><math>\alpha</math>-D-glucose-Ag3</b>		Total Energy
	Dipole Moment	4.237 Debye

Polarizability	237.590 a.u
Temperature	298.150 Kelivin
Pressure	1.00000 atm
Zero Point Energy Correction	1 atom
Thermal Correction to Energy	0.20061 Hartree
Thermal Correction to Entropy	0.219214 Hartree
Thermal Correction to Free Energy	0.220158 Hartree
E Thermal	0147378 Hartree
Heat Capacity	137.599 Kcal/mol
Entropy	62.915 cal/mol. Kelivin

### 3.3.2 Bond Lengths

The bond distance, or bond length, in molecular structure is the normal distance between two bonded atoms in a structure. It is an atomic bond's transferable attribute. Bond length is proportional to bond order; as the number of electrons participating in bond formation increases, so does bond length. Bond strength and bond dissociation energy are also inversely linked to bond length or distance. When all of the components that contribute to bond strength are recognized, a harder bond is smaller. The length of a bond is measured in Angstroms  $1\text{\AA} = 10^{-10} \text{ m}$  [194].

Table 3-5: bond lengths in ( $\text{\AA}$ ) of pure  $\alpha$ -D glucose and glucose with AgNPs at B3LYP and mix basis set 6-311+G\* and LAN2DZ.

code	Assignment	Bound distances	Code	Assignment	Bound distances
<b>pure <math>\alpha</math>-D Glucose <math>\text{C}_6\text{H}_{12}\text{O}_6</math></b>					
<b>R1</b>	C1-C2	1.53	R13	O12-H24	0.97
<b>R2</b>	C2-C3	1.53	R14	C3-H15	1.09
<b>R3</b>	C3-C4	1.53	R15	O11-H23	0.98
<b>R4</b>	C4-O5	1.47	R16	O10-H22	0.97
<b>R5</b>	O5-C6	1.47	R17	C2-H14	1.09
<b>R6</b>	C6-C7	1.52	R18	C1-H13	1.09
<b>R7</b>	C7-O8	1.45	R19	O9-H21	0.97
<b>R8</b>	C1-O9	1.47	R20	C6-H17	1.09
<b>R9</b>	C2-O10	1.49	R21	C7-H19	1.08

<b>R10</b>	C3-O11	1.45	R22	C7-H18	1.08
<b>R11</b>	C4-O12	1.40	R23	O8-H20	0.97
<b>R12</b>	C4-H16	1.08	R24	C6-C1	1.53
<b><i>α-D</i> Glucose with 3AgNPs C<sub>6</sub>H<sub>12</sub>O<sub>6</sub>Ag<sub>3</sub></b>					
<b>R1</b>	C15-C9	1.54	R15	Ag24-Ag27	2.68
<b>R2</b>	C9-C7	1.53	R16	C1-H2	1.09
<b>R3</b>	C7-C6	1.53	R17	C1-H3	1.09
<b>R4</b>	C6-O8	1.44	R18	O4-H5	0.97
<b>R5</b>	O8-C16	1.41	R19	C6-H11	1.09
<b>R6</b>	C16-C15	1.54	R20	C7-H12	1.09
<b>R7</b>	O19-C15	1.42	R21	O10-H21	0.97
<b>R8</b>	C15-O20	1.41	R22	C9-H13	1.09
<b>R9</b>	C9-O14	1.41	R23	O14-H22	0.96
<b>R10</b>	C7-O10	1.43	R24	C15-H18	1.09
<b>R11</b>	C1-O4	1.43	R25	O16-H26	0.96
<b>R12</b>	C6-C1	1.52	R26	O20-H23	0.96
<b>R13</b>	O8-Ag24	2.73	R27	C16-H17	1.09
<b>R14</b>	Ag24-Ag25	2.77			

<b>Two alpha-D Glucose with one AgNP C<sub>12</sub>H<sub>24</sub>O<sub>12</sub>Ag</b>					
<b>R1</b>	C34-C21	1.53	R26	C1-C2	1.54
<b>R2</b>	C21-C20	1.53	R27	C2-C3	1.54
<b>R3</b>	C20-C19	1.51	R28	C3-C4	1.53
<b>R4</b>	C19-C18	1.52	R29	C6-C32	1.53
<b>R5</b>	C18-C17	1.53	R30	C6 - C1	1.54
<b>R6</b>	C17-O16	1.42	R31	C6-O5	1.44
<b>R7</b>	O16-Ag31	3.05	R32	C4-O5	1.43
<b>R8</b>	C34-O35	1.43	R33	O5-Ag31	3.5
<b>R9</b>	C20 - O28	1.42	R34	C32-O33	1.42
<b>R10</b>	C19-O25	1.42	R35	C2-O8	1.45
<b>R11</b>	C18-O30	1.41	R36	C1-O12	1.42
<b>R12</b>	C17-O23	1.38	R37	C3-O11	1.41
<b>R13</b>	H49-O35	0.96	R38	C4-O15	1.40
<b>R14</b>	C34-H48	1.09	R39	O33-H46	0.96
<b>R15</b>	C34-H47	1.08	R40	C32-H45	1.09
<b>R16</b>	C21-H22	1.09	R41	C32-H44	1.09
<b>R17</b>	C20-H27	1.09	R42	C6-H13	1.08
<b>R18</b>	O28-H42	0.96	R43	C1-H7	1.09
<b>R19</b>	C19-H26	1.10	R45	O12-H38	0.97

<b>R20</b>	O25-H41	0.96	R46	C2-H9	1.09
<b>R21</b>	C18-H29	1.10	R47	O8-H36	0.96
<b>R22</b>	O30-H43	0.96	R48	O11-H37	0.96
<b>R23</b>	C17-H24	1.09	R49	C3-H10	1.09
<b>R24</b>	O23-H40	0.98	R50	C4-H14	1.09
<b>R25</b>	O16-C21	1.43	R51	H39-O15	0.97

When comparing the lengths of the bonds between  $\alpha$ -D glucose pure atoms in the table above, there is good agreement between the results and previous experiments using the DFT approach [195]. The length of the distance between carbon and carbon C-C ring atoms in both compounds  $C_6H_{12}O_6Ag_3$ ,  $C_{12}H_{24}O_{12}Ag$ , it is similar and its value is  $1.53 \text{ \AA}$ . Because by the electronic affinity between the atoms of similarity, However, there is a difference in the length of the bond between (C-C)CH<sub>2</sub>O, as its value is in the compound  $C_6H_{12}O_6Ag_3$   $1.43 \text{ \AA}$ , while in the compound  $C_{12}H_{24}O_{12}Ag$   $1.42 \text{ \AA}$ , a decrease occurred in the length of the bond, due to its association with oxygen atoms with high electronegativity and ability to attract electrons, in addition to its association with one silver atom. Carbon-hydrogen bonding, C-H, where the electronegativity is between two atoms, is practically same, as its value is 2.5 for carbon and 2.2 for hydrogen, therefore the distance is equal while its value is  $1.09 \text{ \AA}$  in both compounds. While the hydroxyl group O-H attached to the carbon atoms and the carbon-oxygen group C-O decreases the distance between them and its value,  $0.97 \text{ \AA}$ ,  $0.96 \text{ \AA}$  and  $1.41 \text{ \AA}$ ,  $1.38 \text{ \AA}$ , respectively, in both compounds due to the high electronegativity of oxygen, and is equal 3.44 to its comparison with carbon and hydrogen atoms.

However, we stress that the sort of bonding between the silver atoms and the oxygen atom is an adsorption form, and it is considered a weak binding, similar to the Vanned Waltz forces. Its value in both compounds is 3.5 and 2.7, with the difference related to the distance between them caused by the type of interaction



### 3-3-3 Bond Angles

Within the molecules, the atoms are arranged in a regular geometric structure, and the angle bond may be described as the average distance between two atoms linked together in every molecule, or it can be characterized as the angle created between three atoms joined together. The bond angles are determined by the number of single electron pairs in the chemical structure, generally determined by degrees. Table (3-6) shows the selected bond angles determined using DFT techniques.

Table 3-6: Bond angle in (degree) pure  $\alpha$ -D glucose and  $\alpha$ -D glucose with AgNPs at B3LYP and mix basis set 6-311+G\* and LAN2DZ.

Code	Assignment	Value	Code	Assignment	Value
<b>pure <math>\alpha</math>-D Glucose</b>					
A1	C1-C2-C3	111.4	A2	C3-C4-O5	109.6
A3	O5-C6-C1	110.9	A4	C7-H18-H19	35.7
A5	C6-C7-H17	29.7	A6	C7-O8-H20	107.9
A7	C6-C1-H13	110.3	A8	C1-O9-H21	111.2
A9	C1-C2-H14	108.5	A10	C2-O10-H22	110.9
A11	C2-C3-H15	110	A12	C3-O11-H23	108.1
A13	C3-C4-H16	112.1	A14	O5-C4-O12	107.05
A15	C4-O12-H24	107.4	A16	O5-C4-H16	110
<b><math>\alpha</math>-D Glucose with 3AgNPs</b>					
A1	C6-C7-C9	109.7	A2	C15-C16-O8	112.7
A3	C9-C15-C16	114.1	A4	O8-C6-Ag24	46.5
A5	Ag24-Ag25-Ag27	55.7	A6	O8-C6-C1	106.7
A7	C6-C1-O4	113.3	A8	C1-H3-H2	36
A9	C1-O4-H5	106.4	A10	C1-C6-H11	108.8
A11	C6-C7-H12	108.7	A12	C7-O10-H21	111.4
A13	H13-C9-O14	110.4	A14	C9-O14-H22	106.1
A15	H15-C15-O19	107	A16	C15-O19-H25	106.5
A17	C15-C16-H17	109.9	A18	C16-O20-H23	108.9
<b>2 <math>\alpha</math>-D glucose with one AgNP</b>					
A1	C17-C18-C19	110.4	A2	C19-C20-C21	109.7
A3	C21-O15-C17	114	A4	O15-Ag31-O5	56.2
A5	C17-H24-O23	41.6	A6	C17-O23-H40	111.06
A7	C18-O33-H43	107.5	A8	H29-C18-O33	110.4
A9	C18-C19-H26	108.7	A10	C19-O25-H41	107.6
A11	C20-O28-H42	106.9	A12	C19-C20 -H23	107.8
A13	H22-C21-C34	108.2	A14	C34-H48-H47	35.4
A15	C34-C35-H49	107.2	A16	C6-C1-C2	113
A17	C2-C3-C4	109.4	A18	C4-O5-C6	118.1
A19	H46-O33-C32	107	A20	C32-H44-H45	35.9



A21	C32-C6-C1	115.4	A22	O5-C6-H13	102.3
A23	C2-C1-H7	106.4	A24	C2-O12-H38	109.2
A25	H9-C2-O8	110.5	A26	C2-C3-H10	108.4
A27	C2-O8-H36	108.8	A28	C3-O11-H37	111.2
A29	H14-C4-H39	132.4	A30	C3-C4-O15	112.8

When compared to glucose, the bond angle C-C-C ring for both molecules is equivalent to  $114^\circ$  and  $109^\circ$  in the table above. Because the electron cloud between the carbon atoms is equivalent, the value is the same. As for the bond angle O-C-C, its value in both compounds is  $106.7^\circ$  and  $107.6^\circ$ , respectively. We notice an increase caused by the force of repulsion between the electrons in the outer orbits. According to the repulsion of the electronic pairs, the repulsion of electrons in the valence shell occurs to the maximum extent possible until it reaches the lowest energy and most stable geometric shape.

While the angle bond C-H-H has near values in both compounds  $C_6H_{12}O_6Ag_3$  and  $C_{12}H_{24}O_{12}Ag$  is equal to  $35.5^\circ$  and  $36^\circ$  due to the proximity of the electronegative values of the carbon and hydrogen atoms

The angle of bonding of silver with oxygen (O-C -Ag) and (O- Ag-O ). On the other hand, is a weak bond of its kind vander-Wals ls forces. Due to the uneven electric charge, the values of this bonding differ in both compounds and are  $46.5^\circ$  and  $56.2^\circ$ . The density of electrons is greater near the molecule's tip. A simple transient polarization (instantaneous polarization) happens.

### 3-3-4 dihedral angle

The le generated when two planes cross is known as a dihedral angle. The Cartesian planes are the two intersecting planes here. Cartesian geometry is specified for two- and three-dimensional planes, and it specifies the forms of various things. Table (3-7) show the selected dihedral angles determined using DFT techniques.

Table 3-7: Dihedral angle in (degree) of pure  $\alpha$ -D glucose and  $\alpha$ -D glucose with AgNPs at B3LYP and mix basis set 6-311+G\* and LAN2DZ.

Code	Assignment	Value	Code	Assignment	Value
<i>pure <math>\alpha</math>-D Glucose</i>					
D1	C1-C2-C3-C4	51.6	D2	C4-O5-C6-C1	-53.2
D3	H20-O8-C7-H19	-166.1	D4	H13-C1-O9-H21	70.5
D5	H17-C6-C7-H18	-176.1	D6	H22-O10-C2-H14	46.4
D7	H15-C3-O11-H23	156.4	D8	H24-O12-C4+H16	164.2
<i><math>\alpha</math>-D Glucose with 3AgNPs</i>					
D1	C6-C7-C9-C15	49	D2	C15-C16-O8-C6	-53.1
D3	H3-C1-C6- H11	-59.4	D4	H2-C1-O4-H5	67.5
D5	O8-Ag24-Ag27- Ag25	-79.6	D6	H17-C16-O20-H23	-44.1
D7	H18-C15-O19-H26	-137	D8	H13-C9-O14-H22	-73.9
D9	H121-O18-C7-H12	168.8			
<i>2 <math>\alpha</math>-D glucose with one AgNP</i>					
D1	C1-C2-C3-C4	51.9	D2	C4-O5-C6-C1	-48.4
D3	H46-O33-C32-C6	-61.3	D4	H44-C32-H45-O33	118
D5	H13-C6-O8-Ag31	51.7	D6	H14-C4-O15-H39	-154
D7	H10-C3-O11-H37	-164.2	D8	H36-O8-C2-H9	37.8
D9	H7-C1-O12-H38	160.3	D10	C17-C18-C19-C20	55
D11	C20-C21-O16-C17	-61	D12	H49-O35-C34-H47	-168.5
D13	H48-C34-C21-H22	158	D14	C17-O15-O33-Ag31	-104.5
D15	H40-O23-C17-H24	-162.9	D16	H29-C18-O30-H43	67
D17	H26-C19-O25-H41	-65.8	D18	H27-C20-O28-H42	72.4

Results in the above table indicate a difference in dihedral angles for both compounds, due to the difference in bonds, i.e. the distance between the atoms and the bonding angles, in addition to the rotation of those atoms from -180 to +180. If the rotations of those atoms are clockwise, the value becomes positive. If the rotation is counter clockwise the value becomes negative.

### 3-3-5 Natural Population Analysis (NPA)

The natural charge is directly related to the compound's vibrational characteristics and indicates how the electronic structure changes when one atom is shifted. As a result, it has a direct link with the molecule's chemical bonds. It has an impact on molecule electrical structure, polarizability, dipole moment, and other characteristics [197]. The molecule's native atomic charge distribution has been attained at B3LYP levels in the solid state. Table (3-8), shows the achieved values of the natural charges of alpha-D glucose with nanoparticles. The total natural charge of  $(C_6H_{12}O_6 Ag_3)$  and  $(C_{12}H_{24}O_{12}Ag)$  is zero.

Table 3-8: Natural atomic charges of the  $(C_6H_{12}O_6 Ag_3)$ .

NO.	Atoms	Value	NO.	atoms	Value
1	C1	-0.244	15	C15	-0.073
2	H2	0.256	16	C16	0.135
3	H3	0.271	17	H17	0.267
4	O4	-0.593	18	H18	0.263
5	H5	0.446	19	O19	-0.626
6	C6	-0.100	20	O20	-0.261
7	C7	-0.050	21	H21	0.429
8	O8	-0.369	22	H22	0.411
9	C9	-0.329	23	H23	0.445
10	O10	-0.618	24	Ag24	0.139
11	H11	0.260	25	Ag25	-0.297
12	H12	0.267	26	H26	0.426
13	H13	0.242	27	Ag27	-0.028
14	O14	-0.608	-----	-----	-----

Due to hydrogen atom's strong electronegativity, all hydrogen atoms in the molecular structure have a positive charge. According to Malikh's charge

distribution, all carbon and silver atoms are negatively charged, with the exception of C16 and Ag24, which are positively charged due to their interaction with two oxygen atoms (O8, O20) that have high electronegativity, as shown in the figure 3-7.

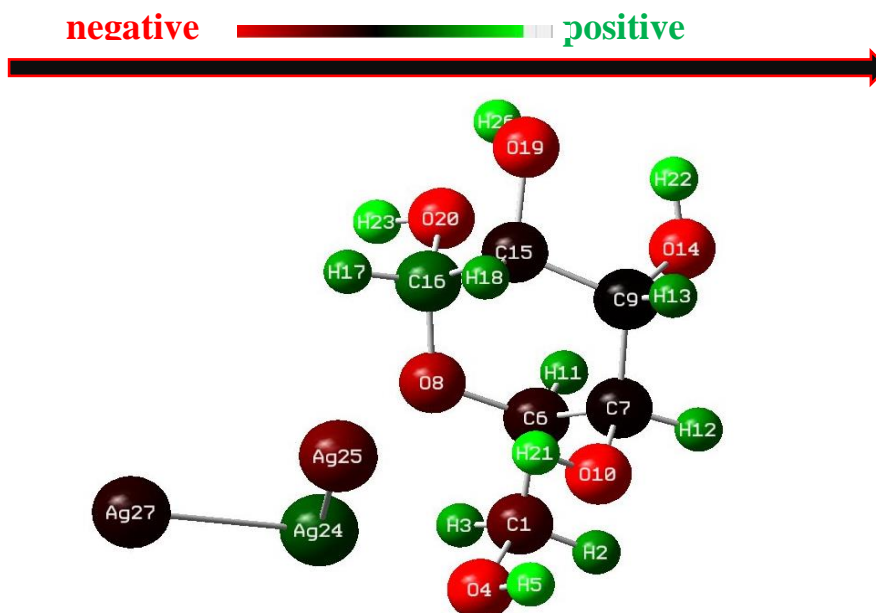


Figure 3- 7: The charge distbustion of  $\alpha$ -D glucose with 3Ag NPs.

When comparing the charge distributions in both compounds, as shown in the table 3-9, all hydrogen atoms have a positive charge due to the flow of their single electron towards oxygen atoms with a negative charge and high electronegativity, whereas carbon and silver atoms have a negative charge, with the exception of carbon 4 and carbon 17, which have a positive charge. because of its high association with the negatively charged oxygen atom, as seen in the figure (3-8)

Table 3-9: Natural atomic charges of the ( $C_{12}H_{24}O_{12}$  Ag).

NO.	Atoms	Value	NO.	atoms	Value
1	C1	-0.028	26	H26	0.228
2	C2	-0.079	27	H27	0.226
3	C3	-0.070	28	O28	-0.631

4	C4	0.010	29	H29	0.231
5	O5	-0.037	30	O30	-0.625
6	C6	-0.183	31	Ag31	-0.104
7	H7	0.256	32	C32	-0.218
8	O8	-0.635	33	O33	-0.607
9	H9	0.255	34	C34	-0.236
10	H10	0.250	35	O35	-0.640
11	O11	-0.595	36	H36	0.450
12	O12	-0.596	37	H37	0.419
13	H13	0.264	38	H38	0.408
14	H14	0.252	39	H39	0.415
15	O15	-0.593	40	H40	0.428
16	O16	-0.359	41	H41	0.430
17	C17	0.114	42	H42	0.431
18	C18	-0.021	43	H43	0.425
19	C19	-0.052	44	H44	0.223
20	C20	-0.041	45	H45	0.246
21	C21	-0.065	46	H46	0.440
22	H22	0.252	47	H47	0.280
23	O23	-0.587	48	H48	0.282
24	H24	0.235	49	H49	0.446
23	O23	-0.587	48	H48	0.282
25	O25	-0.625	-----	-----	-----

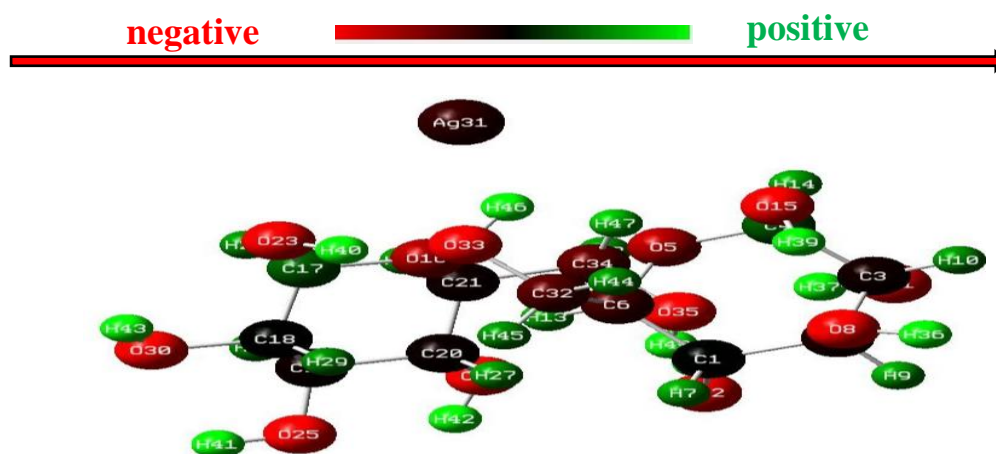


Figure 3-8: The charge distribution of 2 alpha -D glucose with one Ag NP.

### 3-4 HOMO–LUMO Energy

The HOMO-LUMO energies are well-known quantum mechanical descriptors that play a key role in the regulation of a wide range of chemical interactions. Distribution of frontier orbitals offers information about the molecule's reactivity and can be utilized to pinpoint the active site[198]. The HOMO - LUMO energies for  $\alpha$ -D glucose with Ag NPs were estimated using the B3LYP, and the mixed basis. Because HOMO-type molecular orbitals have less energy than LUMO-type molecular orbitals, electrons are naturally maintained HOMO in the ground state, leaving LUMO orbits empty or unoccupied. It is possible that every occupied MO has a pair of electrons with alpha ( $m_s = \frac{1}{2}$ ) or beta ( $m_s = -\frac{1}{2}$ ) spin, resulting in a net spin of zero since all of the alpha electrons cancel out all of the beta electrons. Likewise, no unpaired electrons have been found, supporting the zero total spin and single-single multiplicity.

Table 3-10: Energy gap of alpha-D glucose with and without Ag NPs the DFT method.

Molecule	E LUMO (eV)	E HOMO (eV)	E LUMO – E HOMO gap (eV)
$C_6H_{12}O_6$	-7.253	- 0.217	7.035
$C_{12}H_{24}O_{12}Ag$	- 0.718	- 4.158	3.440
$C_6H_{12}O_6 Ag_3$	- 0.308	- 4.666	4.358

The energies of the deepest core orbitals are almost comparable, meaning that the alpha and beta electrons are in essentially the same spatial orbit. As the energy of the orbital increases, so does the energy differential between the alpha and beta orbitals, resulting in uneven energies in the outer orbits. The first compound is doing  $C_{12}H_{24}O_{12}Ag$ , 526 MOs, were created in this study; the first 106 MOs are totally filled with electrons and are referred to as **occupied MOs**, while the remaining 420 molecular orbitals are vacant and referred to as **unoccupied MOs**. According to the energy level alignment of these orbits, the 106th MO is the highest energy orbital among the occupied MOs while the 107th MO is the lowest energy orbital among the unoccupied ones. The HOMO

and LUMO for the  $\alpha$ -D glucose with AgNPs using the DFT techniques at the mix basis sets are shown in figures (3-9) (3-10.) and (3-11) HOMO and LUMO values for all structures are -0.718 eV, -4.158 eV, -0.308 eV, -4.666 eV, -0.217 eV and -7.253 eV respectively, as shown in table 3-10. The energy gap between them is determined to be  $\Delta E = 3.440$  eV,  $\Delta E = 4.358$  eV and 7.035. By analyzing the energy gap for both structures after adsorbing them with various atoms of nano silver cluster, we see that as the number of silver nano atoms grows, so does the energy gap at the molecular structure. This is owing to the atoms' size and the electronic orbitals overlapping between the silver nanoparticles and the oxygen atom. Because of the localized hybridization nature of  $\alpha$ -D-glucose and silver, the  $\alpha$ -D-glucose HOMO and LUMO states distributed throughout the molecule become strongly localized on O and Ag atoms after adsorption [196].

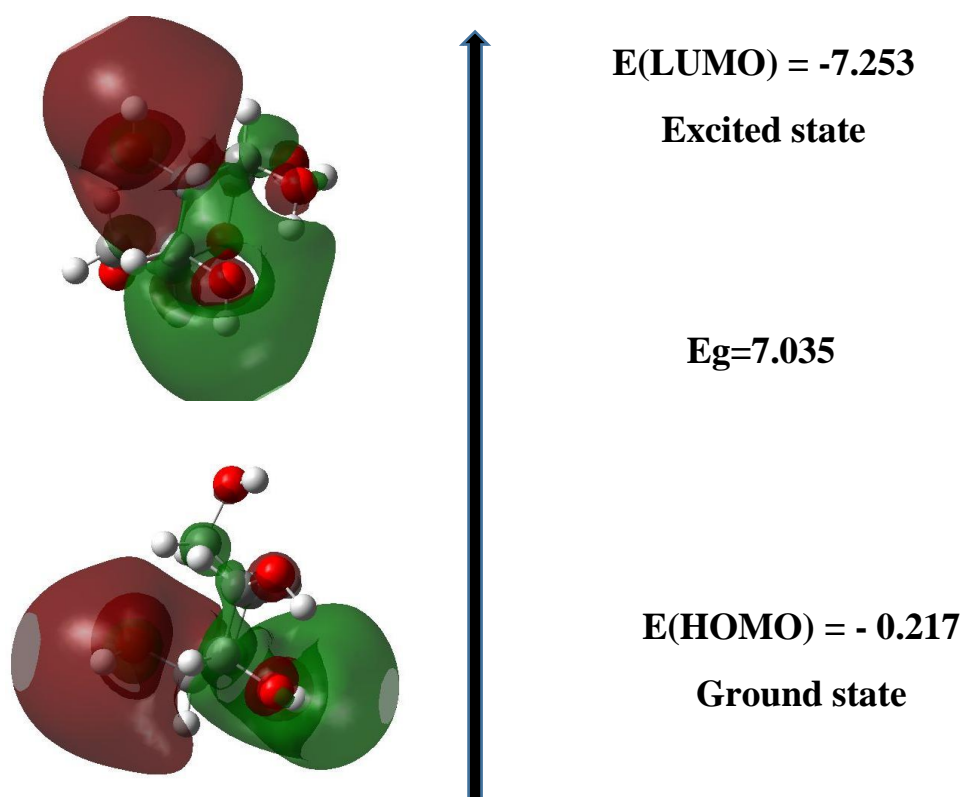
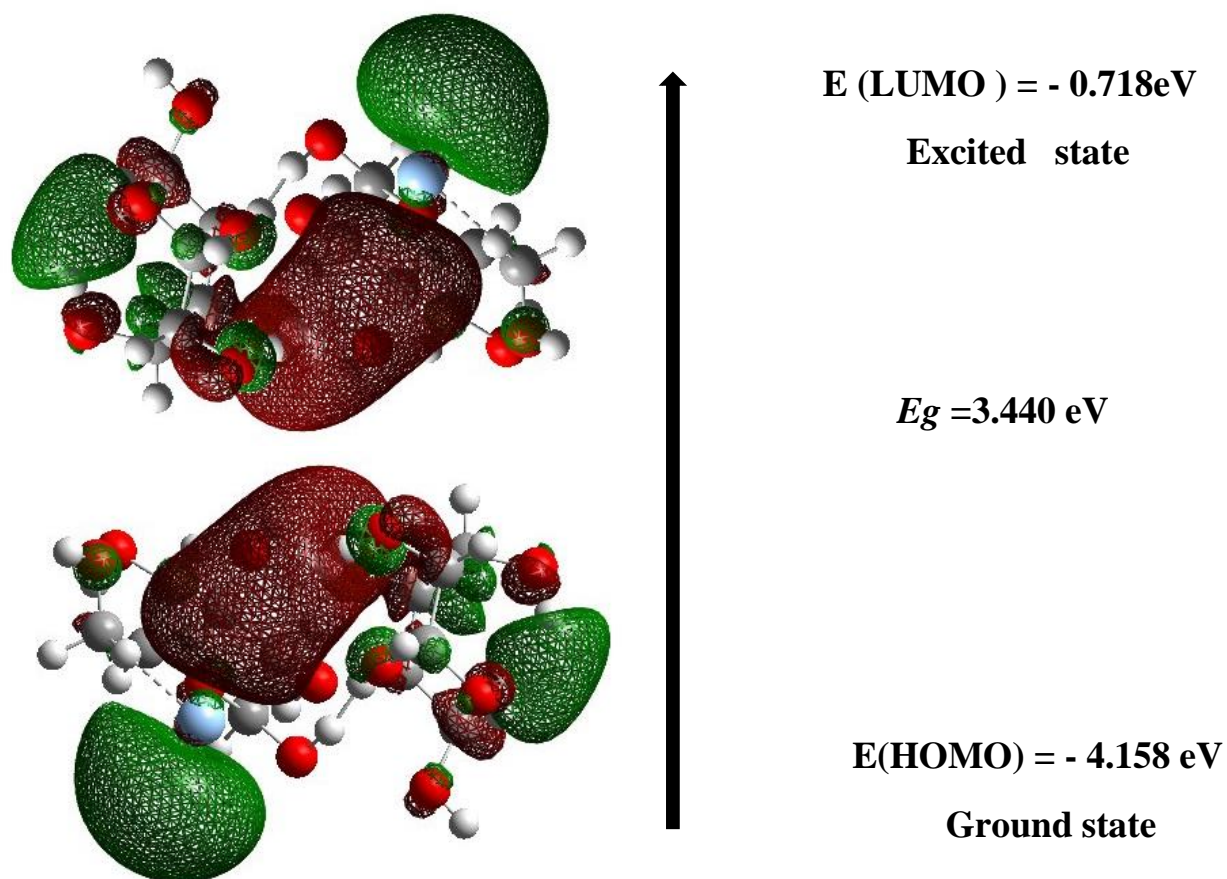
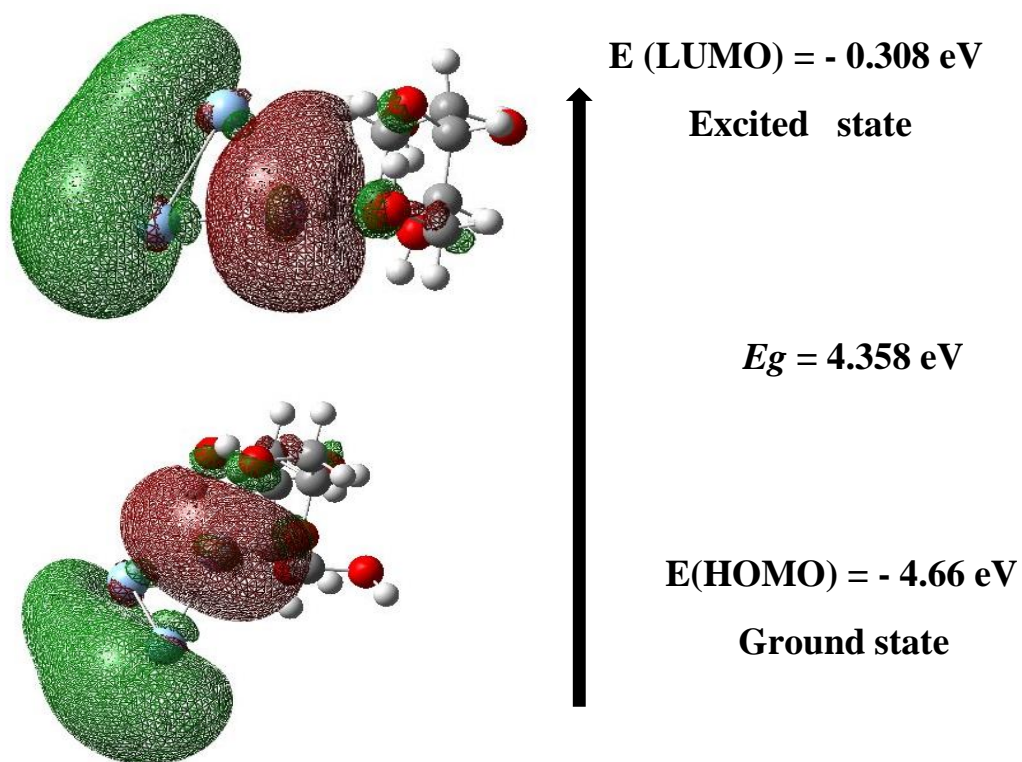


Figure 3-9: HOMO- LUMO state of  $C_6H_{12}O_6$ .

Figure 3-10: HOMO- LUMO state of  $\text{C}_{12}\text{H}_{24}\text{O}_{12}\text{Ag}$ .Figure 3-11: HOMO- LUMO state of  $\text{C}_6\text{H}_{12}\text{O}_6\text{Ag}_3$ .



### **3-5 Molecular Electrostatic Potential (MEP) Surface**

MEP has been calculated at the B3LYP using mix basis sets. The red and blue hues indicate electron-rich and electron-poor areas, respectively, while the green collar represents the neutral electrostatic potential. As illustrated in figure (3-12) there are multiple possible locations for electrophilic attacks over the, Ag31, Ag24, Ag25 and Ag27 atoms. Negative (red) MEP areas are related to electrophilic reactivity, whereas positive (blue) MEP regions have been linked with nucleophilic reactivity. Although areas with a negative potential are over electronegative atoms, areas with a positive potential are above hydrogen atoms.

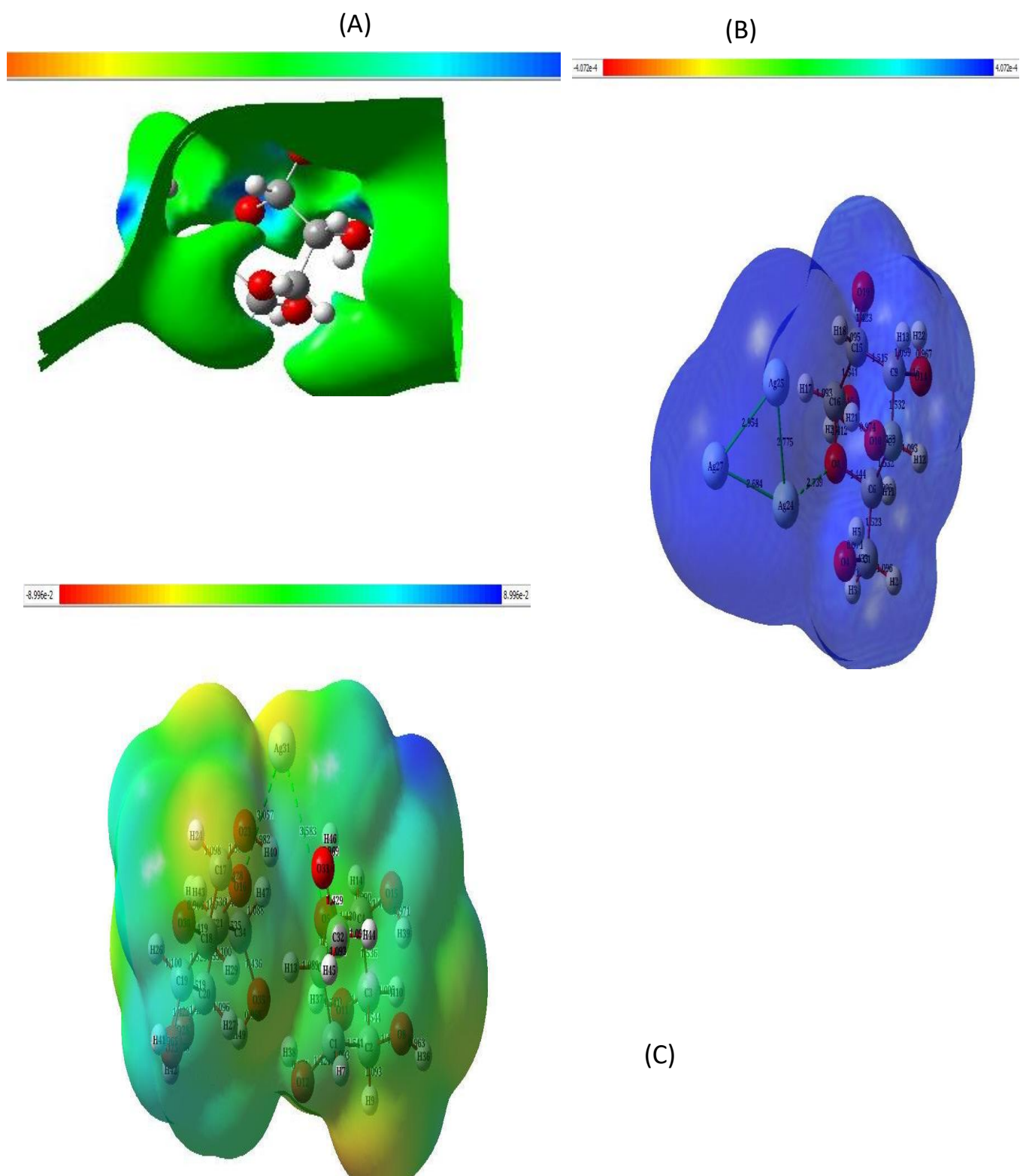


Figure 3-12: Molecular electrostatic potential in 3D (A) pure  $\alpha$ -D glucose (B)  $\alpha$ -D glucose with 3AgNPs and (C) 2 $\alpha$ -D glucose with one AgNP.

Only the top surface is seen if all MEP surfaces are plotted with all iso-surface values. To view all MEP surfaces, plot each surface as a contour around the molecule, as illustrated in figure 3-13

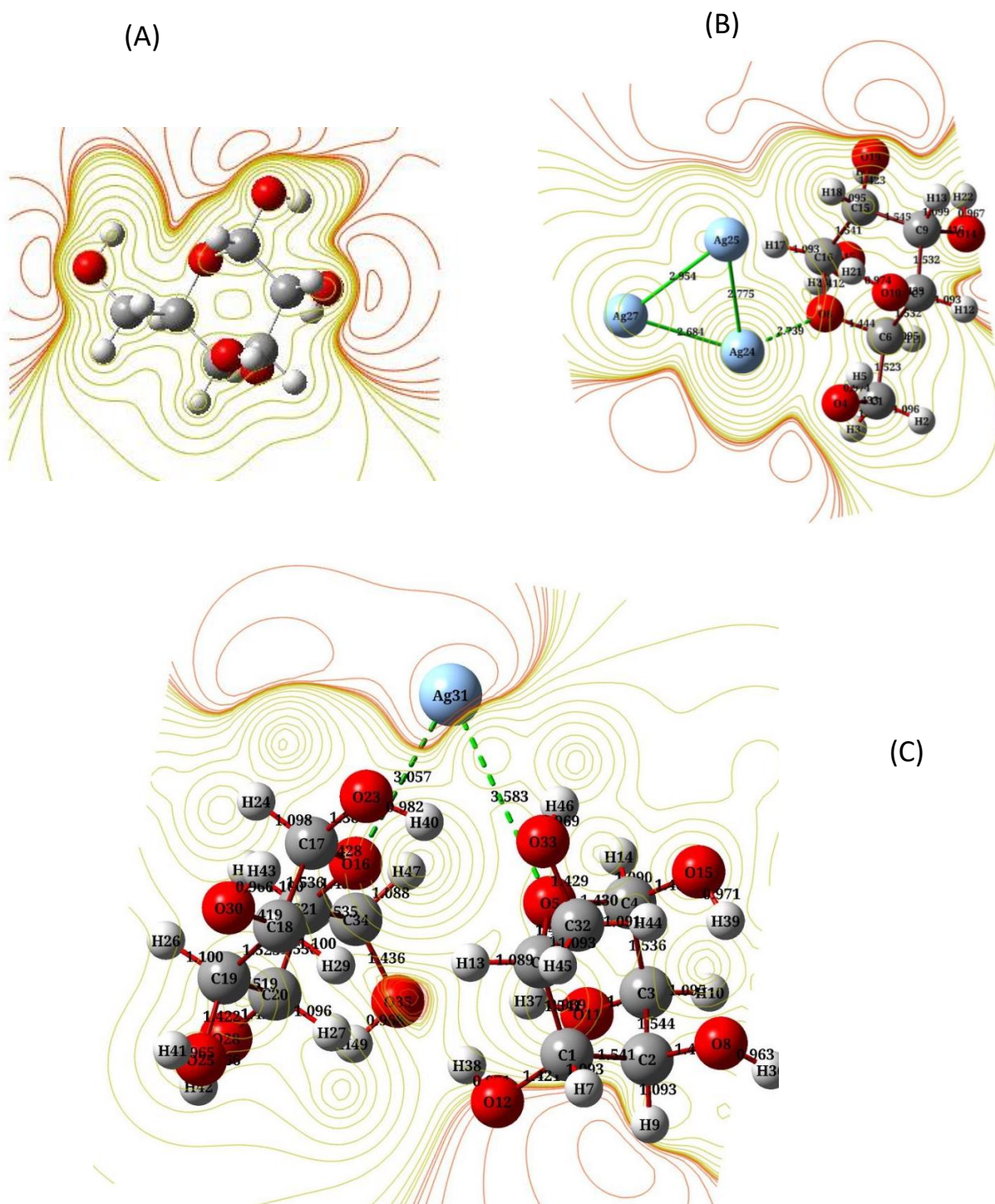


Figure 3- 13: Molecular electrostatic potential contour surface show (A) pure  $\alpha$ -D glucose (B)  $\alpha$ -D glucose with 3AgNPsand (C)  $2\alpha$ -D glucose with one AgNP.

## 3.6 Spectroscopy Properties

### 3.6.1 Vibrational Frequencies & IR spectra analysis.

Both chemical structures have a different number of atoms, hence they have a different number of vibration mode as the first compound,  $C_{12}H_{24}O_{12}Ag$ , has 49 atoms and 141 modes, while the second compound,  $C_6H_{12}O_6Ag_3$ , has 27 atoms and 75 modes. The vibration bands analyzed are assigned using DFT techniques, B3LYP, with the mix basis set. Generally, it is observed from IR spectra analysis distinctive bands from carbohydrates due to the C-O and C-C group's vibration modes at range  $400 - 1500\text{ cm}^{-1}$ . In addition to the C-H and O-H vibration group around  $2900-3700\text{ cm}^{-1}$  [199, 200]. The oxygenated functional groups were taken into consideration in both when they interact directly with silver or are not associated directly with it. The assignment of the most influential groups is shown in figure (3-14). These wavenumbers were found to be matched to those found in the literature for these species indicating the possibility of adsorbed D-glucose on the silver surface, although there are a few minor differences that can be explained by the sample's varied carbohydrate concentration from that used in that literatures[201, 202]. Furthermore, it was observed remarkable red shifts in frequency at the strong bands occurring at  $3703$  and  $3460\text{ cm}^{-1}$  for  $\alpha$ -D glucose/Ag3 appear at  $3615$  (O4-H5) and  $3577$  (O10-H21)  $\text{cm}^{-1}$ , with respect to the  $2\alpha$ -D glucose/Ag structure and this indicates that the C-H bond is affected by the interaction of  $2\alpha$ -D glucose with AgNPs cluster. Red shift means that IR spectrum of  $\alpha$ -D glucose configuration with a closed cluster of Ag3 shifts towards short wavelengths (high energies) confirming the enhancement of nanoparticles surface due to the effect of glucose that works as a camping agent[6]. Additionally, the band at  $796\text{ cm}^{-1}$  appears in the spectra of alpha-D-glucose/Ag structure, suggesting dependence on C-O configuration. This is also confirmed by the frequency shift to  $760\text{ cm}^{-1}$  in the spectrum alpha-D-glucose/Ag3. Analysis of normal coordinates [203] has

shown that CCO, OCO bending and C-O stretching modes contribute to the weak band at  $760\text{ cm}^{-1}$ .

On the other hand, the  $70\text{-}300\text{ cm}^{-1}$  frequency range also contains several interesting bands that were recognized through the animation in the Gaussian view program in the  $\alpha\text{-D}$  glucose/Ag<sub>3</sub> structure. Most of the bands appearing in this region arise from normal modes vibrations involving Ag (24), Ag (25) and Ag(27) motions. The bands at  $71$ ,  $127$  and  $229\text{ cm}^{-1}$  including Ag(24)-Ag(25)-Ag(27) bending (sci.), Ag(24)-Ag(25)-Ag(27) stretching (symm.) and Ag(24)-Ag(25)-Ag(27) stretching (w) motion respectively. However, the motion of AgNPs in the  $2\alpha\text{-D}$  glucose/Ag structure was detected at bands  $94$ ,  $202$  and  $247\text{ cm}^{-1}$  involving O(5)-Ag(31)-O(16) bending (sci.), O-Ag-O stretching (asymm.) and O-Ag-O stretching (mw) motion respectively.

Table 3-11: Comparison of calculated wavenumbers ( $\text{cm}^{-1}$ ) for final adsorption geometries of studied molecules indicating to the vibrational normal modes of main functional groups.

Molecular structure	Most probable assignment	Type of Mode	Approximate wavenumbers/ $\text{cm}^{-1}$
<b><math>\alpha\text{-D-glucose/Ag}_3</math></b>	$\nu$ C-O $\delta$ CCO, OCO	side stretch, bending	760
	$\nu$ C-O, C-C $\delta$ COH	Stretching, Bending	1,066 1,039
	$\nu$ C-C	Stretching	1,309
	$\delta$ ( $\rho_s$ ) C-H	Bending (sci.)	1,468
	$\nu$ C-H	Stretching (sym.)	3,037
	$\nu$ O-H	Stretching	3,577
<b><math>2\alpha\text{-D-glucose/Ag}</math></b>	$\nu$ C-O $\delta$ CCO, OCO	side stretch, bending	796
	$\nu$ C-O, C-C $\delta$ COH	Stretching, Bending	1,038 1,111
	$\nu$ C-C	Stretching	1,309
	$\delta$ ( $\rho_s$ ) C-H	Bending (sci.)	1,500
	$\nu$ C-H	Stretching	3,073
	$\nu$ C-H	Stretching (asym.)	3,148
	$\nu$ O-H	Stretching	3,640

$\nu$ = stretching,  $\delta$ = bending,  $\rho_s$ = Scissoring is change in angle between a group of atoms in the same plane.

Sym. =symmetric, asym. = asymmetric, w= weak, s = strong, m = moderate, w = weak,

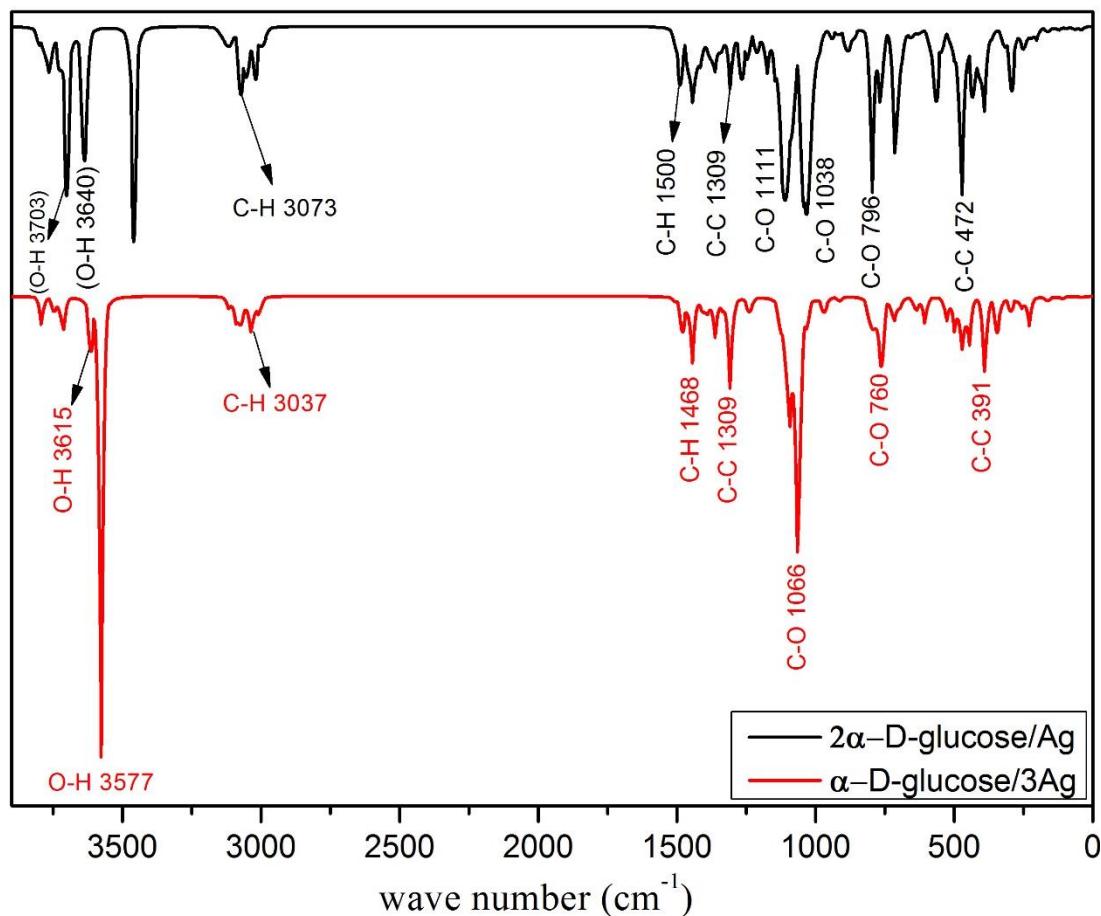


Figure 3-14: IR spectra of structures of glucose with AgNPs;  $\alpha$ -D-glucose-Ag<sub>3</sub> (red), and 2  $\alpha$ -D-Glucose-Ag (black) including the assignment of the most influential groups.

### 3-6-2 Vibrational modes

Vibration of molecules is a property caused by the periodic movement of atoms inside the molecule. The frequency of vibration is the frequency of the periodic movement. This vibration happens as a result of the atoms absorbing a certain amount of energy until the molecule achieves stability. Number of vibrations inside a molecule varies with the number of atoms in the molecule, and each atom has a certain number of degrees of freedom. As seen in the table (3-12), the first compound  $C_6H_{12}O_6Ag_3$  has 75 modes while the second compound  $C_{12}H_{24}O_{12}Ag$  has 141 modes.

Table 3-12: The number of vibrations mode of alpha-D glucose with AgNPs.

Mode	Frequency $\text{cm}^{-1}$	Type of mode
$\text{C}_6\text{H}_{12}\text{O}_6\text{Ag}_3$		
1	13	bending
2	26	stretching
3	28.75	Rocking
4	38.70	Rocking
5	55.20	Rocking
6	71.90	Bending
7	82.91	Rocking
8	103.57	Stretching
9	111.56	Twisting
10	132.54	Rocking
11	161.31	Bending
12	172.01	Rocking
13	207.24	Bending
14	229.23	Twisting
15	253.13	Bending
16	271.71	Twisting
17	295.25	Rocking
18	300.59	Rocking
19	329.98	Rocking
20	344.00	Twisting
21	388.85	Twisting
22	446.36	Rocking
23	468.10	Rocking
24	475.78	Twisting
25	498.44	Twisting
26	528.87	Rocking
27	604.45	Twisting
28	638.58	Rocking
29	694.79	Rocking

30	718.89	Wagging
31	763.35	Wagging
32	791.16	Rocking
33	808.09	Rocking
34	885.46	Twisting
35	912.31	Bending
36	958.43	Twisting
37	970.94	Twisting
38	1033.03	Twisting
39	1060.70	Twisting
40	1068.21	Bending
41	1087.01	Rocking
42	1096.93	Rocking
43	1113.14	Rocking
44	1123.45	Stretching
45	1129.35	Stretching
46	1229.38	Twisting
47	1237.21	Twisting
48	1246.80	Twisting
49	1289.00	Twisting
50	1309.15	Twisting
51	1332.61	Twisting
52	1361.27	Twisting
53	1370.13	Twisting
54	1385.40	Twisting
55	1393.21	Rocking
56	1404.32	Twisting
57	1410.17	Twisting
58	1412.89	Twisting
59	1444.35	Wagging
60	1447.02	Wagging
61	1466.70	Twisting



62	1481.55	Twisting
63	1506.53	Bending
64	3005.94	Stretching
65	3032.89	Stretching
66	3041.49	Stretching
67	3066.50	Stretching
68	3073.27	Stretching
69	3087.58	Stretching
70	3114.60	Stretching
71	3577.14	Stretching
72	3615.41	Stretching
73	3715.93	Stretching
74	3745.46	Stretching
75	3791.42	Stretching
<b>C<sub>12</sub>H<sub>24</sub>O<sub>12</sub>Ag</b>		
1	10.80	Stretching
2	24.70	rocking
3	31.30	rocking
4	36.95	rocking
5	39.66	Stretching
6	53.30	Twisting
7	56.76	Twisting
8	66.25	Twisting
9	91.84	Rocking
10	99.87	Rocking
11	120.36	Rocking
12	127.24	Wagging
13	140.56	Wagging
14	155.86	Twisting
15	166.66	Rocking
16	184.96	Rocking
17	202.16	Rocking
18	211.59	Rocking
19	218.11	Twisting
20	228.47	Twisting
21	228.74	Rocking
22	245.33	Twisting
23	257.19	Twisting
24	284.35	Rocking
25	292.08	Twisting

26	299.85	Wagging
27	313.90	Rocking
28	319.41	rocking
29	324.31	Rocking
30	368.11	Rocking
31	391.94	Rocking
32	392.68	Wagging
33	405.55	Twisting
34	415.53	Twisting
35	427.31	Twisting
36	435.43	Twisting
37	448.04	Rocking
38	455.38	Twisting
39	472.55	Twisting
40	480.59	Twisting
41	501.38	Rocking
42	514.52	Wagging
43	544.22	Rocking
44	560.78	Rocking
45	564.00	Twisting
46	574.46	Rocking
47	590.26	Rocking
48	620.74	Rocking
49	630.41	Twisting
50	655.65	Twisting
51	690.25	Twisting
52	703.69	Rocking
53	714.28	Twisting
54	764.90	Rocking
55	797.28	Twisting
56	859.26	Rocking
57	880.44	Rocking
58	890.79	Rocking
59	917.49	Rocking
60	940.42	Rocking
61	989.34	Rocking
62	1009.32	Wagging
63	1019.56	Stretching
64	1026.21	Wagging
65	1029.18	Rocking
66	1035.37	Rocking
67	1047.60	Rocking
68	1050.80	Rocking
69	1072.85	Rocking
70	1082.67	Twisting
71	1087.29	Stretching
72	1092.56	Bending
73	1099.44	Twisting

74	1103.53	Bending
75	1111.97	Bending
76	1114.06	Stretching
77	1118.05	Bending
78	1125.67	Stretching
79	1143.20	Stretching
80	1145.07	Stretching
81	1176.98	Stretching
82	1206.68	Twisting
83	1215.28	Twisting
84	1242.98	Twisting
85	1245.39	Twisting
86	1248.98	Twisting
87	1264.03	Rocking
88	1271.22	Rocking
89	1275.08	Rocking
90	1305.71	Rocking
91	1307.25	Rocking
92	1330.43	Rocking
93	1336.79	Rocking
94	1345.97	Rocking
95	1354.59	Rocking
96	1359.86	Rocking
97	1366.45	Rocking
98	1377.91	Rocking
99	1382.80	Rocking
100	1386.66	Rocking
101	1405.70	Rocking
102	1413.42	Rocking
103	1415.13	Twisting
104	1421.04	Rocking
105	1423.58	Rocking
106	1429.89	Rocking
107	1434.85	Rocking
108	1439.97	Rocking
109	1440.31	Rocking
110	1444.94	Wagging
111	1457.53	Rocking
112	1459.09	Rocking

113	1463.40	Bending
114	1487.53	Bending
115	1490.61	Bending
116	1502.73	Bending
117	1517.49	Bending
118	2985.29	Stretching
119	2992.34	Stretching
120	2996.15	Stretching
121	3019.27	Stretching
122	3043.17	Stretching
123	3055.44	Stretching
124	3063.14	Stretching
125	3070.52	Stretching
126	3072.59	Stretching
127	3078.03	Stretching
128	3109.44	Stretching
129	3113.88	Stretching
130	3130.17	Stretching
131	3148.11	Stretching
132	3459.23	Stretching
133	3634.19	Stretching
134	3641.63	Stretching
135	3699.83	Stretching
136	3703.89	Stretching
137	3729.75	Stretching
138	3760.66	Stretching
139	3763.72	Stretching
140	3779.65	Stretching
141	3799.17	Stretching

Types of vibration modes vary according to the quantity of energy absorbed by the atoms, and they include stretching (symmetric and asymmetric), wagging, and bending. The illustration 3-15 shows the most prominent kinds of effective vibration in both compounds.

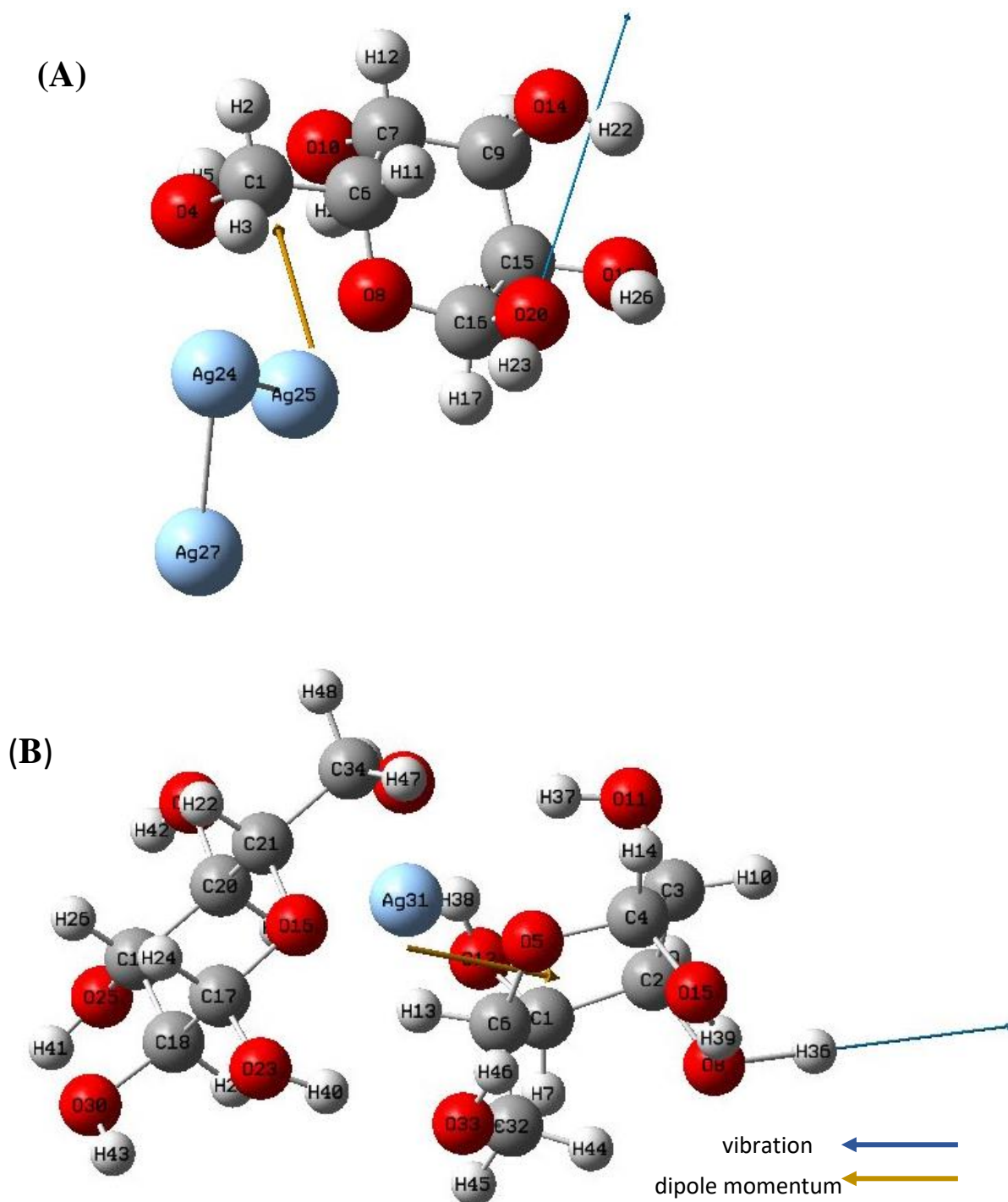


Figure 3-15: The most prominent kinds of effective vibration, (A)  $\alpha$ -D glucose with 3AgNPs and (B) 2  $\alpha$ -D glucose with one AgNP.

Another comparison with experimental and calculated wavenumbers ( $\text{cm}^{-1}$ ) from previous studies that revealed a significant correlation is presented in Table 3-13.

Table 3-13: Comparison of experimental and theoretical wavenumbers for studied molecules and previous studies.

Wavenumbers/ $\text{cm}^{-1}$ (current study)		Theoretical Wavenumbers/ $\text{cm}^{-1}$	Experimental Wavenumbers/ $\text{cm}^{-1}$
2 $\alpha$ -D-glucose/Ag	$\alpha$ -D-glucose/Ag <sub>3</sub>		
391	391	395 [204]	—
472	445	435 [204]	446 [204]
562	526	552[204]	531 [10]
796	760	751 [204]	760 [205], 754 [204]
886	—	850 [204]	806 [205]
940	967	991 [204]	996 [205], 942 [204]
1,038	1,039	1,039 [205], 1,032 [204]	1,039 [205]
—	1,093	1,090 [204]_____	1,095 [205], 1,094 [204]
1,111	—	1,110 [205], 1,103 [204]	1,108 [205]
1,174	—	1,170 [205]	1,176 [205]
1,246	1237	1,254 [204]	1,245 [205]
1,264	—	1,292 [205], 1265 [206]	1,284 [205]
1,309	1309	1,305 [205]	1,307 [205]
1,363	1,363	1,368 [204]	1,363 [205], 1,366 [204]
1,444	1,444	1,440 [204]	1,433 [205], 1,425 [204]
1,500	1,480	1,493 [204]	1,450 [205], 1,494 [204]
2,992	3,001	2,957 [204]	2,958 [204]
3,073	3,037	3,072 [204]	3,068 [204]
3,460	3,577	3,508 [204]	3,510 [204]

### 3-7 Number of surviving lung malignant cells

Lung tissue is made up of light elements with individual mass percentages of H (10.3), C (10.5), N (3.1), O (74.9), Na (0.2), P (0.2), S (0.3), Cl (0.3), and K (0.2), resulting in a low cross-section [207]. The cross-section of the lung is increased by directly injecting glucose with AgNPs into the lung tumor.[72, 111, 112]. It is well known that cancerous tissue has larger vessels than

surrounding healthy tissue [112, 208-210]. As a result, nanoparticles with glucose injected into the tumor will concentrate more than their presence in healthy tissue, and therefore the absorption of ionizing radiation dose inside the tumor would be larger due to the presence of nanoparticles. The interaction of these nanoparticles with high intensity X-rays will result in an increase in free radicals. Following irradiation, the accumulation of free radicals product decreases in surviving cancer cells.

The mass energy absorption coefficient ( $\frac{\mu_{en}}{\rho}$ ) for adding nanoparticles to glucose is obtained from the National Institute of Standards and Technology (NIST) [211]. The mathematical model employed the irradiation equation (2-81) for a lung without and with silver nanoparticles containing glucose that were added to the lung tumor. X-ray radiation with energies ranging from 2 to 15 MeV interacts with nanoparticles containing glucose. Applying the final irradiation equation (2-81) to the lung without and with glucose with AgNPs and X-ray photons with energies ranging from 2 (MeV) to 15 (MeV), we get the table (3-14) and (3-15) which illustrates a decrease in the number of surviving cancer cells is due to the presence of glucose with 3 AgNPs, and this decrease in the number of surviving cancer cells with increasing X-ray energy, as shown in the tables (3-14) (3-15).

Table 3-14 (A): The decreasing the number of cancer cells with increasing energy with Alpha-D glucose add 3 Ag NPs ( $C_6H_{12}O_6Ag_3$ ).

Sessions	Day	Dose (Gy)	Number of surviving cells with glucose aid Ag NPs and high energy from (2MeV – 8 MeV)				
			Without Ag NPs	E= 2 MeV	E= 4 MeV	E= 6 MeV	E= 8 MeV
0		0	$1.00 \times 10^{20}$	$1.00 \times 10^{20}$	$1.00 \times 10^{20}$	$1.00 \times 10^{20}$	$1.00 \times 10^{20}$
1	Saturday	2	$2.00 \times 10^{19}$	$7.00 \times 10^{18}$	$7.00 \times 10^{18}$	$7.00 \times 10^{18}$	$6.00 \times 10^{18}$
2	Sunday	4	$4.00 \times 10^{18}$	$5.00 \times 10^{17}$	$5.00 \times 10^{17}$	$5.00 \times 10^{17}$	$4.00 \times 10^{17}$
3	Monday	6	$8.00 \times 10^{17}$	$3.00 \times 10^{16}$	$3.00 \times 10^{16}$	$3.00 \times 10^{16}$	$2.00 \times 10^{16}$
4	Tuesday	8	$2.00 \times 10^{17}$	$3.00 \times 10^{15}$	$3.00 \times 10^{15}$	$2.00 \times 10^{15}$	$2.00 \times 10^{15}$
5	Wednesday	10	$3.00 \times 10^{16}$	$2.00 \times 10^{14}$	$2.00 \times 10^{14}$	$2.00 \times 10^{14}$	$1.00 \times 10^{14}$
6	Saturday	12	$7.00 \times 10^{15}$	$1.00 \times 10^{13}$	$1.00 \times 10^{13}$	$1.00 \times 10^{13}$	$7.00 \times 10^{12}$
7	Sunday	14	$1.00 \times 10^{15}$	$1.00 \times 10^{11}$	$1.00 \times 10^{12}$	$7.00 \times 10^{11}$	$4.00 \times 10^{11}$
8	Monday	16	$3.00 \times 10^{14}$	$7.00 \times 10^{10}$	77762851532	$5.00 \times 10^{10}$	27861556243
9	Tuesday	18	$5.00 \times 10^{13}$	5223517319	5650914025	3293769199	1780865179
10	Wednesday	20	$1.00 \times 10^{13}$	376282905	410643755	225419979	113829994
11	Saturday	22	$2.00 \times 10^{13}$	27106031	29840888	15427361	7275827
12	Sunday	24	$4.00 \times 10^{11}$	1952618	2168494	1055822	465059
13	Monday	26	86214613383	140659	157581	72259	29726
14	Tuesday	28	17310829391	10133	11451	4945	1900
15	Wednesday	30	3475800708	730	832	338	121
16	Saturday	32	697897847	53	60	23	8
17	Sunday	34	140129267	0	4	2	0
18	Monday	36	28136226	0	0	0	0
19	Tuesday	38	5649407	0	0	0	0
20	Wednesday	40	1134331	0	0	0	0
21	Saturday	42	227760	0	0	0	0
22	Sunday	44	45731	0	0	0	0
23	Monday	46	9182	0	0	0	0
24	Tuesday	48	1844	0	0	0	0
25	Wednesday	50	370	0	0	0	0
26	Saturday	52	74	0	0	0	0
27	Sunday	54	15	0	0	0	0
28	Monday	56	3	0	0	0	0
29	Tuesday	58	1	0	0	0	0
30	Wednesday	60	0	0	0	0	0
	<b>SER</b>			<b>13.86</b>	<b>13.86</b>	<b>13.86</b>	<b>14.75</b>



Table 3-14(B): The decreasing the number of cancer cells with increasing energy with Alpha-D glucose add 3 Ag NPs ( $C_6H_{12}O_6Ag_3$ ).

sessions	Day	Dose (Gy)	Number of surviving cells with glucose aid Ag NPs and high energy from (10MeV – 15 MeV)				
			Without Ag NPs	E= 10 MeV	E= 12 MeV	E= 14 MeV	E= 15 MeV
0		0	$1.00 \times 10^{20}$	$1.00 \times 10^{20}$	$1.00 \times 10^{20}$	$1.00 \times 10^{20}$	$1.00 \times 10^{20}$
1	Saturday	2	$2.00 \times 10^{19}$	$6.00 \times 10^{18}$	$7.00 \times 10^{18}$	$6.00 \times 10^{18}$	$5.00 \times 10^{18}$
2	Sunday	4	$4.00 \times 10^{18}$	$4.00 \times 10^{17}$	$4.00 \times 10^{17}$	$3.00 \times 10^{17}$	$3.00 \times 10^{17}$
3	Monday	6	$8.00 \times 10^{17}$	$2.00 \times 10^{16}$	$3.00 \times 10^{16}$	$2.00 \times 10^{16}$	$1.00 \times 10^{16}$
4	Tuesday	8	$2.00 \times 10^{17}$	$1.00 \times 10^{15}$	$2.00 \times 10^{15}$	$1.00 \times 10^{15}$	$7.00 \times 10^{14}$
5	Wednesday	10	$3.00 \times 10^{16}$	$8.00 \times 10^{13}$	$1.00 \times 10^{14}$	$7.00 \times 10^{13}$	$4.00 \times 10^{13}$
6	Saturday	12	$7.00 \times 10^{15}$	$5.00 \times 10^{12}$	$9.00 \times 10^{12}$	$4.00 \times 10^{12}$	$2.00 \times 10^{12}$
7	Sunday	14	$1.00 \times 10^{15}$	$3.00 \times 10^{11}$	$6.00 \times 10^{11}$	$2.00 \times 10^{11}$	99716319179
8	Monday	16	$3.00 \times 10^{14}$	16293842689	$4.00 \times 10^{10}$	$1.00 \times 10^{10}$	5162685883
9	Tuesday	18	$5.00 \times 10^{13}$	973927119	$3.00 \times 10^9$	$8.00 \times 10^8$	267291510
10	Wednesday	20	$1.00 \times 10^{13}$	58214262	$2.00 \times 10^8$	$5.00 \times 10^7$	13838679
11	Saturday	22	$2.00 \times 10^{13}$	3479624	$1.00 \times 10^7$	$3.00 \times 10^6$	716480
12	Sunday	24	$4.00 \times 10^{11}$	207988	$7.00 \times 10^5$	$2.00 \times 10^5$	375095
13	Monday	26	86214613383	12432	273	55	1921
14	Tuesday	28	17310829391	743	60	44	99
15	Wednesday	30	3475800708	44	15	8	0
16	Saturday	32	697897847	3	3	2	0
17	Sunday	34	140129267	0	1	0	0
18	Monday	36	28136226	0	1	0	0
19	Tuesday	38	5649407	0	0	0	0
20	Wednesday	40	1134331	0	0	0	0
21	Saturday	42	227760	0	0	0	0
22	Sunday	44	45731	0	0	0	0
23	Monday	46	9182	0	0	0	0
24	Tuesday	48	1844	0	0	0	0
25	Wednesday	50	370	0	0	0	0
26	Saturday	52	74	0	0	0	0
27	Sunday	54	15	0	0	0	0
28	Monday	56	3	0	0	0	0
29	Tuesday	58	1	0	0	0	0
30	Wednesday	60	0	0	0	0	0
	<b>SER</b>			<b>14.75</b>	<b>13.95</b>	<b>14.83</b>	<b>15.64</b>

Table 3-15 (A): The decreasing the number of cancer cells with increasing energy with the aid of 2 alpha-D glucose add 1 Ag NPs ( $C_{12}H_{24}O_{12}Ag$ ).

Sessions	Day	Dose (Gy)	Number of surviving cells with glucose aid Ag NPs and high energy from (2MeV – 8 MeV)				
			Without Ag NPs	E= 2 MeV	E= 4 MeV	E= 6 MeV	E= 8 MeV
0		0	$1.00 \times 10^{20}$	$1.00 \times 10^{20}$	$1.00 \times 10^{20}$	$1.00 \times 10^{20}$	$1.00 \times 10^{20}$
1	Saturday	2	$2.00 \times 10^{19}$	$7.00 \times 10^{18}$	$8.00 \times 10^{18}$	$8.00 \times 10^{18}$	$8.00 \times 10^{18}$
2	Sunday	4	$4.00 \times 10^{18}$	$7.00 \times 10^{17}$	$6.00 \times 10^{17}$	$6.00 \times 10^{17}$	$6.00 \times 10^{17}$
3	Monday	6	$8.00 \times 10^{17}$	$3.00 \times 10^{16}$	$4.00 \times 10^{16}$	$5.00 \times 10^{16}$	$5.00 \times 10^{16}$
4	Tuesday	8	$2.00 \times 10^{17}$	$2.00 \times 10^{15}$	$3.00 \times 10^{15}$	$4.00 \times 10^{15}$	$4.00 \times 10^{15}$
5	Wednesday	10	$3.00 \times 10^{16}$	$1.00 \times 10^{14}$	$2.00 \times 10^{14}$	$3.00 \times 10^{14}$	$3.00 \times 10^{14}$
6	Saturday	12	$7.00 \times 10^{15}$	$1.00 \times 10^{13}$	$2.00 \times 10^{13}$	$2.00 \times 10^{13}$	$2.00 \times 10^{13}$
7	Sunday	14	$1.00 \times 10^{15}$	$7.00 \times 10^{11}$	$1.00 \times 10^{12}$	$2.00 \times 10^{12}$	$2.00 \times 10^{12}$
8	Monday	16	$3.00 \times 10^{14}$	47051491303	$1.00 \times 10^{11}$	$1.00 \times 10^{11}$	$1.00 \times 10^{11}$
9	Tuesday	18	$5.00 \times 10^{13}$	3211035205	8179405293	10608731313	11579667715
10	Wednesday	20	$1.00 \times 10^{13}$	219137519	619317043	826806407	911302015
11	Saturday	22	$2.00 \times 10^{13}$	14955069	46892602	64438321	71718065
12	Sunday	24	$4.00 \times 10^{11}$	1020611	3550550	5022091	5644101
13	Monday	26	86214613383	69652	268836	391404	444182
14	Tuesday	28	17310829391	4753	20355	30505	34956
15	Wednesday	30	3475800708	324	1541	2377	2751
16	Saturday	32	697897847	22	117	185	217
17	Sunday	34	140129267	0	9	14	17
18	Monday	36	28136226	0	1	1	1
19	Tuesday	38	5649407	0	0	0	0
20	Wednesday	40	1134331	0	0	0	0
21	Saturday	42	227760	0	0	0	0
22	Sunday	44	45731	0	0	0	0
23	Monday	46	9182	0	0	0	0
24	Tuesday	48	1844	0	0	0	0
25	Wednesday	50	370	0	0	0	0
26	Saturday	52	74	0	0	0	0
27	Sunday	54	15	0	0	0	0
28	Monday	56	3	0	0	0	0
29	Tuesday	58	1	0	0	0	0
30	Wednesday	60	0	0	0	0	0
<b>SER</b>				<b>13.7</b>	<b>12.9</b>	<b>12.9</b>	<b>12.9</b>

Table 3-15(B): The decreasing the number of cancer cells with increasing energy with the aid of 2 alpha-D glucose add 1 Ag NPs (C<sub>12</sub>H<sub>24</sub>O<sub>12</sub>Ag).

Sessions	Day	Dose (Gy)	Number of surviving cells with glucose aid Ag NPs and high energy from (10MeV – 15 MeV)				
			Without Ag NPs	E= 10 MeV	E= 12 MeV	E= 14 MeV	E= 15 MeV
0		0	1.00×10 <sup>20</sup>	1.00×10 <sup>20</sup>	1.00×10 <sup>20</sup>	1.00×10 <sup>20</sup>	1.00×10 <sup>20</sup>
1	Saturday	2	2.00×10 <sup>19</sup>	8.00×10 <sup>18</sup>	9.00×10 <sup>18</sup>	8.00×10 <sup>18</sup>	8.00×10 <sup>18</sup>
2	Sunday	4	4.00×10 <sup>18</sup>	6.00×10 <sup>17</sup>	7.00×10 <sup>17</sup>	7.00×10 <sup>17</sup>	6.00×10 <sup>17</sup>
3	Monday	6	8.00×10 <sup>17</sup>	5.00×10 <sup>16</sup>	7.00×10 <sup>16</sup>	6.00×10 <sup>16</sup>	5.00×10 <sup>16</sup>
4	Tuesday	8	2.00×10 <sup>17</sup>	4.00×10 <sup>15</sup>	6.00×10 <sup>15</sup>	5.00×10 <sup>15</sup>	4.00×10 <sup>15</sup>
5	Wednesday	10	3.00×10 <sup>16</sup>	3.00×10 <sup>14</sup>	6.00×10 <sup>14</sup>	4.00×10 <sup>14</sup>	3.00×10 <sup>14</sup>
6	Saturday	12	7.00×10 <sup>15</sup>	2.00×10 <sup>13</sup>	5.00×10 <sup>13</sup>	4.00×10 <sup>13</sup>	2.00×10 <sup>13</sup>
7	Sunday	14	1.00×10 <sup>15</sup>	2.00×10 <sup>13</sup>	5.00×10 <sup>12</sup>	3.00×10 <sup>12</sup>	2.00×10 <sup>12</sup>
8	Monday	16	3.00×10 <sup>14</sup>	1.00×10 <sup>12</sup>	4.00×10 <sup>11</sup>	3.00×10 <sup>11</sup>	1.00×10 <sup>11</sup>
9	Tuesday	18	5.00×10 <sup>13</sup>	1.00×10 <sup>11</sup>	36676808035	22403757275	10405275770
10	Wednesday	20	1.00×10 <sup>13</sup>	915666506	3280881853	1897292490	809206849
11	Saturday	22	2.00×10 <sup>13</sup>	72095982	293487528	160674781	62931126
12	Sunday	24	4.00×10 <sup>11</sup>	5676554	26253591	13606961	4894084
13	Monday	26	86214613383	446950	2348485	1152324	380608
14	Tuesday	28	17310829391	35191	210081	97586	29599
15	Wednesday	30	3475800708	2771	18793	8264	2302
16	Saturday	32	697897847	218	1681	700	179
17	Sunday	34	140129267	17	150	59	14
18	Monday	36	28136226	1	13	5	1
19	Tuesday	38	5649407	0	1	0	0
20	Wednesday	40	1134331	0	0	0	0
21	Saturday	42	227760	0	0	0	0
22	Sunday	44	45731	0	0	0	0
23	Monday	46	9182	0	0	0	0
24	Tuesday	48	1844	0.	0	0	0
25	Wednesday	50	370	0	0	0	0
26	Saturday	52	74	0	0	0	0
27	Sunday	54	15	0	0	0	0.
28	Monday	56	3	0	0	0	0
29	Tuesday	58	1	0	0	0	0
30	Wednesday	60	0	0	0	0	0
<b>SER</b>				<b>12.9</b>	<b>12.5</b>	<b>12.8</b>	<b>12.9</b>

Because the vascularity of cancer tumors is greater than that of healthy tissue, AgNPs add α-D glucose are predicted to be more concentrated within tumors than in healthy tissue. The target has already been injected with nanoparticles

with a high mass energy absorption coefficient, the quantity of absorbed dose by the tumor, particularly the ionizing zone, would increase.

This would increase the amount of malignant cells killed when compared to the same target at same energy but without nano-particles[212]. The energy of x-ray beam may be regarded another component that may aid in the improvement of the radio-sensitivity ratio due to its significant contribution in boosting the quantity of free radicals' yield, which can lead to an increase in the number of damaged cancer cells. In this study, it was discovered that the SER was It increases by increasing the energy in the presence of silver nanoparticles with glucose as shown in table 3-14 At the lowest value of energy (2 Mev), the SER is 13.8, and at the highest value of energy at (15Mev). We find that the value of SER has increased w ith the increase of energy and has become 15.64. An increase in the number of destroyed cancer cells. An increase in destructive cancer cells offset by a decrease in the number of radiotherapy sessions. As show in figure (3-15) Compared to prior studies, the  $\alpha$ -D glucose molecules adsorbed with silver nanoparticles gave precise and good results regarding radiation sensitivity. in this study was found that the value of radiation sensitivity using  $\alpha$ -D glucose absorbed on silver nanoparticles is 15.68 from energy 15 Mev greater than. The value of radiation sensitivity while using only silver is equivalent to 14.70 at the same amount of energy this is a good improvement in the value of radiation sensitivity as show in the figure 3-16 [213].

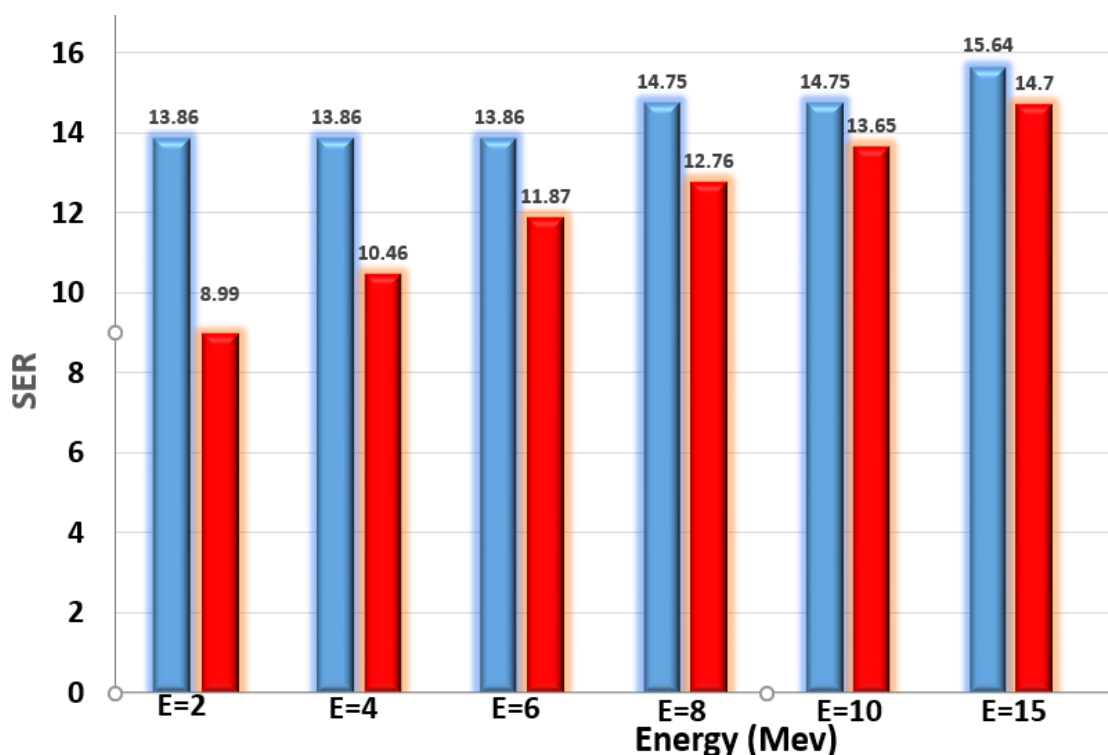


Figure 3-16: Compars SER of lung with the presence of 3 silver nanoparticles with  $\alpha$ -D glucose ( $C_6H_{12}O_6Ag_3$ ) and X-ray energy ranging from 2 to 15 (MeV) with the presence of 3 silver nanoparticles with  $\alpha$ -D glucose ( $C_6H_{12}O_6Ag_3$ ) and X-ray energy ranging from 2 to 15 (MeV) between thyrtical study(Blue column) and pruivous study (red column) [219].

In figure (3-16), when the energy delivered to the organ (lung) is increased from 2 MeV, 4 MeV and 6 MeV, the radiation sensitivity is equal to 13.8 in all energy levels. When the energy is increased, the lung organ's compound and energy absorption coefficient remain unchanged. Furthermore, increasing the energy from 8 MeV to 10 MeV results in an increase in radiation sensitivity of 14.7. This is due to an increase in the energy absorption coefficient of the molecule and the organ, leading to an increase in the reaction's cross-sectional area. When the energy increases to 12 mega-electronvolt, the radiation sensitivity drops to 13.9. This is due to a drop in the values of the mass-energy absorption coefficient for both the human organ and the compound, as

shown in the figure (3-17). The connection between the energy delivered to the organ and the mass-energy absorption coefficient [211].

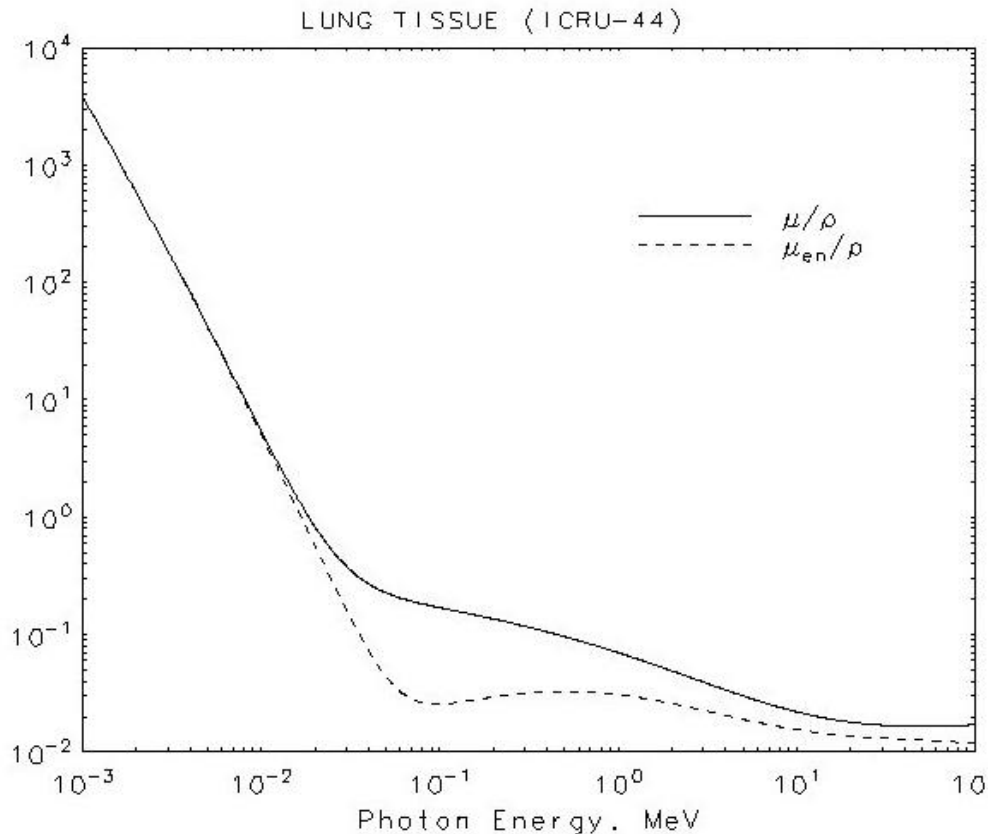


Figure 3-17: The relationship between photon energy and mass-energy absorption coefficient of lung [217].

Finally, increasing the energy from 14 MeV to 15 MeV results in a gradual increase in radiation sensitivity levels ranging from 14.8 to 15.6. On the other hand, radiation sensitivity is greatest when the energy applied to the organ is as high as possible, which is offset by reducing the number of radiotherapy sessions to 15 instead of 30, i.e. the number of sessions has been reduced in half, and this result is good and identical to the practical results.

In general, the results of both tables 3-14 and 3-15 showed a decrease in the number of radiotherapy sessions, and this decrease can be estimated from 11-15 sessions, i.e. almost half of the radiotherapy sessions (30 sessions). Table 3-15

data, on the other hand, showed a decrease in SER values despite an increase in energy in the presence of two glucose molecules with one silver atom ( $C_{12}H_{24}O_{12}Ag$ ) as show figure (3-18). The drop in SER values may be explained at the maximum energy of 15Mev, which is equivalent to 12.9. There are two possible explanations for the reduction in radiation sensitivity. The first explanation is that the compound has an abundance of glucose molecules, which is compensated by a poverty of silver nanoparticles. Glucose is the body's main supply of energy. The  $\alpha$ -D glucose molecule can take as much energy from the lung organ as possible and deliver it to the body. This results in a drop or loss of a portion of the radiation interaction with silver atoms, i.e. a decrease in the reaction's cross-sectional area, followed by a decrease in the radiation sensitivity value. in comparison to the compound ( $C_6H_{12}O_6Ag_3$ ). The second reason is the variance (increase and decrease) in the mass energy absorption coefficient of the silver atom, as shown in the illustration (3-19), which causes fluctuation in the radiation sensitivity value as the energy increases.

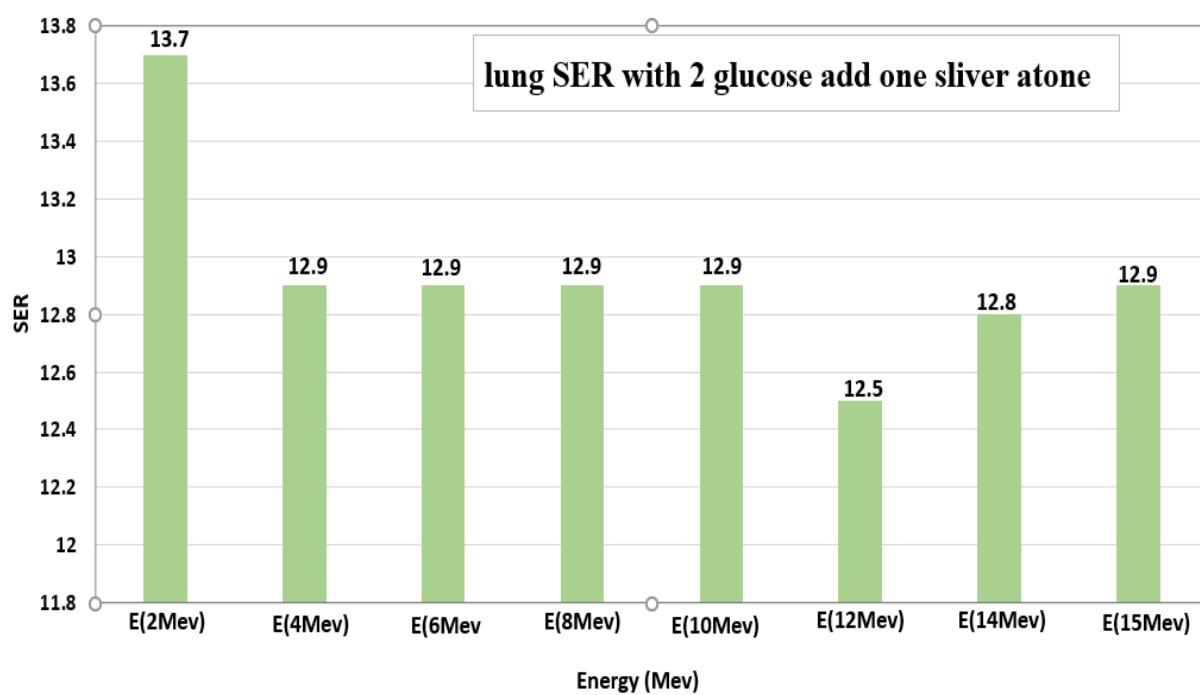


Figure 3-18: The enhancement of lung SER with the presence of one silver nanoparticle with 2 $\alpha$ -D glucose ( $C_{12}H_{24}O_{12}Ag$ ) and X-ray energy ranging from 2 (MeV) to 15 (MeV).

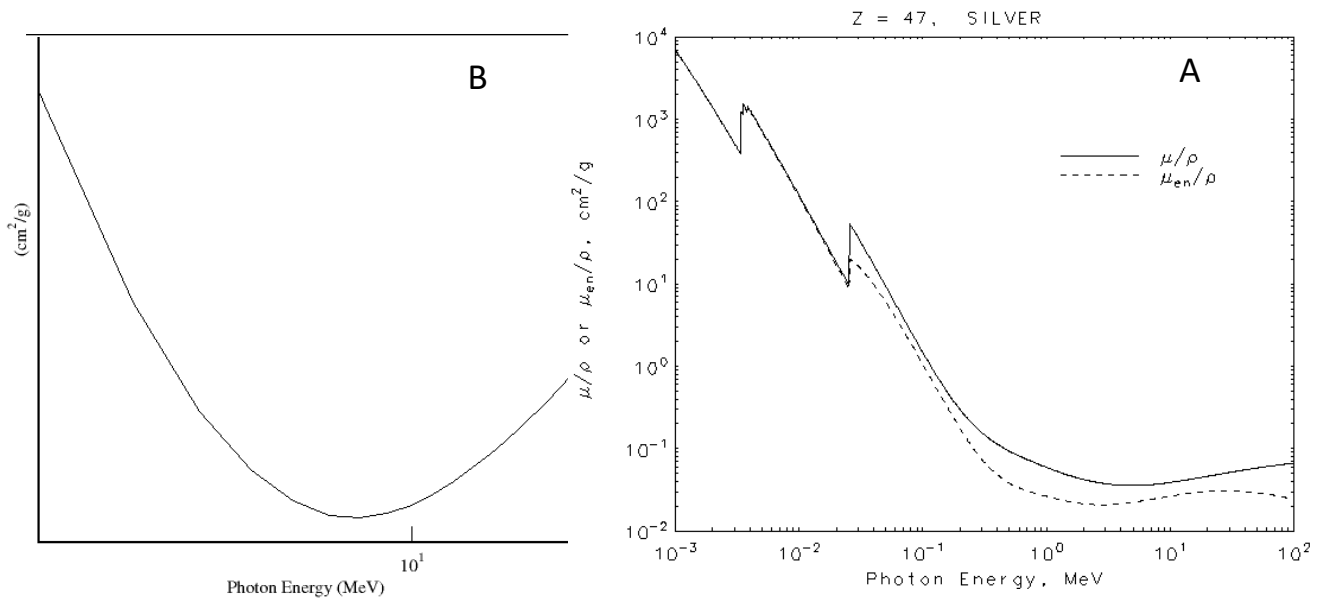


Figure 3-19: (A) Relationship between photon energy and mass-energy absorption coefficient of silver. (B) relationship between photon energy and mass-energy absorption coefficient of  $\text{C}_{12}\text{H}_{24}\text{O}_{12}\text{Ag}$  [217].

According to the data in tables 3-14 and 3-15, the number of remaining cancer cells decreases gradually with both compounds, with increasing doses of radiation in the presence of glucose molecules with silver nanoparticles at high X-ray energies until it reaches the absence of cancer cells, that is, all malignant cells were killed. The decrease in the number of remaining cancer cells is offset by a decrease in the number of radiation sessions, as shown in the figures below. This can be considered as an advancement in the treatment of malignant diseases in general, and lung cancer in particular.



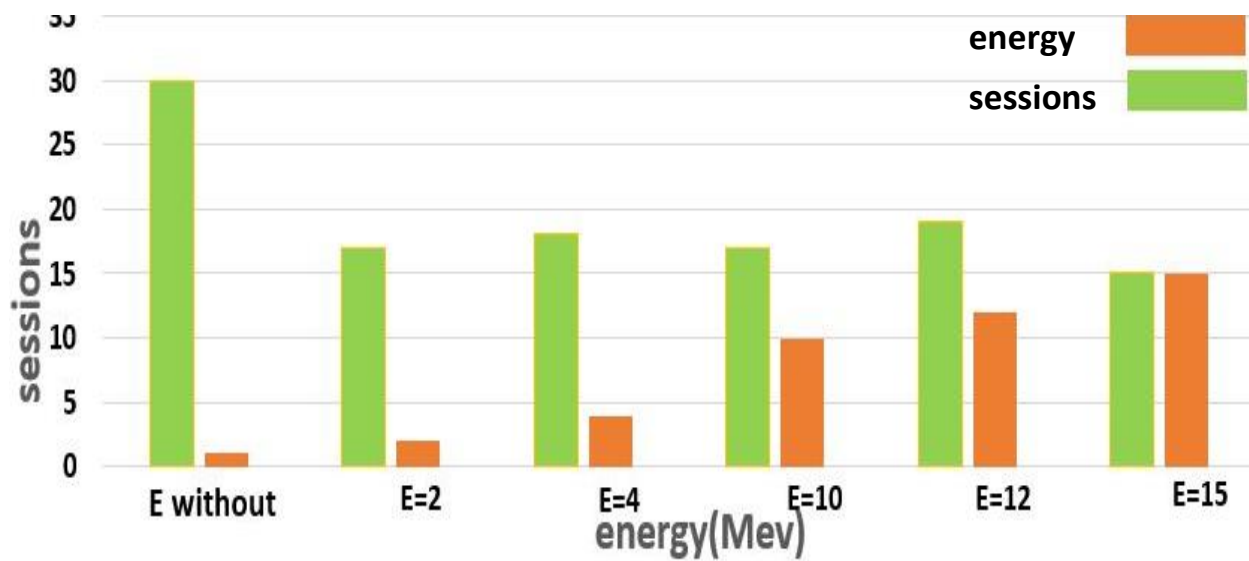


Figure 3-20: Relationship between energy and sessions radio therapy existence alpha-D glucose with three silver nanoparticles.

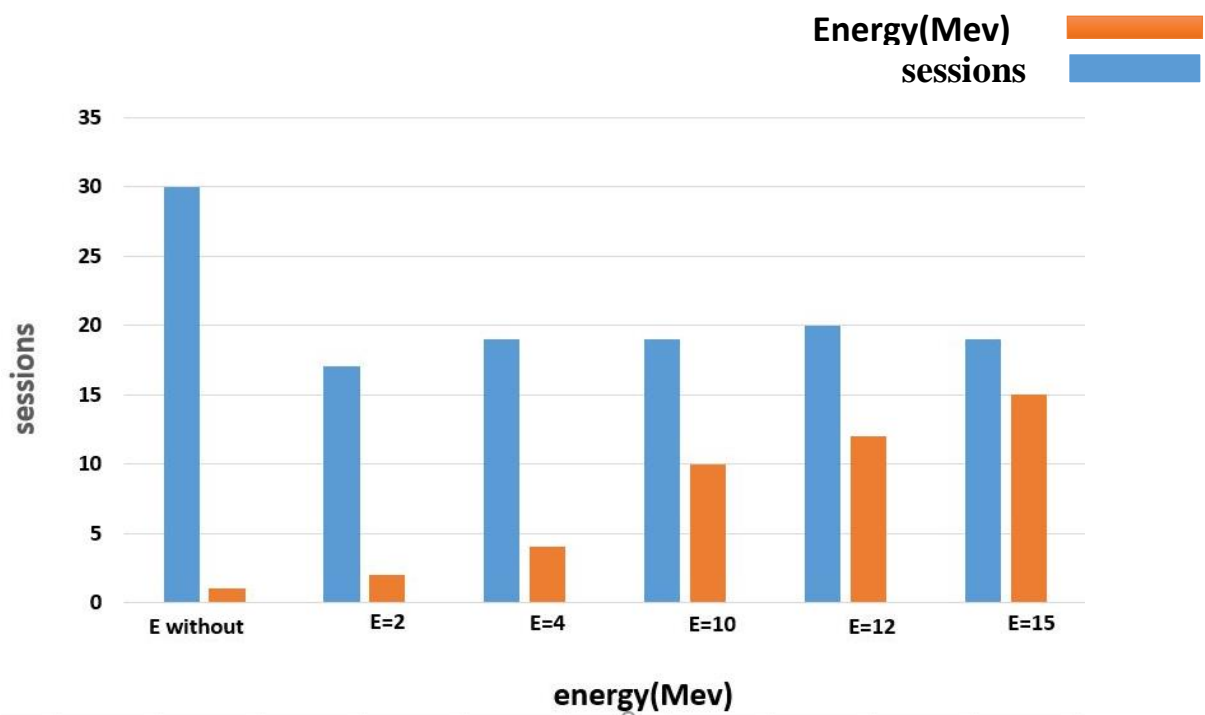


Figure 3-21: Relationship between energy and sessions radio therapy existence two alpha -D glucose with one silver nanoparticle.

Figure (3-20) and (3-21) show the relationship between the number of radiotherapy sessions in the presence and absence of  $\alpha$ -D glucose with silver nanoparticles with high energies of the X-ray rays. By using the energy of the X-ray rays without  $\alpha$ -D glucose with the silver nanoparticles, malignant cells disappear at 30th session, which is equivalent to the dose delivered from radiation 60 Gy for a period of approximately six weeks. However, in the presence of  $\alpha$ -D glucose with silver and high energies of X-ray radiation when the energy is equal to 2 Mev, the cancer cells were found to fade at the 17th session, which is approximately 34 Gy of the administered dose, with a treatment period estimated at three to four weeks, and this is a significant improvement in the treatment period. However, in figure (3-20) when the energy increases from 2 Mev to 15 MeV, it was found that the cancer cells fade and die at the 15th session, approximately. 30 Gy of the dose of radiation delivered during a treatment period estimated at three weeks. This reduction in the number of treatment sessions for patients gives patients a greater chance of recovering from the disease.

On the other hand, with increasing the energy from 2 Mev to 15 MeV, it was found that the cancer cells fade and die obtained at the 19th session, approximately as shown in figure (3-21). 38 Gy of the dose of radiation delivered during a treatment period estimated at four weeks.

Figures 3-20 and 3-21 show a reduction in the treatment time frame or the number of radiation treatments. It was found that the number of radiation treatments might be reduced to three or four weeks, depending on the type of chemical injected with high X-ray energy. This method is considered an improvement or enhancement of the therapeutic methods for cancerous diseases. When the findings of this study were compared to previous experiment [214-216] investigations, they gave good results and content for improving radiotherapy.

### 3-8 Conclusions

The application of density functional theory to the hybrid function B3LYB and the set of the mix basis set that selected for C, O, and H atoms was 6-311 + G\*, whereas the LANL2DZ\_basis set was used for Ag atoms. It yielded profitable and promising results in the electrical and structural characteristics of the  $\alpha$ -D glucose molecule before and after adsorption by silver Nanoparticles. To achieve the most stable structural arrangements. Inserting them into mathematical formulae to improve radiation therapy by estimating the radiation sensitivity of the cells and calculating the number of destroyed cancer cells in the lung. Review the most important conclusions obtained in this study, which are as the following:

- 1- Obtaining the optimum structural configurations of  $\alpha$ -D glucose before and after the addition of silver nanoparticles, where the total energy of  $C_6H_{12}O_6$  was -687.140 Hatree. The value for the compound was  $C_{12}H_{24}O_{12}Ag$  -1520.447 Hatree, and the value for the compound was  $C_6H_{12}O_6Ag_3$  -1124.712 Hatree.
- 2- The length of the bond in both compounds  $C_{12}H_{24}O_{12}Ag$ , ( $C_6H_{12}O_6Ag_3$ ) at C-C and C-H is identical, with values of 1.53 Å and 1.09 Å respectively, however, there is a tiny variance in the hydroxyl group, with values of 0.96 Å and 0.97 Å. Ag- O bonds with, having values of 2.73 Å and 3.5 Å respectively.
- 3- The bond angle for both compounds at C-C-C is equal and its value is 114.109 degrees, the angle bond C-O- Ag for the complex  $C_6H_{12}O_6Ag_3$  is equal to 46.5 degrees, while the angle bond O-Ag-O compound ( $C_{12}H_{24}O_{12}Ag$ ) is equivalent to 56.2 degrees.
- 4- Dihedral angle of both compounds were found to be different due to the difference in the level in which the atoms rotate clockwise or counterclockwise.

- 5- The energy gap increases with the increase of silver nanoparticles.
- 6- There is good agreement between the infrared spectrum and the functional group and their experiment values.
- 7- The vibration modes increase with the increase in the number of atoms involved in the formation of the compound.
- 8- The improvement of the sensitivity enhancement ratio was raised by increasing the high energies of X-rays in the presence of glucose with silver nanoparticles, as its values for both compounds reached the highest energy values of 15.6 and 12.9.
- 9- Increasing the dose of radiation delivered to the organ with the high energy of X-rays in the presence of  $\alpha$ -D glucose with silver nanoparticles corresponds to a decrease in the number of destroyed cancer cells.
- 10- By increasing the dose of radiation with an increase in the high energies of x-rays in the presence of  $\alpha$ - D glucose with silver nanoparticles, the number of radiation treatment sessions was reduced by nearly half.

### 3-9 Future work

- 1- This study's mathematical model is accessible to improve SER in radiation clinical physical planning. It should be noted that the concept of SER enhancement is confined to radiotherapy utilizing high photon X-ray contrast agents with nanoparticles.
- 2- The mathematical model described uses  $\beta$ -d glucose with AgNPs as a starting point for radio sensitizing contrast agents; however, a more promising candidate for additional study may be iodine with atomic number (53) and bismuth with atomic number (83).
- 3- Because tumor vasculature is irregular and broader than normal tissue, the nanoparticle distribution in the tumor is still greater than in healthy cells surrounding the tumor tissue, therefore we may use this attribute to detect the cancer tumor using X-ray methods.

## References

---

- [1] M. Hall, "Challenges with nonfiber carbohydrate methods," *Journal of animal science*, vol. 81, no. 12, pp. 3226-3232, 2003.
- [2] A. Shendurse and C. Khedkar, "Glucose: properties and analysis," *Encyclopedia of food and health*, vol. 3, pp. 239-247, 2016.
- [3] A. S. Marggraf, *Experiences chimiques faites dans le dessein de tirer un veritable sucre de diverses plantes, qui croissent dans nos contrées*. 1748.
- [4] A. J. Domb, J. Kost, and D. Wiseman, *Handbook of biodegradable polymers*. CRC press, 1998.
- [5] F. W. Schenck, "Glucose and glucose-containing syrups," *Ullmann's Encyclopedia of Industrial Chemistry*, 2000.
- [6] A. González Fá, I. López-Corral, R. Faccio, A. Juan, and M. S. Di Nezio, "Surface enhancement Raman spectroscopy and density functional theory study of silver nanoparticles synthesized with d-glucose," *Journal of Raman Spectroscopy*, vol. 49, no. 11, pp. 1756-1764, 2018.
- [7] L. L. Koekkoek, J. D. Mul, and S. E. La Fleur, "Glucose-sensing in the reward system," *Frontiers in neuroscience*, vol. 11, p. 716, 2017.
- [8] Y. Serlin, I. Shelef, B. Knyazer, and A. Friedman, "Anatomy and physiology of the blood–brain barrier," in *Seminars in cell & developmental biology*, 2015, vol. 38: Elsevier, pp. 2-6.
- [9] S. H. Fairclough and K. Houston, "A metabolic measure of mental effort," *Biological psychology*, vol. 66, no. 2, pp. 177-190, 2004.
- [10] M. T. Gailliot *et al.*, "Self-control relies on glucose as a limited energy source: willpower is more than a metaphor," *Journal of personality and social psychology*, vol. 92, no. 2, p. 325, 2007.
- [11] M. T. Gailliot and R. F. Baumeister, "The physiology of willpower: Linking blood glucose to self-control," *Personality and social psychology review*, vol. 11, no. 4, pp. 303-327, 2007.
- [12] D. S. Dwyer, T. D. Ardizzone, and R. J. Bradley, "Psychoactive drugs affect glucose transport and the regulation of glucose metabolism," *International Review of Neurobiology*, vol. 51, pp. 503-530, 2002.
- [13] W. Kang and Z. Zhang, "Selective production of acetic acid via catalytic fast pyrolysis of hexoses over potassium salts," *Catalysts*, vol. 10, no. 5, p. 502, 2020.

## References

---

- [14] L. Bosch, T. Fyles, and T. D. James, "Binary and ternary phenylboronic acid complexes with saccharides and Lewis bases," *Tetrahedron*, vol. 60, no. 49, pp. 11175-11190, 2004.
- [15] M. Mathlouthi, "Relationship between the structure and the properties of carbohydrates in aqueous solutions: solute-solvent interactions and the sweetness of D-fructose, D-glucose and sucrose in solution," *Food chemistry*, vol. 13, no. 1, pp. 1-16, 1984.
- [16] L. G. Sánchez-Lozada *et al.*, "Comparison of free fructose and glucose to sucrose in the ability to cause fatty liver," *European journal of nutrition*, vol. 49, pp. 1-9, 2010.
- [17] A. Ugolev, "Membrane digestion," *Gut*, vol. 13, no. 9, p. 735, 1972.
- [18] R. P. Ferraris, S. Yasharpour, K. Lloyd, R. Mirzayan, and J. M. Diamond, "Luminal glucose concentrations in the gut under normal conditions," *American Journal of Physiology-Gastrointestinal and Liver Physiology*, vol. 259, no. 5, pp. G822-G837, 1990.
- [19] J. Mayer, "Glucostatic mechanism of regulation of food intake," *New England Journal of Medicine*, vol. 249, no. 1, pp. 13-16, 1953.
- [20] A. B. Fernandes *et al.*, "Postingestive modulation of food seeking depends on vagus-mediated dopamine neuron activity," *Neuron*, vol. 106, no. 5, pp. 778-788. e6, 2020.
- [21] L. V. Gromova, S. O. Fetissov, and A. A. Gruzdkov, "Mechanisms of glucose absorption in the small intestine in health and metabolic diseases and their role in appetite regulation," *Nutrients*, vol. 13, no. 7, p. 2474, 2021.
- [22] N. B. Grimm and S. G. Fisher, "Exchange between interstitial and surface water: implications for stream metabolism and nutrient cycling," *Hydrobiologia*, vol. 111, pp. 219-228, 1984.
- [23] H.-G. Joost and B. Thorens, "The extended GLUT-family of sugar/polyol transport facilitators: nomenclature, sequence characteristics, and potential function of its novel members," *Molecular membrane biology*, vol. 18, no. 4, pp. 247-256, 2001.
- [24] K. Birsoy *et al.*, "Metabolic determinants of cancer cell sensitivity to glucose limitation and biguanides," *Nature*, vol. 508, no. 7494, pp. 108-112, 2014.

## References

---

- [25] C. Scafoglio *et al.*, "Functional expression of sodium-glucose transporters in cancer," *Proceedings of the National Academy of Sciences*, vol. 112, no. 30, pp. E4111-E4119, 2015.
- [26] C. R. Scafoglio *et al.*, "Sodium-glucose transporter 2 is a diagnostic and therapeutic target for early-stage lung adenocarcinoma," *Science translational medicine*, vol. 10, no. 467, p. eaat5933, 2018.
- [27] O. Warburg, "On the origin of cancer cells," *Science*, vol. 123, no. 3191, pp. 309-314, 1956.
- [28] J. Berg, J. Tymoczko, and L. Stryer, "The regulation of cellular respiration is governed primarily by the need for ATP," *Biochemistry, 5th ed.*; *WH Freeman: New York, NY, USA*, 2002.
- [29] J. Fan *et al.*, "Glutamine-driven oxidative phosphorylation is a major ATP source in transformed mammalian cells in both normoxia and hypoxia," *Molecular systems biology*, vol. 9, no. 1, p. 712, 2013.
- [30] F. Weinberg *et al.*, "Mitochondrial metabolism and ROS generation are essential for Kras-mediated tumorigenicity," *Proceedings of the National Academy of Sciences*, vol. 107, no. 19, pp. 8788-8793, 2010.
- [31] I. Sussman, M. Erecińska, and D. F. Wilson, "Regulation of cellular energy metabolism. The Crabtree effect," *Biochimica et Biophysica Acta (BBA)-Bioenergetics*, vol. 591, no. 2, pp. 209-223, 1980.
- [32] H. Leese and A. M. Barton, "Pyruvate and glucose uptake by mouse ova and preimplantation embryos," *Reproduction*, vol. 72, no. 1, pp. 9-13, 1984.
- [33] D. Bhattacharya, A. P. Azambuja, and M. Simoes-Costa, "Metabolic reprogramming promotes neural crest migration via yap/tead signaling," *Developmental cell*, vol. 53, no. 2, pp. 199-211. e6, 2020.
- [34] V. Mohanraj and Y. Chen, "Nanoparticles-a review," *Tropical journal of pharmaceutical research*, vol. 5, no. 1, pp. 561-573, 2006.
- [35] E. J. Chung, L. Leon, and C. Rinaldi, *Nanoparticles for biomedical applications: fundamental concepts, biological interactions and clinical applications*. Elsevier, 2019.
- [36] S. Dwivedi, "Nanoelectronics," in *Nanotechnology*: CRC Press, 2022, pp. 93-117.



## References

---

- [37] S. Prabhu and E. K. Poullose, "Silver nanoparticles: mechanism of antimicrobial action, synthesis, medical applications, and toxicity effects," *International nano letters*, vol. 2, pp. 1-10, 2012.
- [38] L. Xu, Y.-Y. Wang, J. Huang, C.-Y. Chen, Z.-X. Wang, and H. Xie, "Silver nanoparticles: Synthesis, medical applications and biosafety," *Theranostics*, vol. 10, no. 20, p. 8996, 2020.
- [39] D. R. Lide, *CRC handbook of chemistry and physics*. CRC press, 2004.
- [40] Q. Zheng, H. Yang, J. Wei, J.-l. Tong, and Y.-q. Shu, "The role and mechanisms of nanoparticles to enhance radiosensitivity in hepatocellular cell," *Biomedicine & Pharmacotherapy*, vol. 67, no. 7, pp. 569-575, 2013.
- [41] L. Xu, Y. Y. Wang, J. Huang, C. Y. Chen, Z. X. Wang, and H. Xie, "Silver nanoparticles: Synthesis, medical applications and biosafety," *Theranostics*, vol. 10, no. 20, pp. 8996-9031, 2020, doi: 10.7150/thno.45413.
- [42] R. Balachandar *et al.*, "Plant-mediated synthesis, characterization and bactericidal potential of emerging silver nanoparticles using stem extract of *Phyllanthus pinnatus*: a recent advance in phytonanotechnology," *Journal of Cluster Science*, vol. 30, pp. 1481-1488, 2019.
- [43] P. Asharani, M. P. Hande, and S. Valiyaveetil, "Anti-proliferative activity of silver nanoparticles," *BMC cell biology*, vol. 10, pp. 1-14, 2009.
- [44] L. Li, H. Wu, W. J. Peijnenburg, and C. A. van Gestel, "Both released silver ions and particulate Ag contribute to the toxicity of AgNPs to earthworm *Eisenia fetida*," *Nanotoxicology*, vol. 9, no. 6, pp. 792-801, 2015.
- [45] J. D. Tward, C. J. Anker, D. K. Gaffney, and G. M. Bowen, "Radiation therapy and skin cancer," *Modern practices in radiation therapy. Rijeka: InTech*, pp. 207-246, 2012.
- [46] S. Gianfaldoni, R. Gianfaldoni, U. Wollina, J. Lotti, G. Tchernev, and T. Lotti, "An overview on radiotherapy: from its history to its current applications in dermatology," *Open access Macedonian journal of medical sciences*, vol. 5, no. 4, p. 521, 2017.
- [47] W. C. Röntgen, "Über eine neue Art von Strahlen," *Sitzung Physikal-Medicin Gesellschaft*, vol. 137, pp. 132-141, 1895.

## References

---

- [48] E. H. Grubbé, "Priority in the therapeutic use of X-rays," *Radiology*, vol. 21, no. 2, pp. 156-162, 1933.
- [49] H. Coutard, "Principles of x ray therapy of malignant diseases," *The lancet*, vol. 224, no. 5784, pp. 1-8, 1934.
- [50] M. L. Boone, J. H. Lawrence, W. G. Connor, R. Morgado, J. A. Hicks, and R. C. Brown, "Introduction to the use of protons and heavy ions in radiation therapy: historical perspective," *International Journal of Radiation Oncology\* Biology\* Physics*, vol. 3, pp. 65-69, 1977.
- [51] D. Fry, R. R.-S.-HARVIE, L. Mullett, and W. Walkinshaw, "A travelling-wave linear accelerator for 4-MeV. electrons," *Nature*, vol. 162, no. 4126, pp. 859-861, 1948.
- [52] H. Suit *et al.*, "Evaluation of the clinical applicability of proton beams in definitive fractionated radiation therapy," *International Journal of Radiation Oncology\* Biology\* Physics*, vol. 8, no. 12, pp. 2199-2205, 1982.
- [53] S. Jayaraman and L. H. Lanzl, *Clinical radiotherapy physics*. Springer Science & Business Media, 2003.
- [54] E. B. Podgorsak, "Review of radiation oncology physics: a handbook for teachers and students," *Vienna, Austria: IAE Agency*, vol. 19, p. 133, 2003.
- [55] D. I. Thwaites and J. B. Tuohy, "Back to the future: the history and development of the clinical linear accelerator," *Physics in Medicine & Biology*, vol. 51, no. 13, p. R343, 2006.
- [56] E. Podgorsak, "Basic Radiobiology," *Radiation Oncology Physics: A Handbook for Teachers and Students*, pp. 488-91, 2005.
- [57] L. Xiong, Z.-H. Tong, J.-J. Chen, L.-L. Li, and H.-Q. Yu, "Morphology-dependent antimicrobial activity of Cu/Cu x O nanoparticles," *Ecotoxicology*, vol. 24, pp. 2067-2072, 2015.
- [58] Y. Hao, Y. Altundal, M. Moreau, E. Sajo, R. Kumar, and W. Ngwa, "Potential for enhancing external beam radiotherapy for lung cancer using high-Z nanoparticles administered via inhalation," *Physics in Medicine & Biology*, vol. 60, no. 18, p. 7035, 2015.

## References

---

- [59] S. M. Khalil, G. M. Al-Mazaideh, and N. M. Ali, "DFT calculations on corrosion inhibition of Aluminum by some carbohydrates," *J. Biochem. Res. & Rev*, vol. 14, pp. 1-7, 2016.
- [60] Z. Ouyang, B. Liu, S. Yasmin-Karim, E. Sajo, and W. Ngwa, "Nanoparticle-aided external beam radiotherapy leveraging the Čerenkov effect," *Physica Medica*, vol. 32, no. 7, pp. 944-947, 2016.
- [61] A. J. González Fá, A. Juan, and M. S. Di Nezio, "Synthesis and characterization of silver nanoparticles prepared with honey: the role of carbohydrates," *Analytical Letters*, vol. 50, no. 5, pp. 877-888, 2017.
- [62] S. S. Gowda *et al.*, "Gallic acid-coated silver nanoparticle alters the expression of radiation-induced epithelial-mesenchymal transition in non-small lung cancer cells," *Toxicology in Vitro*, vol. 52, pp. 170-177, 2018.
- [63] R. E. Ambrusi *et al.*, "Density functional theory model for carbon dot surfaces and their interaction with silver nanoparticles," *Physica E: Low-dimensional Systems and Nanostructures*, vol. 114, p. 113640, 2019.
- [64] M. Zangeneh, H. A. Nedaei, H. Mozdarani, A. Mahmoudzadeh, and M. Salimi, "Enhanced cytotoxic and genotoxic effects of gadolinium-doped ZnO nanoparticles on irradiated lung cancer cells at megavoltage radiation energies," *Materials Science and Engineering: C*, vol. 103, p. 109739, 2019.
- [65] R. E. A. Jeison Manuel Arroyave, María Estela Pronsato, and M. F. P. Alfredo Juan, and María Eugenia Centurión, "Experimental and DFT Studies of Hybrid Silver/Cdots Nanoparticles," 2020, doi: 10.1021/acs.jpcc.9b10430.
- [66] J. Han *et al.*, "Combining doxorubicin-conjugated polymeric nanoparticles and 5-aminolevulinic acid for enhancing radiotherapy against lung cancer," *Bioconjugate Chemistry*, vol. 33, no. 4, pp. 654-665, 2022.
- [67] G. Venkatesha, Y. S.-L. b. , e, P. V. , Y. S. M. d. , J. Correa-Basurtoe, and Y. S. M. d. , A. Manikandanf, "An investigation on the molecular structure, interaction with metal lusters, anti-Covid-19 ability of 2-deoxy-D-glucose: DFT calculations, MD and docking simulations," 2022, doi: 10.1016/j.molstruc.2022.132678.

## References

---

- [68] I. Vukoje *et al.*, "Influence of glucose, sucrose, and dextran coatings on the stability and toxicity of silver nanoparticles," *Int J Biol Macromol*, vol. 194, pp. 461-469, Jan 1 2022, doi: 10.1016/j.ijbiomac.2021.11.089.
- [69] R. Iyer *et al.*, "Lung Cancer Targeted Chemoradiotherapy via Dual-Stimuli Responsive Biodegradable Core-Shell Nanoparticles," *Pharmaceutics*, vol. 14, no. 8, p. 1525, 2022.
- [70] Y. Chen *et al.*, "Albumin-Modified Gold Nanoparticles as Novel Radiosensitizers for Enhancing Lung Cancer Radiotherapy," *International Journal of Nanomedicine*, pp. 1949-1964, 2023.
- [71] H. Nosrati *et al.*, "Enhanced in vivo radiotherapy of breast cancer using gadolinium oxide and gold hybrid nanoparticles," *ACS Applied Bio Materials*, vol. 6, no. 2, pp. 784-792, 2023.
- [72] W. Ni *et al.*, "Development of an intelligent heterojunction fenton catalyst for chemodynamic/starvation synergistic cancer therapy," *Journal of Materials Science & Technology*, vol. 141, pp. 11-20, 2023.
- [73] E. Schrödinger, "An undulatory theory of the mechanics of atoms and molecules," *Physical review*, vol. 28, no. 6, p. 1049, 1926.
- [74] Y. Yamaguchi, Y. Osamura, J. D. Goddard, and H. F. Schaefer III, *A new dimension to quantum chemistry: analytical derivative methods in ab-initio molecular electronic structure theory*. Oxford University Press, 1994.
- [75] W. Demtröder, *Molecular physics: theoretical principles and experimental methods*. John Wiley & Sons, 2008.
- [76] R. Ahlrichs, S. Elliot, and U. Huniar, "Ab Initio Treatment of Large Molecules," *Modern Methods and Algorithms of Quantum Chemistry. NIC, Jülich*, 2000.
- [77] B. O. Roos, *Lecture Notes in Quantum Chemistry: European Summer School in Quantum Chemistry*. Springer Berlin Heidelberg, 1997.
- [78] G. o. Institute of Theoretical Physics, b, and G. o. Institute of Theoretical Physics, "<born-opperheimer-translated-s-m-blinder.pdf>," 1927.
- [79] J. P. Goss, "A FIRST PRINCIPLES STUDY OF DEFECTS IN SEMICONDUCTORS," 1997.

## References

---

- [80] D. R. Hartree, "The wave mechanics of an atom with a non-Coulomb central field. Part I. Theory and methods," in *Mathematical Proceedings of the Cambridge Philosophical Society*, 1928, vol. 24, no. 1: Cambridge university press, pp. 89-110.
- [81] V. Fock, "Näherungsmethode zur Lösung des quantenmechanischen Mehrkörperproblems," *Zeitschrift für Physik*, vol. 61, pp. 126-148, 1930.
- [82] D. Zhou, "An Introduction of Density Functional Theory and its Application," *Physics. Drexel. Edu*, 2007.
- [83] W. Pauli, "On the connexion between the completion of electron groups in an atom with the complex structure of spectra," *Zeitschrift für Physik*, vol. 31, p. 765, 1925.
- [84] A. Szabo and N. S. Ostlund, *Modern quantum chemistry: introduction to advanced electronic structure theory*. Courier Corporation, 2012.
- [85] A. S. a. N. Ostlund, "Modern quantum chemistry," *New York.;* Macmillan Pub. Co., 1982.
- [86] H. Dorsett and A. White, "Overview of molecular modelling and ab initio molecular orbital methods suitable for use with energetic materials," DEFENCE SCIENCE AND TECHNOLOGY ORGANIZATION SALISBURY (AUSTRALIA), 2000.
- [87] A. O. Acheampong, "Economic growth, CO2 emissions and energy consumption: what causes what and where?," *Energy Economics*, vol. 74, pp. 677-692, 2018.
- [88] V. Magnasco, *Methods of molecular quantum mechanics: An introduction to electronic molecular structure*. John Wiley & Sons, 2009.
- [89] C. Bjørnholt, P. Mercebach, M. S. Rudner, and F. S. Nathan, "The Hartree-Fock Method," 2019.
- [90] P. E. Hoggan, M. B. Ruiz, and T. Özdoğan, "Molecular integrals over slater-type orbitals. From pioneers to recent developments," *Quantum Frontiers of Atoms and Molecules*, pp. 64-90, 2011.
- [91] P. E. Hoggan, M. B. Ruiz, and T. Özdoğan, "Molecular integrals over slater-type orbitals. From pioneers to recent developments," 2011.
- [92] E. Gross and R. Dreizler, "Density functional theory: an approach to the quantum many-body problem," ed: Springer, Berlin, 1990.

## References

---

- [93] R. G. Parr and Y. Weitao, "Aspects of atoms and molecules," in *Density-functional theory of atoms and molecules*: Oxford University Press, 1994.
- [94] W. Kohn, A. D. Becke, and R. G. Parr, "Density functional theory of electronic structure," *The Journal of Physical Chemistry*, vol. 100, no. 31, pp. 12974-12980, 1996.
- [95] K. Capelle, "A bird's-eye view of density-functional theory," *Brazilian journal of physics*, vol. 36, pp. 1318-1343, 2006.
- [96] J. B. Foresman, "Computational Chemistry: A Practical Guide for Applying Techniques to Real World Problems By David Young (Cytoclonal Pharmaceuticals Inc.). Wiley-Interscience: New York. 2001. xxvi+ 382 pp. \$69.95. ISBN: 0-471-33368-9," ed: ACS Publications, 2001.
- [97] P. Hohenberg and W. Kohn, "Inhomogeneous electron gas," *Physical review*, vol. 136, no. 3B, p. B864, 1964.
- [98] W. Kohn and L. J. Sham, "Self-consistent equations including exchange and correlation effects," *Physical review*, vol. 140, no. 4A, p. A1133, 1965.
- [99] M. Levy, "Universal variational functionals of electron densities, first-order density matrices, and natural spin-orbitals and solution of the v-representability problem," *Proceedings of the National Academy of Sciences*, vol. 76, no. 12, pp. 6062-6065, 1979.
- [100] G. Vignale and M. Rasolt, "Density-functional theory in strong magnetic fields," *Physical review letters*, vol. 59, no. 20, p. 2360, 1987.
- [101] O. A. A. Al-Owaedi, *Electronic properties of nano and molecular quantum devices*. Lancaster University (United Kingdom), 2016.
- [102] R. van Leeuwen, *Kohn-Sham potentials in density functional theory*. Vrije Universiteit Amsterdam, The Netherlands, 1994.
- [103] S. V. Kohut, "Construction and Analysis of Accurate Exchange-Correlation Potentials," The University of Western Ontario (Canada), 2017.
- [104] P. Motamarri, "Large-scale real-space Kohn-Sham density functional theory calculations using adaptive finite-element discretization," University of Michigan, 2014.

## References

---

- [105] S. Cottenier, "Density Functional Theory and the family of (L) APW-methods: a step-by-step introduction," *Instituut voor Kern-en Stralingsfysica, KU Leuven, Belgium*, vol. 4, no. 0, p. 41, 2002.
- [106] D. W. Rogers, *Computational Chemistry using the PC*. John Wiley & Sons, 2003.
- [107] E. Engel, *Density functional theory*. Springer, 2011.
- [108] G.-X. Zhang, "Understanding the role of van der Waals forces in solids from first principles," 2014.
- [109] R. A. Matzner, "Dictionary of Material Science and High Energy Physics," 2001.
- [110] W. J. Hehre, *A guide to molecular mechanics and quantum chemical calculations*. Wavefunction Irvine, CA, 2003.
- [111] A. R. Leach, *Molecular modelling: principles and applications*. Pearson education, 2001.
- [112] H. Englisch and R. Englisch, "Exact density functionals for ground-state energies II. Details and remarks," *physica status solidi (b)*, vol. 124, no. 1, pp. 373-379, 1984.
- [113] J. E. Klepeis, "Introduction to first-principles electronic structure methods: Application to actinide materials," *Journal of materials research*, vol. 21, no. 12, pp. 2979-2985, 2006.
- [114] D. M. Ceperley and B. J. Alder, "Ground state of the electron gas by a stochastic method," *Physical review letters*, vol. 45, no. 7, p. 566, 1980.
- [115] E. Lewars, *Computational Chemistry: Introduction to the Theory and Applications of Molecular and Quantum Mechanics*. 2011, pp. 1-664.
- [116] K. V. Bohoussou, A. Benié, M. G.-R. Koné, A. B. Kakou, K. Bamba, and N. Ziao, "Theoretical Study of the Reaction of (2, 2)-Dichloro (Ethyl) Arylphosphine with Bis (2, 2)-Dichloro (Ethyl) Arylphosphine by Hydrophosphination Regioselective by the DFT Method," *Computational Chemistry*, vol. 5, no. 03, p. 113, 2017.
- [117] D. Willock, "Richard Dronskowski. Computational chemistry of solid-state materials: a guide for materials scientists, chemists, physicists and others. Wiley-VCH, 2005, 294 pp; ISBN 3-978-3-527-31410-2 (hardcover)," ed: Wiley Online Library, 2007.

## References

---

- [118] M. R. Mueller, *Fundamentals of quantum chemistry: molecular spectroscopy and modern electronic structure computations*. Springer, 2001.
- [119] W. Walkosz, *Atomic Scale Characterization and First-Principles Studies of Si<sub>3</sub>N<sub>4</sub> Interfaces*. Springer Science & Business Media, 2011.
- [120] H. Chen and A. Zhou, "Orbital-free density functional theory for molecular structure calculations," *Numerical Mathematics: Theory, Methods and Applications*, vol. 1, no. 1, pp. 1-28, 2008.
- [121] J. P. Perdew, A. Ruzsinszky, J. Tao, V. N. Staroverov, G. E. Scuseria, and G. I. Csonka, "Prescription for the design and selection of density functional approximations: More constraint satisfaction with fewer fits," *The Journal of chemical physics*, vol. 123, no. 6, p. 062201, 2005.
- [122] A. D. Becke, "A new mixing of Hartree-Fock and local density-functional theories," *The Journal of chemical physics*, vol. 98, no. 2, pp. 1372-1377, 1993.
- [123] K. Kim and K. Jordan, "Comparison of density functional and MP2 calculations on the water monomer and dimer," *The Journal of Physical Chemistry*, vol. 98, no. 40, pp. 10089-10094, 1994.
- [124] P. J. Stephens, F. J. Devlin, C. F. Chabalowski, and M. J. Frisch, "Ab initio calculation of vibrational absorption and circular dichroism spectra using density functional force fields," *The Journal of physical chemistry*, vol. 98, no. 45, pp. 11623-11627, 1994.
- [125] A. C. Slov, "Book Review: Exploring Chemistry with Electronic Structure Methods, James B. Foresman and AEleen Frisch. Published by Gaussian, Inc., Pittsburgh, PA, 15106 USA. 354 pages. Soft cover: \$42.00 ISBN 0-9636769-3-8, Hard cover: \$100.00 ISBN 0-9636769-4-6 Abraham F. Jalbout," *Acta Chim. Slov*, vol. 50, pp. 159-160, 2003.
- [126] J. Reel, "A comparative review of computational methods as applied to gold (I) complexes and mechanisms," Duke University, 2016.
- [127] S. Huzinaga, J. Andzelm, E. Radzio-Andzelm, Y. Sakai, H. Tatewaki, and M. Klobukowski, *Gaussian basis sets for molecular calculations*. Elsevier, 2012.
- [128] P. Duffy, D. P. Chong, M. E. Casida, and D. R. Salahub, "Assessment of Kohn-Sham density-functional orbitals as approximate Dyson orbitals for



## References

---

- the calculation of electron-momentum-spectroscopy scattering cross sections," *Physical Review A*, vol. 50, no. 6, p. 4707, 1994.
- [129] J. Foresman and E. Frish, "Exploring chemistry," *Gaussian Inc., Pittsburg, USA*, vol. 21, 1996.
- [130] D. C. Young, "A practical guide for applying techniques to real-world problems," *Computational Chemistry, New York*, vol. 9, p. 390, 2001.
- [131] M. Towler, "An introductory guide to Gaussian basis sets in solid-state electronic structure calculations," *European Summer School "Ab initio modelling in solid-state chemistry"*, Turin, 2000.
- [132] A. Tomberg, "Gaussian 09w tutorial," *An introduction to computational chemistry using G09W and Avogadro software*, pp. 1-36, 2013.
- [133] W. J. Hehre, R. F. Stewart, and J. A. Pople, "Self-consistent molecular-orbital methods. I. Use of Gaussian expansions of Slater-type atomic orbitals," *The Journal of Chemical Physics*, vol. 51, no. 6, pp. 2657-2664, 1969.
- [134] J. A. Pople, M. Head-Gordon, D. J. Fox, K. Raghavachari, and L. A. Curtiss, "Gaussian-1 theory: A general procedure for prediction of molecular energies," *The Journal of Chemical Physics*, vol. 90, no. 10, pp. 5622-5629, 1989.
- [135] N. A. Jasim, "Density Functional Theory (Dft,B3lyp/6-31g) Of Acyclovir And Some Its Derivatives," *European Journal of Molecular & Clinical Medicine*, vol. 7, no. 9, pp. 513-523, 2020. [Online]. Available: [https://ejmcm.com/article\\_3516\\_8ce51f697c90467bfe641d1c2a5e4d08.pdf](https://ejmcm.com/article_3516_8ce51f697c90467bfe641d1c2a5e4d08.pdf).
- [136] R. Dennington, T. A. Keith, and J. M. Millam, "GaussView 6.0. 16," *Semichem Inc.: Shawnee Mission, KS, USA*, 2016.
- [137] O. Adnanhatem, F. S. A. Suhail, and A. M. Juda, "Optimized programs and methods required for the computational study of beta blockers," in *Journal of Physics: Conference Series*, 2020, vol. 1664, no. 1: IOP Publishing, p. 012088.
- [138] M. M. Kadhim and R. M. Kubba, "Theoretical investigation on reaction pathway, biological activity, toxicity and NLO properties of diclofenac drug and its ionic carriers," *Iraqi Journal of Science*, pp. 936-951, 2020.

## References

---

- [139] T. A. Julboev, M. M. Sultonov, and K. Abduvaliyeva, "Teaching Chemistry computer software to students of chemistry in pedagogical higher education institutions," *European Journal of Research and Reflection in Educational Sciences*, vol. 9, no. 3, 2021.
- [140] A. Beiser, *Concepts of modern physics*. 2003.
- [141] v. Jeremy I and S. Nir, "Modern Physics An Introductory Text " 2000 by Imperial College Press
- [142] A. Zarrouk *et al.*, "A theoretical investigation on the corrosion inhibition of copper by quinoxaline derivatives in nitric acid solution," *Int. J. Electrochem. Sci*, vol. 7, no. 7, p. 6353, 2012.
- [143] N. S. Babu and P. P. Kumar, "Computational Studies and Multivariate Analysis of Global and Local Reactivity Descriptors of Five Membered Heterocycles Molecules by Density Functional Theory (DFT)," 2015.
- [144] M. Miar, A. Shiroudi, K. Pourshamsian, A. R. Oliayey, and F. Hatamjafari, "Theoretical investigations on the HOMO–LUMO gap and global reactivity descriptor studies, natural bond orbital, and nucleus-independent chemical shifts analyses of 3-phenylbenzo [d] thiazole-2 (3 H)-imine and its para-substituted derivatives: Solvent and substituent effects," *Journal of Chemical Research*, vol. 45, no. 1-2, pp. 147-158, 2021.
- [145] B. G. Kim, *Mercury-containing species and carbon dioxide adsorption studies on inorganic compounds using density functional theory*. The University of Arizona, 2010.
- [146] İ. Sıdır, Y. G. Sıdır, M. Kumalar, and E. Taşal, "Ab initio Hartree–Fock and density functional theory investigations on the conformational stability, molecular structure and vibrational spectra of 7-acetoxy-6-(2, 3-dibromopropyl)-4, 8-dimethylcoumarin molecule," *Journal of Molecular Structure*, vol. 964, no. 1-3, pp. 134-151, 2010.
- [147] V. Balachandran and K. Parimala, "Tautomeric purine forms of 2-amino-6-chloropurine (N9H10 and N7H10): Structures, vibrational assignments, NBO analysis, hyperpolarizability, HOMO–LUMO study using B3 based density functional calculations," *Spectrochimica Acta Part A: Molecular and Biomolecular Spectroscopy*, vol. 96, pp. 340-351, 2012.

## References

---

- [148] R. Gangadharan and S. Sampath Krishnan, "Natural bond orbital (NBO) population analysis of 1-azanaphthalene-8-ol," *Acta Physica Polonica A*, vol. 125, no. 1, pp. 18-22, 2014.
- [149] A. Lakshmi and V. Balachandran, "Rotational isomers, NBO and spectral analyses of N-(2-hydroxyethyl) phthalimide based on quantum chemical calculations," *Journal of Molecular Structure*, vol. 1033, pp. 40-50, 2013.
- [150] A. A. Pinkerton, E. A. Zhurova, and Y.-S. Chen, "X-ray crystallography-Beyond structure in energetic materials," *Theoretical and Computational Chemistry*, vol. 12, pp. 215-245, 2003.
- [151] J. S. Murray, M. C. Concha, and P. Politzer, "Molecular surface electrostatic potentials as guides to Si-ON angle contraction: tunable  $\sigma$ -holes," *Journal of molecular modeling*, vol. 17, pp. 2151-2157, 2011.
- [152] S. Chand, F. A. Al-Omary, A. A. El-Emam, V. K. Shukla, O. Prasad, and L. Sinha, "Study on molecular structure, spectroscopic behavior, NBO, and NLO analysis of 3-methylbezothiazole-2-thione," *Spectrochimica Acta Part A: Molecular and Biomolecular Spectroscopy*, vol. 146, pp. 129-141, 2015.
- [153] C. B. Lingam and S. P. Tewari, "Theoretical studies on aminoborane oligomers," *Computational and Theoretical Chemistry*, vol. 1020, pp. 151-156, 2013.
- [154] A. D. Zdetsis, "Optical and electronic properties of small size semiconductor nanocrystals and nanoclusters," *Rev. Adv. Mater. Sci*, vol. 11, pp. 56-78, 2006.
- [155] W. Gao, Z. Li, and N. M. Sammes, *Introduction to Electronic Materials for Engineers*, an. World Scientific Publishing Company, 2011.
- [156] W. Strehlow and E. L. Cook, "Compilation of energy band gaps in elemental and binary compound semiconductors and insulators," *Journal of Physical and Chemical Reference Data*, vol. 2, no. 1, pp. 163-200, 1973.
- [157] P. W. Atkins and R. S. Friedman, *Molecular quantum mechanics*. Oxford university press, 2011.
- [158] S. Hokenek, "Characterization of conductive polycarbonate films," 2009.
- [159] D. S. Chang *et al.*, "Interactions of Electromagnetic Radiation with Matter," *Basic Radiotherapy Physics and Biology*, pp. 35-41, 2014.

## References

---

- [160] A. B. Chaves, L. F. d. S. G. Peralta, C. M. A. de Sousa Oliveira, and U. d. Lisboa, *Monte Carlo simulation applied to dosimetry of narrow high-energy photon beams used in radiosurgery*. 2004.
- [161] L. Korhonen, "Methods for dose calculation and beam characterization in external photon beam radiotherapy," 2009.
- [162] Y. Yan and E. G. Moros, "Radiation Oncology Physics: A Handbook for Teachers and Students, EB Podgorsak (Ed.), International Atomic Energy Association, Vienna, Austria (2005), 657 pages, Euro 65, paperbound, ISBN 92-0-107304-6," ed: Elsevier, 2006.
- [163] D. S. Chang, F. D. Lasley, I. J. Das, M. S. Mendonca, and J. R. Dynlacht, "Basic radiotherapy physics and biology," Springer, 2014.
- [164] F. H. ATTIX, "INTRODUCTION TO RADIOLOGICAL PHYSICS AND RADIATION DOSIMETRY," 2004 WILEY-VCH Verlag GmbH & Co. KGaA, Weinheim
- [165] W. Meredith and J. Massey, "Chapter XVI-The properties of the X-ray film," *Fundamental Physics of Radiology (Third Edition): Butterworth-Heinemann*, pp. 175-190, 1977.
- [166] J. P. S. W. S. K. R. SHORTT, "DOSIMETRIC PRINCIPLES, QUANTITIES AND UNITS," VIENNA, 2005.
- [167] M. C. Joiner and A. J. van der Kogel, *Basic clinical radiobiology*. CRC press, 2018.
- [168] R. A. Powsner and E. R. Powsner, *Essential nuclear medicine physics*. John Wiley & Sons, 2008.
- [169] P. D. FAIZ M. KHAN, "THE PHYSICS OF RADIATION THERAPY THIRD EDITION," 2003.
- [170] J. K. SHULTIS, R. E. FAW, K. S. University, and K. Manhattan, U.S., "FUNDAMENTALS OF NUCLEAR SCIENCE AND ENGINEERING," 2002.
- [171] P. Mayles, A. Nahum, and J.-C. Rosenwald, *Handbook of radiotherapy physics: theory and practice*. CRC Press, 2007.

## References

---

- [172] J. Hubbell, "Review of photon interaction cross section data in the medical and biological context," *Physics in Medicine & Biology*, vol. 44, no. 1, p. R1, 1999.
- [173] M. Berger *et al.*, "XCOM: photon cross section database (version 1.5), National Institute of Standards and Technology, Gaithersburg, MD, 2010," Available on <http://physics.nist.gov/xcom> (9 August, 2017, date last accessed), 2011.
- [174] S. G. Gounhalli, A. Shantappa, and S. Hanagodimath, "Studies on mass attenuation coefficient, effective atomic numbers and electron densities of some narcotic drugs in the energy range 1KeV-100GeV," *Journal of Applied Physics*, vol. 2, no. 4, pp. 40-48, 2012.
- [175] E. M. Zeman, E. C. Schreiber, and J. E. Tepper, "Basics of radiation therapy," in *Abeloff's clinical oncology*: Elsevier, 2020, pp. 431-460. e3.
- [176] E. B. P. N. Suntharalingam, J.H. Hendry, "Basic Radiobiology -Radiation Oncology Physics: A Handbook for Teachers and Students," 2012.
- [177] W. N. Rahman *et al.*, "Enhancement of radiation effects by gold nanoparticles for superficial radiation therapy," *Nanomedicine: Nanotechnology, Biology and Medicine*, vol. 5, no. 2, pp. 136-142, 2009.
- [178] C.-J. Liu *et al.*, "Enhancement of cell radiation sensitivity by pegylated gold nanoparticles," *Physics in Medicine & Biology*, vol. 55, no. 4, p. 931, 2010.
- [179] D. F. Ismail, D. o. R. Oncology, and U. K. M. M. Centre, "DRUG RADIATION INTERACTION Radiation Sensitizers and Protectors," 2012.
- [180] J. F. Hainfeld, F. A. Dilmanian, D. N. Slatkin, and H. M. Smilowitz, "Radiotherapy enhancement with gold nanoparticles," *Journal of pharmacy and pharmacology*, vol. 60, no. 8, pp. 977-985, 2008.
- [181] H. Dote *et al.*, "Enhancement of in vitro and in vivo tumor cell radiosensitivity by the DNA methylation inhibitor zebularine," *Clinical cancer research*, vol. 11, no. 12, pp. 4571-4579, 2005.
- [182] S. H. Cho, "Estimation of tumour dose enhancement due to gold nanoparticles during typical radiation treatments: a preliminary Monte Carlo study," *Physics in Medicine & Biology*, vol. 50, no. 15, p. N163, 2005.

## References

---

- [183] F. H. Attix, *Introduction to radiological physics and radiation dosimetry*. John Wiley & Sons, 2008.
- [184] J. D. Chapman and A. E. Nahum, *Radiotherapy treatment planning: linear-quadratic radiobiology*. CRC Press, 2016.
- [185] M. Beyzadeoglu, G. Ozyigit, and C. Ebruli, *Basic radiation oncology*. Springer, 2010.
- [186] J. F. Fowler, "21 years of biologically effective dose," *The British journal of radiology*, vol. 83, no. 991, pp. 554-568, 2010.
- [187] R. D. Stewart and X. A. Li, "BGRT: Biologically guided radiation therapy—The future is fast approaching!," *Medical Physics*, vol. 34, no. 10, pp. 3739-3751, 2007.
- [188] K. Chadwick and H. Leenhouts, "Molecular theory of cell survival," Instituut voor Toepassing van Atoomenergie in de Landbouw, Wageningen ..., 1973.
- [189] H. D. Thames, "An 'incomplete-repair' model for survival after fractionated and continuous irradiations," *International Journal of Radiation Biology and Related Studies in Physics, Chemistry and Medicine*, vol. 47, no. 3, pp. 319-339, 1985.
- [190] P. H. K. SACHS and R. DJ BRENNER, "Review the link between low-LET dose-response relations and the underlying kinetics of damage production/repair/misrepair," *International journal of radiation biology*, vol. 72, no. 4, pp. 351-374, 1997.
- [191] "Radiation Biology: A Handbook for Teachers and Students," *INTERNATIONAL ATOMIC ENERGY AGENCY*, VIENNA, 2010
- [192] A. Barrett, S. Morris, J. Dobbs, and T. Roques, *Practical radiotherapy planning*. CRC Press, 2009.
- [193] E. C. Halperin, "Perez and Brady's principles and practice of radiation oncology," (*No Title*), 2008.
- [194] A. N. Ayaash, "Theoretical study for potential energy curves, dissociation energy and molecular properties for (LiH, H<sub>2</sub>, HF) molecules," 2015.

## References

---

- [195] S. M. Khalil, E. E. Ali-Shattle, and N. M. Ali, "A theoretical study of carbohydrates as corrosion inhibitors of iron," *Zeitschrift für Naturforschung A*, vol. 68, no. 8-9, pp. 581-586, 2013.
- [196] J. M. Arroyave, R. n. E. Ambrusi, M. a. E. Pronsato, A. Juan, M. F. Pistonesi, and M. a. E. Centurión, "Experimental and DFT studies of hybrid silver/cdots nanoparticles," *The Journal of Physical Chemistry B*, vol. 124, no. 12, pp. 2425-2435, 2020.
- [197] G. Nageswari, G. George, S. Ramalingam, and M. Govindarajan, "Molecular analyses using FT-IR, FT-Raman and UV spectral investigation; quantum chemical calculations of dimethyl phthalate," *Journal of Molecular Structure*, vol. 1195, pp. 331-343, 2019.
- [198] M. Saranya, S. Ayyappan, R. Nithya, R. Sangeetha, and A. Gokila, "Molecular structure, NBO and HOMO-LUMO analysis of quercetin on single layer graphene by density functional theory," *Dig. J. Nanomater. Biostruct*, vol. 13, pp. 97-105, 2018.
- [199] R. N. Jones and F. Herling, "CHARACTERISTIC GROUP FREQUENCIES IN THE INFRARED SPECTRA OF STEROIDS<sup>1</sup>," *The Journal of Organic Chemistry*, vol. 19, no. 8, pp. 1252-1268, 1954.
- [200] P. Vennila *et al.*, "Synthesis, spectroscopic characterization, molecular docking studies and DFT calculation of novel Mannich base 1-((4-ethylpiperazin-1-yl)(2-hydroxyphenyl) methyl) naphthalen-2-ol," *Journal of Molecular Structure*, vol. 1246, p. 131164, 2021.
- [201] R. Goodacre, B. S. Radovic, and E. Anklam, "Progress toward the rapid nondestructive assessment of the floral origin of European honey using dispersive Raman spectroscopy," *Applied Spectroscopy*, vol. 56, no. 4, pp. 521-527, 2002.
- [202] E. Corbett, V. Zichy, J. Goral, and C. Passingham, "Fourier transform Raman studies of materials and compounds of biological importance—II. The effect of moisture on the molecular structure of the alpha and beta anomers of d-glucose," *Spectrochimica Acta Part A: Molecular Spectroscopy*, vol. 47, no. 9-10, pp. 1399-1411, 1991.
- [203] M. Hineno, "Infrared spectra and normal vibration of  $\beta$ -d-glucofuranose," *Carbohydrate Research*, vol. 56, no. 2, pp. 219-227, 1977.

## References

---

- [204] G. Venkatesh *et al.*, "An investigation on the molecular structure, interaction with metal clusters, anti-Covid-19 ability of 2-deoxy-D-glucose: DFT calculations, MD and docking simulations," *Journal of Molecular Structure*, vol. 1258, p. 132678, 2022/06/15/ 2022, doi: <https://doi.org/10.1016/j.molstruc.2022.132678>.
- [205] A. González Fa, I. Lopez-Corral, R. Faccio, A. Juan, and M. S. Di Nezio, "Surface enhancement Raman spectroscopy and density functional theory study of silver nanoparticles synthesized with d-glucose," *Journal of Raman Spectroscopy*, vol. 49, no. 11, pp. 1756-1764, 2018, doi: 10.1002/jrs.5466.
- [206] J. M. Arroyave, R. E. Ambrusi, M. E. Pronsato, A. Juan, M. F. Pistonesi, and M. E. Centurion, "Experimental and DFT Studies of Hybrid Silver/Cdots Nanoparticles," *The Journal of Physical Chemistry B*, vol. 124, no. 12, pp. 2425-2435, 2020/03/26 2020, doi: 10.1021/acs.jpcc.9b10430.
- [207] J. G. Webster, *Encyclopedia of medical devices and instrumentation*. United States of America, 2006.
- [208] H. Rieger, T. Fredrich, and M. Welter, "Physics of the tumor vasculature: Theory and experiment," *The European Physical Journal Plus*, vol. 131, pp. 1-24, 2016.
- [209] J. W. Baish *et al.*, "Scaling rules for diffusive drug delivery in tumor and normal tissues," *Proceedings of the National Academy of Sciences*, vol. 108, no. 5, pp. 1799-1803, 2011.
- [210] A. S. Thakor and S. S. Gambhir, "Nanooncology: the future of cancer diagnosis and therapy," *CA: a cancer journal for clinicians*, vol. 63, no. 6, pp. 395-418, 2013.
- [211] J. H. Hubbell, "Review and history of photon cross section calculations," *Physics in Medicine & Biology*, vol. 51, no. 13, p. R245, 2006.
- [212] N. Scher *et al.*, "Review of clinical applications of radiation-enhancing nanoparticles," *Biotechnology Reports*, vol. 28, p. e00548, 2020.
- [213] T. A. Abdulwahid, "Mathematical Model for Calculating Radiation Dose used to Treat Malignant Cells and Improved SER with Aid of Nanoparticles " 2017.



## References

---

- [214] Z. Liu *et al.*, "Enhancement of radiotherapy efficacy by silver nanoparticles in hypoxic glioma cells," *Artificial Cells, Nanomedicine, and Biotechnology*, vol. 46, no. sup3, pp. 922-930, 2018.
- [215] I. Kiran *et al.*, "Emerging Nanomaterials as Radio-Sensitizer in Radiotherapy," in *Harnessing Materials for X-ray Based Cancer Therapy and Imaging*: Springer, 2022, pp. 59-75.
- [216] J. Ma, R. Xu, J. Sun, D. Zhao, J. Tong, and X. Sun, "Nanoparticle surface and nanocore properties determine the effect on radiosensitivity of cancer cells upon ionizing radiation treatment," *Journal of nanoscience and nanotechnology*, vol. 13, no. 2, pp. 1472-1475, 2013.



جامعة كربلاء

كلية العلوم

قسم الفيزياء

تحسين العلاج الاشعاعي نظرياً بواسطة جزيئات النانو كعامل حساس للإشعاع

رسالة مقدمة الى مجلس كلية العلوم / جامعة كربلاء  
كجزء من متطلبات نيل درجة الماجستير في علوم الفيزياء

كتبت بواسطة

ولاء شعلان سرحان عبد

بكالوريوس 2008

بإشراف

ا.م.د نغم محي التميمي

## الخلاصة

يتضمن هذا البحث دراسة نظرية لتعزيز العلاج الإشعاعي باستخدام جزيئات النانو كعامل حساس للإشعاع. تم استخدام هياكل مختلفة من جزيئة الفا دي كليكوز بعد امتزازها على سطح ذرات الفضة النانوية  $C_{12}H_{24}O_{12}Ag$ ،  $C_6H_{12}O_6Ag_3$ . تم تقييم خواص هذه المركبات باستخدام نظرية الكثافة الوظيفية (DFT) مع الدالة الهجينة B3LYP مع مزيج من مجموعات الأساس لذرات الكربون والاكسجين والهيدروجين ( $6-311+G^*$ ) وللفضة النانوية (LANL2DZ).

تم دراسة الخواص الالكترونية والتركيبية من خلال اجراء التحسين الهندسي للحصول على أفضل التكوينات المستقرة لهياكل الجلوكوز مع الفضة من خلال الحصول على طاقات الاستقرار لكل من  $C_6H_{12}O_6Ag_3$ ،  $C_{12}H_{24}O_{12}Ag$  and  $C_6H_{12}O_6$  قيمها على التوالي كانت  $-1124.712$ ،  $-1520.447$ ،  $-687.140$  - بوحدة الهاتري. الهياكل الجزيئية المستقرة المدروسة تم حساب اطوال الاواصر بين الذرات، زوايا الربط وزوايا ثنائية السطوح ودراسة خواص الالكترونية منها الطاقات الالكترونية وتوزيع الشحنات الالكترونية وحساب فجوة الطاقة لكل للمركب بوحدة الالكترون فولط. كما تم حساب أنماط الاهتزاز لكل مركب . من جهة أخرى تم تحليل ودراسة أطياف FTIR حيث وجد انه هناك توافق بين الدراسة النظرية والعملية بعد دراسة خواص واستقراره هذه الجزيئات. وقد استخدمت مع فوتونات ذو طاقات عالية ناتجة من المعجلات الخطية او من المصادر المشعة.

ان الغرض كان من استخدام هذه الجزيئات هو لزيادة مساحة الجرعة الممتصة من الإشعاع داخل الخلايا المصابة بالسرطان في الأعضاء البشرية (الرئة). الية تفاعل هذه الجزيئات مع فوتونات الطاقة العالية لأشعة X-Ray داخل الخلايا المصابة ينتج من تفاعل الالكترون - بوزترون. الهدف من هذا التفاعل زيادة مساحة المقطع العرضي للتفاعل داخل الورم بواسطة جزيئات كلوكوز مع الفضة النانوية من اجل زيادة الجرعة الممتصة داخل الورم دون الضرر بالخلايا السليمة المحاطة بالورم

استخدمت المركبات  $C_6H_{12}O_6Ag_3$ ،  $C_{12}H_{24}O_{12}Ag$  كعامل حساس للإشعاع لزيادة حساسية الإشعاعية داخل الورم (الرئة) من تفاعل هذه الجزيئات مع الطاقات العالية لأشعة X-Ray بمدى يتراوح من 2-15 ميكا الالكترون فولط. وكانت حساسية الإشعاع SER نظريا عند المركب  $C_6H_{12}O_6Ag_3$  عندما  $E=2MeV$  ،  $E=4MeV$  و  $E=6MeV$  قيمتها تساوي 13.86 بينما عند  $E=8MeV$ ،  $E=10MeV$  قيمتها تساوي 14.75 وعند  $E=12MeV$  تساوي 13.95 ،  $E=14MeV$  تساوي 14.83 عند اعظم قيمة للطاقة  $E=15MeV$  قيمتها تساوي 15.64 لكن المركب  $C_{12}H_{24}O_{12}Ag$ . عندما  $E=2MeV$  قيمتها 13.7 ،  $E=4MeV$ ،  $E=6MeV$ ،  $E=10MeV$  قيمتها تساوي 12.9 ،  $E=12MeV$  تساوي 12.5،  $E=14MeV$  ،  $E=12.8$  عند اعظم قيمة للطاقة  $E=15MeV$  قيمتها تساوي 12.9

هذه القيم من حساسية الاشعاع أحدث تقليص في عدد جلسات العلاج الاشعاعي تقريبا الى نصف المدة الزمنية العلاجية وهذا يعتبر تحسن ملحوظ في تحسين العلاج الاشعاعي ما يعكس شيء إيجابي على نفسية المرضى المصابين.